FINAL REPORT

MULTI-OBJECTIVE AND MULTIDISCIPLINARY DESIGN OPTIMISATION (MDO) OF UNMANNED AERIAL VEHICLE SYSTEMS USING HIERARCHICAL ASYNCHRONOUS PARALLEL MULTI-OBJECTIVE EVOLUTIONARY ALGORITHMS

L. Damp, L.F. Gonzalez and K. Srinivas
School of Aerospace, Mechanical & Mechatronic Engineering, University of Sydney, NSW, Australia

AFOSR Contract Number: AOARD-044078

Report Documentation Page

Form Approved
OMB No. 0704-0188

Public reporting burden for the collection of information is estimated to average 1 hour per response, including the time for reviewing instructions, searching existing data sources, gathering and maintaining the data needed, and completing and reviewing the collection of information. Send comments regarding this burden estimate or any other aspect of this collection of information, including suggestions for reducing this burden, to Washington Headquarters Services, Directorate for Information Operations and Reports, 1215 Jefferson Davis Highway, Suite 1204, Arlington VA 22202-4302. Respondents should be aware that notwithstanding any other provision of law, no person shall be subject to a penalty for failing to comply with a collection of information if it does not display a currently valid OMB control number.

1. REPORT DATE	2. REPORT TYPE	3. DATES COVERED
17 SEP 2007	**FInal**	**01-08-2005 to 01-04-2006**

4. TITLE AND SUBTITLE
Multi-objective and Multidisciplinary Design Optimisation of UAV Systems using Hierarchical Asynchronous Parallel Evolutionary Algorithms

5a. CONTRACT NUMBER
FA520905P0585

5b. GRANT NUMBER

5c. PROGRAM ELEMENT NUMBER

6. AUTHOR(S)
Karkenahalli Srinivas

5d. PROJECT NUMBER

5e. TASK NUMBER

5f. WORK UNIT NUMBER

7. PERFORMING ORGANIZATION NAME(S) AND ADDRESS(ES)
University of Sydney,School of Aerospace, Mechanical and Mechatronic Engr,Sydney, NSW 2006,Australia,AU,2006

8. PERFORMING ORGANIZATION REPORT NUMBER
N/A

9. SPONSORING/MONITORING AGENCY NAME(S) AND ADDRESS(ES)
AOARD, UNIT 45002, APO, AP, 96337-5002

10. SPONSOR/MONITOR'S ACRONYM(S)
AOARD

11. SPONSOR/MONITOR'S REPORT NUMBER(S)
AOARD-044078

12. DISTRIBUTION/AVAILABILITY STATEMENT
Approved for public release; distribution unlimited

13. SUPPLEMENTARY NOTES

14. ABSTRACT
Project report from basic science initiative to use Hierarchical Asynchronous Parallel Evolutionary Algorithms for MDO of a UAV system using high fidelity analysis tools. Two production UAV wings were examined for aerodynamic and structural properties. Optimization was performed over 48 design variables.

15. SUBJECT TERMS

16. SECURITY CLASSIFICATION OF:			17. LIMITATION OF ABSTRACT	18. NUMBER OF PAGES	19a. NAME OF RESPONSIBLE PERSON
a. REPORT	b. ABSTRACT	c. THIS PAGE			
unclassified	**unclassified**	**unclassified**	**Same as Report (SAR)**	**99**	

TABLE OF CONTENTS

NOMENCLATURE

AR	= Aspect ratio	Γ_{rc}	= Inboard dihedral angle, *deg*
S	= Wing wetted area, m^2	Γ_{ct}	= Outboard dihedral angle, *deg*
C_R	= Root chord length	M_∞	= Freestream Mach number
b	= Semi span length	Re	= Reynolds number
λ_{rc}	= Inboard taper ratio	α	= Angle of attack, *deg*
λ_{ct}	= Outboard taper ratio	ψ	= Yaw angle, *deg*
Λ_{rc}	= Inboard sweep angle, *deg*	C_L	= Lift coefficient
Λ_{ct}	= Outboard sweep angle, *deg*	C_D	= Drag coefficient
$BP_{Inboard}$	= Inboard break point	C_{D0}	= Drag coefficient at zero lift
$BP_{Outboard}$	= Outboard break point	L/D	= Lift to drag ratio
C_f	= Friction coefficient	$SrTr$	= Spar Root Thickness Taper Ratio
$crank_l$	= Crank Location	$WsRt$	= Wing Skin Root Thickness, *m*
Ns	= Number of Spars	$WstTr$	= Wing Skin Thickness Tip Taper Ratio
Nr	= Number of Ribs	$WsTre$	= Wing Skin Thickness Edge Taper Ratio
Rrt	= Rib Root Thickness, *m*	Sc	= Spar Cap Root Area, m^2
$RrTr$	= Rib Root Thickness Taper Ratio	Rc	= Rib Cap Root Area, m^2
Srt	= Spar Root Thickness, *m*		

SUMMARY

The overall objective of this project was to realise the practical application of Hierarchical Asynchronous Parallel Evolutionary Algorithms for Multi-objective and Multidisciplinary Design Optimisation (MDO) of UAV Systems using high fidelity analysis tools. The project looked at the aerodynamics and structure of two production UAV wings and attempted to optimise these wings in isolation to the rest of the vehicle. The project was sponsored by the Asian Office of the Air Force Office of Scientific Research.

The two vehicles wings which were optimised were the Northrop Grumman Global Hawk (GH) and the General Atomics Altair (Altair). The optimisations for both vehicles were performed at cruise altitude with MTOW minus 5% fuel and a 2.5g load case. The GH was assumed to use NASA LRN 1015 aerofoil at the root, crank and tip locations with five spars and ten ribs. The Altair was assumed to use the NACA4415 aerofoil at all three locations with two internal spars and ten ribs. Both models used a parabolic variation of spar, rib and wing skin thickness as a function of span, and in the case of the wing skin thickness, also chord.

The work was carried out by integrating the current University of Sydney designed Evolutionary Optimiser (HAPMOEA) with Computational Fluid Dynamics (CFD) and Finite Element Analysis (FEA) tools. The variable values computed by HAPMOEA were subjected to structural and aerodynamic analysis. The aerodynamic analysis computed the pressure loads using a Morino class panel method code named PANAIR. These aerodynamic results were coupled to a FEA code, MSC.Nastran® and the strain and displacement of the wings computed. The fitness of each wing was computed from the outputs of each program.

In total, 48 design variables were defined to describe both the structural and aerodynamic properties of the wings subject to several constraints. These variables allowed for the alteration of the three aerofoil sections describing the root, crank and tip sections. They also described the internal structure of the wings allowing for variable flexibility within the wing box structure. These design variables were manipulated by the optimiser such that two fitness functions were minimised. The fitness functions were the overall mass of the simulated wing box structure and the inverse of the lift to drag ratio. Furthermore, six penalty functions were added to further penalise genetically inferior wings and force the optimiser to not pass on their genetic material.

The results indicate that given the initial assumptions made on all the aerodynamic and structural properties of the HALE and MALE wings, a reduction in mass and drag is possible through the use of the HAPMOEA code. The code was terminated after 300 evaluations of each hierarchical level due to plateau effects. These evolutionary optimisation results could be further refined through a gradient based optimiser if required. Even though a reduced number of evaluations were performed, weight and drag reductions of between 10 and 20 percent were easy to achieve and indicate that the wings of both vehicles can be optimised.

1 INTRODUCTION

The development and use of Unmanned Aerial Vehicles (UAVs) for military and civilian applications is rapidly increasing. Similar to their manned counterparts, the challenge is to develop trade-off studies of optimal configurations to produce high performance aircraft that satisfy mission requirements. There are difficulties with these concepts due to the varied nature of the missions that have to be performed. These complexities in engineering design, and the more demanding industrial requirements, have pushed the need to speed up the development of robust and fast numerical techniques to overcome difficulties associated with traditional deterministic optimisers.

In aerospace engineering design and optimisation the designer is usually presented with a problem which involves not just one objective, but numerous objectives and multi-physics. Hence a systematic approach, which is regarded as Multidisciplinary Design Optimisation (MDO) and which accounts for the coupling between the variables and objectives, is required. Problems in aeronautics usually involve a number of disciplines and objectives; therefore the search space can be multi-modal, non convex or discontinuous. Wing design is an example of a multi-objective MDO problem where there is a strong interaction between the aerodynamics and the forced structural response.

The goal of the present report is to address this issue from a multi-objective and multidisciplinary aircraft design optimisation (MDO) standpoint.

In today's world of advancing technology, engineers are faced with the problem of designing increasingly complicated multidisciplinary systems. This is a difficult task, as these systems not only involve coupling amongst the different physics involved, but also a large number of variables and a series of objectives and constraints. At the same time, engineers need to optimise and address several requirements which include the reduction of the time spent on design and reducing the cost of research and development, while improving the performance, reliability, quality and safety of the product or process under consideration.

These complex interactions have generated a growing interest in the area of multi-objective and Multidisciplinary Design Optimisation (MDO). Here the designer is interested not only in a single global optimal solution but in a set of solutions that represent the trade-off between the different objectives. MDO refers to an approach to formalise a design process which accounts for the interaction between the different physics involved, while optimising for a number of objectives and constraints.

When applied to aeronautics, the necessity of optimisation and MDO is clear, given that even a very small improvement in weight or a reduction in aerodynamic drag will have a tremendous impact on the overall performance of the design. The application of MDO to the design and optimisation of aerospace vehicles can be represented as in Figure 1. Cleary in MDO a number of disciplines (aerodynamics, structures, propulsion, aero-acoustics, etc) are present and interact.

The task of the designer or team of designers is to develop a solution that conforms to all the disciplines while satisfying the requirements and constraints. When optimisation is intended, the different objectives (for example, aerodynamic performance, purchase price, take-off weight) need to be considered in order to find an optimal solution or set of solutions.

A common approach for optimisation is the use of aggregating functions in which different weights are assigned to each objective. The problem with this approach is that the weight for each objective needs to be known in advance. Another approach is to compute or produce a set of solutions in what will be referred to in this thesis as a Pareto optimal front or surface. This Pareto optimal front represents the optimal set of non-dominated solutions and the trade-off between the objectives and disciplines involved.

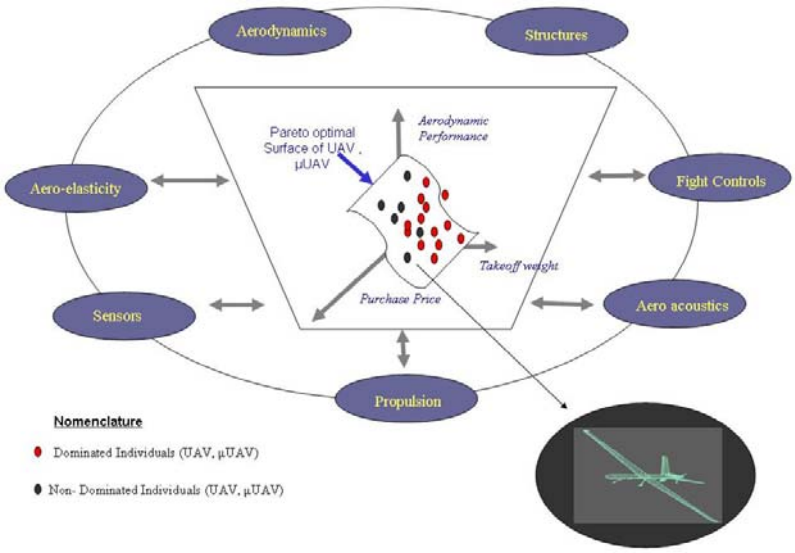

Figure 1: UAV MDO process

The process of MDO involves the use of several analysis tools such as Computational Fluid Dynamics (CFD) software or Finite Element Analysis (FEA) and also optimisation tools. These analysis tools are under constant development and have reached a point where a confident application to aeronautical design in conjunction with MDO is possible (Mason 1998; Agarwal 1999; Thomas 1999)

However, there are limitations on the application of these tools within MDO at an industrial level, due to the computational expense involved. A single high-fidelity Navier-Stokes CFD computation around an aircraft wing, for example, might take several hours on a supercomputer. Therefore, the continuing challenge has been to develop methodologies such as Design of Experiments (DOE) (Giunta 1997), approximation methods and variable fidelity models that combine and use different fidelity analysis tools during the design and optimisation process to minimise the computational expense.

While the area of traditional optimisation tools for a single discipline is quite mature, the area of robust optimisation tools and approaches for MDO is still at the initial stages of development (Alexandrov and Lewis 2000), (Sobieszczanski-Sobieski 1997; Bartholomew 1998)

The conventional approach in aeronautical design and MDO has been the use of traditional deterministic optimisers. These optimisers are efficient for finding optimal global solutions if the objective and constraints are differentiable. However, robust alternative numerical tools are required if a broader application of the optimiser is desired, or the problem is multi-modal, involves approximations, is non-differentiable or involves multiple objectives and physics, as is usually the case in the design of complex multidisciplinary systems in aeronautics.

A relatively new technique for optimisation is the use of Evolutionary Algorithms (EAs). These are based on Darwinian theories of evolution, where populations of individuals evolve over a search space and adapt to the environment through the use of different mechanisms such as mutation, crossover and selection. EAs require no derivatives or gradients of the objective function and have the capability of finding globally optimum solutions amongst many local optima. They are easily executed using parallel computing techniques and can be adapted to arbitrary analysis codes without much major modification. Another major advantage of EAs is that they can tackle multi-objective problems directly. Together these characteristics give EAs substantial advantages over more conventional deterministic approaches.

Interest in EAs for problems in engineering and aeronautics has grown substantially in the past fifteen years. These methods have been successfully applied to different aeronautical design problems including airframe, wing, aerofoil and rotor blade design, (Obayashi 1998), (Oyama, Liou et al. September, 2002), (Parmee and Watson July 1999), (Raymer 2003; Gonzalez 2005).

The application of EAs for MDO problems has been limited. This is mainly because one of the drawbacks of EAs is that they are slow when compared to traditional deterministic methods, as they require a larger number of function evaluations to converge to an optimal solution.

Hence the continuing challenge in evolutionary optimisation has been to reduce the number of function evaluations and the computational expense. To achieve this, several approaches have been proposed; these include a combination of variable fidelity models, parallelisation strategies and hybridisation techniques (Coello, Veldhuizen et al. 2002), (Deb 2003), (Kim 1997).

This report describes the theory and application of a methodology for multi-objective multidisciplinary design of UAV Wings. The method is based on a robust evolutionary optimiser, an aero-structural solver, parallel computing, asynchronous evaluation and a hierarchical topology of different fidelity solvers that reduce the computational expense for multi-objective and MDO problems. The method is applicable to single and multi-objective, inverse or direct complex engineering problems that can be multi-modal, involve approximations, are non-differentiable, with convex, non-convex or discontinuous Pareto optimal fronts.

The method simplifies the task of the designer or design team by integrating several components so that they can focus on the engineering problem itself. The methods are developed in a sequence of steps consisting of: defining the requirements, formulating the method, identifying several promising robust analysis and optimisation tools, the creation of algorithms and practical real-world problems in aeronautics.

Section 2 of the report describes the concept of multidisciplinary design optimisation; section 3 the main components of the MDO methodology. Section 4 details the Evolutionary Optimiser; Section 5 details and tests the aero-structural solver for two baseline designs. Section 6 details the aero-structural optimisation process and section 7 presents the application of the method for two test cases related to aero-structural UAV wing design optimisation.

2 MULTIDISCIPLINARY DESIGN OPTIMISATION

In aerospace engineering the designer is usually presented with a problem which involves considering not only one objective but numerous objectives and multi-physics. A systematic approach that accounts for the coupling between the disciplines and variables regarded as Multidisciplinary Design Optimisation (MDO), is required. In aircraft design, for example, the multi-physics include aerodynamics, structures, propulsion and control. These multi-physics are interrelated and interdisciplinary constraints must be satisfied to solve the problem. The area of MDO has matured itself as a separate discipline as evidenced in different journals, specialised technical committees, conferences and publications devoted solely to the topic.

The need for, and benefits of MDO are clear given that even a small improvement in the performance of the aircraft can have significant impact on the overall operation of the vehicle. An MDO process also allows an evaluation of the constraints on multiple disciplines from the early stages of the design, thus the expense of re-designing an aircraft system is reduced. A comprehensive survey of MDO methods, their development and limitations is provided by Sobieski (Sobieski and Haftka 1996). The research has classified the different methods and highlighted some important needs, including a multi-platform operation, the use of parallel computation to reduce computational expense and space visualisation as the designer might be interested in the space around the optimum rather than the optimum itself. In most of the methods described in the survey, the optimisation algorithms for MDO use traditional gradient methods for the solution, but as has been discussed, these methods have some limitations. Sobieski and Haftka (Sobieski and Haftka 1996) have evaluated recent developments in multidisciplinary aerospace design and optimisation and identified several categories of problem formulations and also two main challenges for MDO - the computational expense and organisational (architectural) complexity. A more recent survey by Giesing and Barthel (Giesing 1998) identifies several industrial applications and summarises some of the needs for MDO. Most of the applications are related to detailed design; few applications are developed for conceptual or preliminary MDO studies. On the classification of needs, their research also describes how a MDO framework should be flexible to accept whatever functions is needed and should address the issue of low - and high - fidelity models, but not to compromise the optimisation. It also points out the need for efficient models that describe the physics to keep computing time at a reasonable level. A critical issue mentioned in the paper is the need for accurate and realistic design by identification of the constraints, mechanisms and underlying physics of the various disciplines involved.

An open issue with MDO studies is the fact that many high-fidelity processes such as CFD or FEA are complex to couple within MDO as many of them are not automated, robust or fast enough. Also, the need for approximation techniques, such as Response Surface Methodology (RSM) (Giunta 1997) or Design and Analysis of Computer Experiments (DACE) (Sacks, Welch et al. 1989), arises because of the computational expense of using an analysis code for all the evaluations during the optimisation process and also from the fact that some analysis codes cannot be directly integrated with the MDO architecture.

In MDO framework architectures, there is a requirement for more efficient, robust flexible framework architectures and methods with industrial codes. These codes should be easily coupled and reconfigurable, and adaptable to commercial solvers. One of the problems with current MDO architectures is that these are usually developed at universities and in industries with restrictions on their use, and sometimes these are specialised and difficult to generalise for other applications.

When implementing the optimisation tools for MDO, it is important to determine the presence of multi-modalities, non-linearities and multiple objectives that might cause a traditional deterministic method to fail. The computational cost of calculating the gradients and the presence of multiple disciplines is also an important consideration.

The continuing challenge has been on developing and improving numerical optimisation techniques and enhancing their speed and robustness for their use within MDO. One of the emerging optimisation techniques for MDO is Evolutionary Algorithms (EAs), but they have found limited application in MDO due to the computational burden associated with them.

Giesing and Barthel (Giesing 1998) also presented a short discussion on supporting design space search methods such as EAs, and explained how they are gaining popularity for MDO because they are simple to couple with analysis modules and do not incur the cost of computing derivatives.

One example of MDO is the minimisation of wing drag and weight in a two-discipline problem: namely aerodynamics and structures. The design variables can be wing sweep, wing span, twist or taper. With an integrated approach the optimiser sends the values of these variables to an integral system of equations that represent the aerodynamic and structural analysis codes. These calculations are iteratively performed to conform and converge on each discipline to a consistent solution. The objective function and constraints are then evaluated and manipulated by the optimiser to improve the design.

This approach is conceptually very simple. Once all disciplines are coupled to form a single multidisciplinary analysis module, the same techniques that are used for a single-discipline optimisation may be used. The disadvantage of this approach is that the solution of a single system could be very expensive and does not enable the potential decoupling of the individual disciplines into analysis modules that can be computed in parallel.

As will be illustrated in Section 7.1, the benefits of parallelisation can be exploited by using an EA which sends candidate individuals to different processors where they are evaluated by the complete MDO analysis and returned to the optimiser.

2.1 Limitations of Current Optimisation Techniques for MDO

As discussed in the previous sections, most of the optimisation methods used for MDO use traditional deterministic techniques. While the use of these methods is largely successful and efficient in finding optimal global solutions, problems do arise. Gradient-based methods usually work best with unimodal functions, but their effectiveness decreases with the presence of local optima or ridges in the fitness landscape. Also, the presence of numerical noise inhibits the application of many gradient-based optimisation techniques. The numerical noise causes an inaccurate calculation of gradients, which in turn slows or prevents convergence during optimisation as shown by Giunta (Giunta 1997).

In aircraft design, for example, the problem of numerical noise is of special concern when an accurate solution is sought through a high-fidelity analysis but the computation of gradients is complex and a single aerodynamic or structural analysis might take several CPU hours on a supercomputer.

An emerging optimisation technique for MDO is Evolutionary Algorithms (EAs); these techniques are robust in finding optimal solutions for single- and multi-objective problems, but have found limited applications to MDO due to the computational burden associated with them. The challenge is then to study, develop, apply and improve the speed and robustness of these methods so that confident applications and within an MDO operational framework is possible.

It is important to highlight that in this work the use of EAs will be restricted to conceptual and preliminary MDO studies where the number of variables is still relatively small, less than a hundred, and where the use of EAs is still of potential benefit. On a larger scale, the use of EAs can be extended for an increased number of variables and coupled with other techniques such as Design of Experiments (DOE).

3 FORMULATION OF THE MDO PROBLEM

The general MDO is formulated to seek a vector X of design variables that minimises an objective function $F(X)$ subject to disciplinary interdisciplinary and side constraints according to $(X_i)_L \leq X \leq (X_i)_U$, $i = 1,...,N$ where N is the number of design variables and $(X_i)_L$ and $(X_i)_U$ are the lower and upper bounds placed upon the design variable X_i. Two different classes of design variables are specified:

- Aerodynamics
- Structures

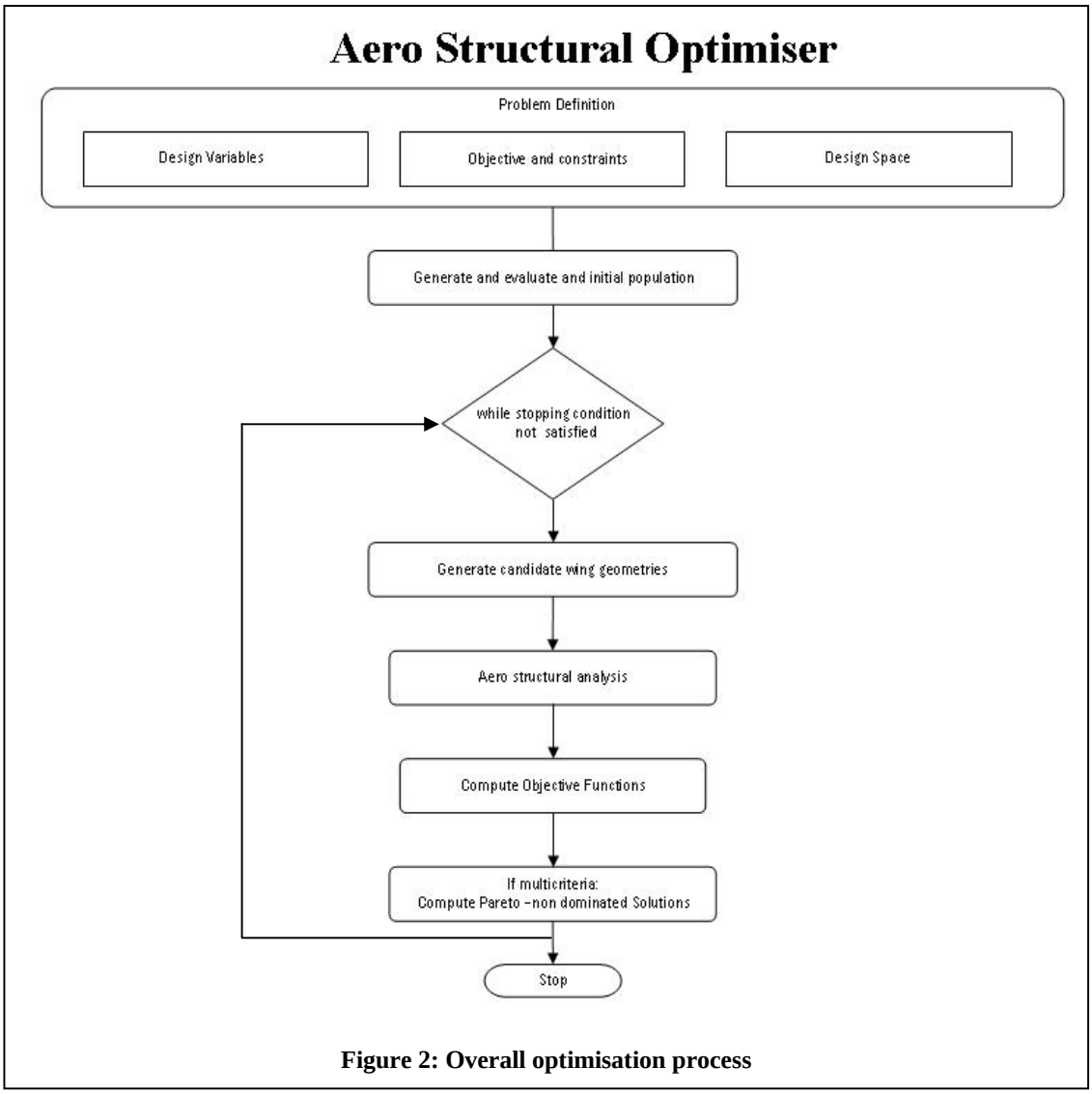

Figure 2: Overall optimisation process

3.1 METHOD

The method couples the proven Evolutionary Optimiser (HAPMOEA) and an Aero-Structural solver. The Aero-Structural solver integrates two commercial high fidelity analysis tools for FEA and CFD analysis using MATLAB as the controlling operating system.

The optimisation process consists of the eight main steps as illustrated in Figure 2. In the first step, the design variables, design constraints, flow conditions and fitness functions are defined. The second step consists of generating an initial population of wing geometries at random. Then while the stopping condition has not been reached, the optimiser generates new candidate geometries in steps three and four respectively. In step five, each candidate geometry is evaluated by the aero-structural solver. These analyses provide the necessary information to compute the fitness function or functions in step six. If the problem is multi-objective the optimiser computes the Pareto fronts in step seven. The optimisation terminates if the stopping condition has been met in step eight.

4 EVOLUTIONARY OPTIMISER

4.1 EA FUNDAMENTALS

Evolutionary algorithms are design and optimisation algorithms which mimic the natural process of 'survival of the fittest' within a generation of candidate solutions. Broadly speaking EAs operate simply through the iterated mapping of one population of solutions to another population of solutions. This is in contrast with the conventional deterministic search techniques such as the simplex method, conjugate gradient method and others, which proceed from one given sub-optimal solution to another, until a converged optimum solution is reached. EAs are not deterministic, so that for identical problems and identical starting conditions, the evolution of the solution will not follow the same path on repeated applications. It is for this reason that EAs fall into the category of stochastic (randomised) optimisation methods. Some other stochastic methods that are used are the Monte-Carlo approach, the directed random walk and simulated annealing. The process of evolution in EAs is of course not completely random because in this case the performance of the algorithm would be no better than simple guessing, and at worst would be equivalent to complete enumeration of the parameter search space. Evolutionary algorithms work by exploiting population statistics to some greater or lesser extent, so that when newer individual solutions or offspring are generated from parents, some will have inferior characteristics and some will have superior characteristics. The general working principles of the iterated mapping then reduces to generating an offspring population, removing a certain number of inferior individuals, and obtaining the subsequent population. This can be summarised as the repeated application of two operators on the population, the first being the variation operator (the generation of offspring) and the second, the selection operator (the survival of the fittest) (Goldberg 1989)

The origin of evolutionary algorithms for parameter optimisation seems to have appeared independently in two separate streams, the Genetic Algorithm (GA) and the Evolution Strategy (ES). The Genetic Algorithm was founded on principles developed by Holland (Holland 1975), and has been extensively researched and applications developed. It is generally accepted however, that the modern GA was placed on its strong foundation in optimisation research by Goldberg (Goldberg 1989). His initial applications of the GA were in real-world topics such as gas pipeline control. The original GA technique revolved around a single binary string (or base - 2) encoding of the chromosomes, which is the genetic material each individual carries. The binary coded GA's variation operator is comprised of two parts, crossover and mutation. Crossover interchanges portions of parental chromosomes while mutation involves the random switching of letters in the chromosome. The selection operator has taken many forms, the most basic being the stochastic fitness-proportionate (or roulette wheel) method (Goldberg 1989).

Evolutionary techniques other than GA's and ES's exist, such as Evolutionary Programming (EP) and Genetic Programming (GP). Evolutionary Programming has been applied to real coded optimisation problems (Koza 1992) but has not seen widespread use in this field. For comparisons between ES and EP refer to Back (Bäck, Rudolph et al. 1993). Genetic Programming (Koza 1992) is devoted to the generation of computer programs rather than number sets as the solution to a given problem. Together with GA's and ES's these methodologies form the basic four 'schools' of evolutionary algorithms (GA, ES, EP and GP).

Evolution Strategies were first developed at the Technical University of Berlin, (Bäck, Rudolph et al. 1993). The first algorithm worked using only two individuals, one parent and one offspring. Each individual was real coded; each problem variable was assigned a floating point value in the chromosome. The variation operator involved applying a random mutation to each floating point value in the parental chromosome to arrive at the offspring individual. The selection operator was entirely deterministic, and was simply the result of a competition between parent and offspring to determine which one remained. In the standard nomenclature this strategy is denoted the (1+1) ES, the first digit indicating the number of parents, the ' + ' indicating competition between parents and offspring and the final digit indicating the number of offspring's. From the beginning the ES has been designed almost exclusively with real coding in mind, as opposed to original GA variants where real parameter optimisation comes about by the piecewise interpretation of the binary chromosome associated with each individual. An evolution strategy would therefore seem a logical starting point for evolutionary optimisation using real coded problem variables.

Subsequent developments in ES's introduced multi-membered populations, and the first algorithm of this type was the (μ+1) ES (Bäck and Schwefel 1995). This worked by applying some variation operator to μ parents to produce a single offspring. The offspring is selected by determining whether it is better than the worst member of μ^2, and if so it replaces the worst member μ. Both the (1+1) ES and the (μ+1) ES used deterministic control of the mutation size (variations applied to design variables) which were normally distributed when applied to real coded problems.

A pseudo code of a canonical evolution strategy is illustrated in Figure 3. A population (μ_0) is initialised and then evaluated. For a number of generations (g), and while a stopping condition (maximum number of function evaluation or target fitness value) is not yet met, offspring (λ^{g+1}) go recursively through the process of recombination, mutation, evaluation and selection.

Initialise: $init(\mu_o)$

Evaluate: $f(\mu_o)$

g=0

while stopping condition not met,

Recombine: $\lambda_R^{g+1} = reco(\mu^g)$

Mutate: $\lambda_M^{g+1} = mut(\lambda_R^{g+1})$

Evaluate: $\lambda^{g+1} = f(\lambda_M^{g+1})$

Select: $\mu^{g+1} = sel(\mu + \lambda)$ (Plus strategy) or,

$\mu^{g+1} = sel(\lambda)$ (Comma strategy)

g=g+1

loop

Figure 3: Label Canonical Evolution Strategy

The recent developments in both GAs and ESs have greatly modified their variation and selection operators, to the point where it is not clear whether such a nomenclature division is nowadays particularly justified. The main difference that exists between them today is still the predominance of adaptive mutations in ES's, which have made them very attractive for real coded optimisation, although GA research has produced some related concepts (Collard and Escazut 1995; Sefioui, Periaux et al. 1996; Thierens 2002)

Some of the advantages of EAs are that they require no derivatives or gradients of the objective function, have the capability of finding globally optimum solutions amongst many local optima, are easily executed in parallel and can be adapted to arbitrary solver codes without major modification. Another major advantage of EAs is that they can tackle multi-objective problems directly. EAs have been successfully applied to different aeronautical design problems and there have been different efforts to explore the benefits and capabilities of EAs for MDO, aircraft, wing, aerofoil and rotor blade design (Mäkinen 1998; Obayashi 1998; Sasaki 2004; Gonzalez 2005).

4.2 The Development of Evolutionary Algorithms for Design and Optimisation in Aeronautics

The potential benefits of EAs for optimisation problems in engineering have been recognised for some time. Different studies explore the potential benefits of EAs for wing design and optimisation (Obayashi 1998), (Oyama, Liou et al. September, 2002), (Oyama 2000). Obayashi, for example, has applied EAs for several wing platform design problems

In these studies, different niching and elitist models are applied to a Multi Objective Genetic Algorithm (MOGA) to find optimal Pareto fronts for transonic and supersonic wing design. The transonic case considered three (3) objectives: minimise aerodynamic drag, minimise aircraft weight and maximise fuel weight stored in the wing. The constraints imposed were lift greater than given aircraft weight and structural strength greater than aerodynamic loads.

Other applications of EAs for wing design include the work by Obayashi (Obayashi 1998) , (Anderson 1996; Takahashi 1997), (González, Whitney et al. 2004). Gonzalez, Whitney et al. (Gonzalez, Whitney et al. 2004) for example studied and illustrated the application of a hierarchical topology of EAs for multi-objective multidisciplinary wing design using low fidelity analysis tools. The main results of these studies indicate the importance of variable fidelity models, the broad applicability and the ability of EAs to find optimal Pareto solutions for three-dimensional applications and problems with more than two objectives.

Crispin (Crispin 1994) applied GAs for aircraft conceptual and preliminary design and found it useful to obtain reasonable and feasible solutions. Crossley et al (Crossley 1996) applied a GA for helicopter conceptual design and were able to show the effectiveness of GAs and obtain optimal feasible configurations. One of the results of his work was that the use of parametric variations conducted by GAs can significantly reduce the amount of time and money in the early stages of aircraft design.

Ruben et al. (Ruben and . 2000) conducted some work on GAs for aircraft conceptual design and found a 5% weight savings when compared to a conventional design. Ali and Behdinan (Ali 2002) applied GAs to determine an optimal combination of design variables for a medium-size transport aircraft. They studied different selection and crossover strategies and indicated that with a GA approach it was possible to generate feasible and efficient conceptual designs. In these studies, the authors also highlighted the effectiveness and importance of EAs in saving money in the initial stages of the design process.

Parmee and Watson (Parmee and Watson 1999) proposed a preliminary airframe design using co-evolutionary multi-objective genetic algorithms. Their algorithm was able to find local objective optimal solutions after a few generations and identify paths to trace the trade-off surface to some extent. This research also mentions that on-line sensitivity analysis has a role to play as the number of objectives increases and suggests that quicker, less detailed runs can easily be achieved using smaller population sizes.

Other applications of EAs for aircraft design include the work by Cvetkovick et al. (Cvetkovic 2000) and Raymer (Raymer 2002; Raymer 2003). Traditional transport or commercial aircraft have been studied and optimised using EAs. A few studies on the benefits of EAs in exploring large variations in the design space have been conducted for novel, non-notional configurations such as Unmanned Aerial Vehicles (UAVs/UCAVs) and Micro Aircraft Vehicles (Ng 2002), (González, Whitney et al. 2004), (Gonzalez, Whitney et al. 2004), (Whitney 2003).

All these works provide an indication of the broad applicability and robustness of Evolutionary Algorithms to find optimal solutions and how industry is increasingly applying them to solve complex problems in engineering.

Little work has been conducted on comparing the application of EAs and other methods for MDO. Raymer and Crossley (Raymer 2002; Raymer 2003) applied and compared different MDO methods, Monte Carlo, Random Walk, Simulated Annealing, GAs and orthogonal steepest descent search to enhance aircraft conceptual design and MDO. In his research Raymer applied these methods to four aircraft concepts: a fighter, a commercial airliner, an asymmetrical light twin and a tactical UAV showing a broad applicability of GAs. One of the conclusions of his work is that aircraft conceptual design can be improved by proper application of optimisation methods for MDO. He found that the proper selection of a technique can reduce the weight and cost of an aircraft concept by minor changes in the design variables. His results also indicate that the orthogonal steepest descent method provides a slightly better result with the same number of function evaluations, but, as the number of variables is increased, the evolutionary methods seem to be superior. It should be noted that Raymer limited his research to single-objective problems, used only one type of fidelity model for the aircraft analysis and limited his research to seven design variables and the inclusion of any propulsion variables other than engine size via Thrust/Weight.

4.3 ADVANTAGES AND LIMITATIONS OF TRADITIONAL EAS FOR AERONAUTICAL PROBLEMS

Even though there are definite advantages to using EAs they have not seen a widespread use in industry or for multidisciplinary design optimisation applications. The main reason for this is the computational expense involved, as they require more function evaluations than gradient-based methods. Therefore, the continuing challenge has been to improve their performance and develop new numerical techniques.

It is clear that a possible and realistic avenue is the application of robust and efficient evolutionary methods for MDO. One of the viable alternatives is the Hierarchical Asynchronous Parallel Multi-Objective Evolutionary Algorithms (HAPMOEA) described in the next section. These algorithms have proven to be robust and will be extended in this research for multi-objective and multidisciplinary design optimisation problems in aeronautics.

4.4 HIERARCHICAL ASYNCHRONOUS PARALLEL MULTI-OBJECTIVE EVOLUTIONARY ALGORITHMS

One drawback of EAs is that they are slow to converge in that they require a large number of function evaluations to refine the global optimum position once found. Gradient based optimisation techniques do not suffer from this problem. Furthermore, a EAs performance decreases as the number of variables increase. Hence the continuing challenge with EAs has been to develop robust and fast numerical techniques to overcome these known difficulties and facilitate the complex task of design and optimisation in aeronautics. In this direction we developed and use the Hierarchical Asynchronous Parallel Evolutionary Algorithm (HAPMOEA) approach (Whitney, Sefrioui et al. 2002; Gonzalez 2005; Gonzalez 2005) with some extensions for Multi-Disciplinary and Multi-Objective analysis introduced recently. The foundations of the algorithm lie upon traditional evolution strategies and incorporate the concepts of covariance matrix adaptation (CMA) (Hansen and Ostermeier 2001), multi-objective optimisation, hierarchical topology, parallel computing (parallel EAs) and asynchronous evaluation of candidate solutions, Pareto tournament selection for single and multi-objective problems and a constraint handling mechanism.

4.4.1 MULTI-CRITERIA OPTIMISATION

Often aeronautical design problems require a simultaneous optimisation of conflicting objectives and associated number of constraints. Unlike single objective optimisation problems, the solution is a set of points known as Pareto optimal set. Solutions are compared to other solutions using the concept of Pareto dominance. A multi-criteria optimisation problem can be formulated as:

$$\begin{aligned} &\textit{Maximise} / \textit{Minimise} \\ &f_i(x)_i = 1,.....,N \\ &\textit{Subject to constraints}: \\ &g_j(x) = 0 \quad j = 1,.....,M \\ &h_k(x) \le 0 \quad k = 1,.....,M \end{aligned}$$

Where f_i are the objective functions, N is the number of objectives; x is an n – dimensional vector where its arguments are the decision variables. For a minimisation problem, a vector x_1 is said partially less than vector x_2 if:

$$\forall_i f_i(x_1) \le f_i(x_2) \text{ and } \exists_i f_i(x_1) \le f_i(x_2)$$

In this case the solution x_1 dominates the solution x_2.

Figure 4 shows Pareto optimality for a two objective problem. The objective of the optimisation is then to provide a set of Pareto optimal solutions that represent a trade-off of information amongst the objectives.

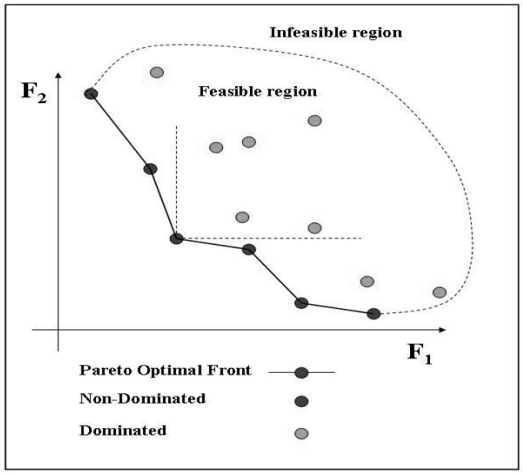

Figure 4: Pareto Optimality

As EAs evaluate multiple populations of solution points, they are capable of finding a number of solutions in a Pareto set. Pareto selection ranks the population and selects the non-dominated individuals for the Pareto fronts. An Evolutionary Algorithm that has capabilities for Multi-Objective optimisation is termed Multi-Objective Evolution Algorithms (MOEAs). Theory and applications of MOEAs can be found in Deb (Deb 2003) and Coello-Coello et al (Coello, Veldhuizen et al. 2002).

4.4.2 HIERARCHICAL POPULATION TOPOLOGY

A hierarchical population topology, when integrated into an evolution algorithm, means that a number of separate populations are established in a hierarchical layout to solve the given problem, rather than a single 'cure-all' type single population layout. This method was proposed by Sefrioui (Sefrioui and Périaux 2000) and is shown in Figure 5. The bottom layer can be entirely devoted to exploration, the intermediate layer is a compromise between exploitation and exploration and the top layer concentrates on promising solutions.

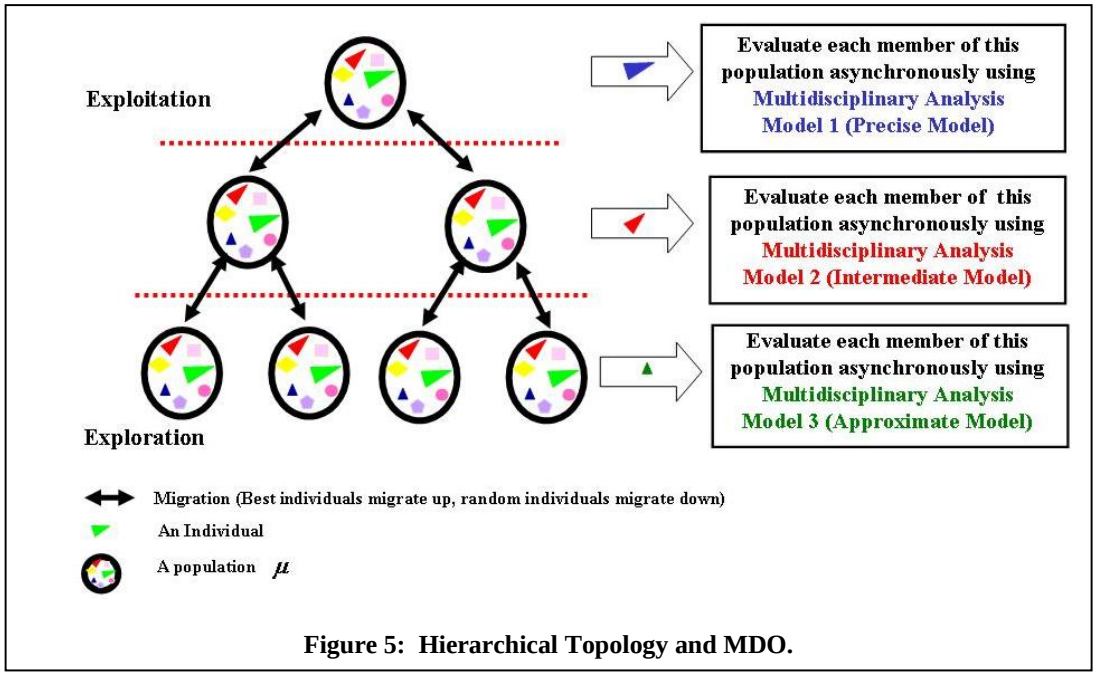

Figure 5: Hierarchical Topology and MDO.

4.4.3 Parallelisation Of The Algorithm

The algorithm is similar to hybrid parallel Multi-Objective Evolutionary Algorithms (pMOEA) (Cantu-Paz 2000; Veldhuizen, Zydallis et al. 2003); it uses a master slave approach but incorporates the concept of isolation and migration through a hierarchical binary tree structure where each level has different parameters for the MOEAs . The parallel environment used in this work is a cluster of PCs, wherein the master carries on the optimisation process while remote nodes perform the analysis (CFD, FEA). The message-passing model used is the Parallel Virtual Machine (PVM) (Geist, Beguelin et al. 1994). The algorithm has been tested in a cluster of heterogeneous CPUs available at the School of Aerospace, Mechanical and Mechatronic Engineering at the University of Sydney and with different RAMs frequencies, caches, memory access times, storage capabilities and communication attributes. The cluster can be configured with up to 18 machines with performances varying between 2.0 and 3.4 GHz.

4.4.4 Asynchronous Evaluation

When considering the solution to Multi-objective and Multidisciplinary Optimisation cases, several problems arise as many methods of solution used in engineering today may take different times to complete their operation. The classic example of this is the modern CFD solver. With a typical industrial code used for external aerodynamic analysis of airplanes, the time for the residual of the solution to converge to a specified level (either machine zero or an arbitrarily selected higher value) can vary over a significant range depending on the geometry, boundary condition, the algorithm and CPU used. The previous generation of evolutionary algorithms have mostly used a generation-based approach and so are the traditional genetic algorithm and evolution strategy. A difficulty with generational models is that they may create an unnecessary bottleneck when used on parallel computers. If the population size is approximately equal to the number of processors, and most of the candidate offspring's that are sent for solution can be successfully evaluated, it may so happen that some processors will complete their task quicker with the remainder taking more time. With a generational approach, those processors that have already completed their solutions will remain idle until all processors have completed their work.

The approach used here is to ignore any concept of a generation based solution and is similar to work by Wakunda and Zell (Wakunda and Zell 2002) and other non-generational approaches. The difference is that the selection operator couples a one-by-one (steady-state) function evaluation with a direct multi-objective fitness criterion. Whilst a parent population exists, offspring are not sent as a complete 'block' space to the parallel slaves for solution. Instead one candidate is generated at a time, and is sent to any idle processor where it is evaluated at its own speed. When candidates have been evaluated, they are returned to the optimiser and either accepted by insertion into the main population or rejected. This requires a new selection operator because the offspring cannot now be compared one against the other, or even against the main population due to the variable-time evaluation. The recently evaluated offspring are compared against a previously established rolling-benchmark and if successful, replace (according to some rule) a pre-existing individual in the population. This benchmarking is implemented via a separate evaluation buffer (*B*), which provides a statistical 'background check' on the comparative fitness of the solution. The length of the buffer should represent a reasonable statistical sample size, but need not be too large; approximately twice the population size is more than ample. When an individual has had a fitness assigned, it is then compared to past individuals (both accepted and rejected) to determine whether or not it should be inserted into the main population. If it is to be accepted, then some replacement strategy is invoked and it replaces a member of the main population. The replace-worst-always method is exclusively used in this work. A schematic of the asynchronous and parallelization approach is shown in Figure 5

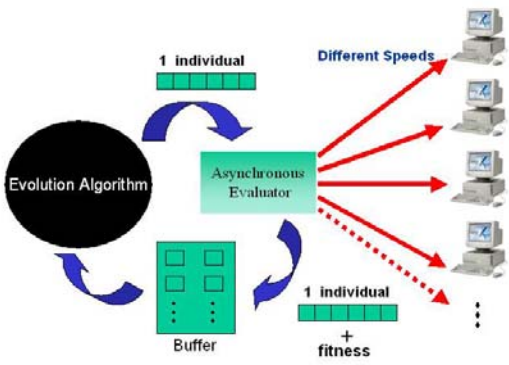

Figure 6: Parallel Computing and Asynchronous Evaluation

4.4.5 PARETO TOURNAMENT SELECTION

An on-the-fly selection operator is implemented by means of a Pareto tournament selection operator. To implement an optimisation algorithm that is equally applicable to both single and multi-objective problems, a suitable selection operator capable of handling either situation must be developed. An extension of the standard tournament operator popular in many approaches is proposed (Goldberg 1989; Michalewicz 1992). Most evolutionary algorithms configured for multi-objective optimisation currently use the non-dominated sorting approach. This is a straightforward way to adapt an algorithm that is designed as a single objective optimiser into a multi-objective optimiser, and is used by many researchers (Michalewicz 1992; Deb 2003)]. The problem with sorting approaches is that the method is not a fully integrated one. Briefly, a sorting method works by computing the set of non-dominated solutions amongst a large statistical sampling (either a large population or previous data), and assigning these solutions a rank one. Then ignoring these points, the process is repeated until a 'second' Pareto front is found, and this is assigned rank two. This process continues until all points are ranked, and then the value of the rank is assigned to the individual as a new single objective fitness. A problem arises now on whether it is fair to assign individuals in the second rank numerically half the fitness of the first, and whether the third rank deserves a third of the fitness of the first. This poses a dilemma regarding the level of equality present amongst the solutions, as often solutions

with excellent information may lie adjacent to, but not in, rank one. To solve this 'artificial scaling' problem, it is possible to introduce scaling, sharing and niching schemes, however all of these require problem-specific parameters or knowledge, even in adaptive approaches. It is of course always desirable to compose an algorithm that does not introduce such unnecessary parameters.

The current operator is a novel approach in that it requires no additional 'tuning' parameters, works seamlessly with the asynchronous selection buffer (B), and is very easy to encode. As illustrated in Figure 7 to determine whether a new individual x is to be accepted into the main population, we compare it with the selection buffer by assembling a small subset of the buffer called the tournament $Q = [q_1,q_2,...,q_n]$. We assemble Q by selecting individuals from the buffer, exclusively at random, until it is full. We then simply ensure that the new individual is not dominated by any in the tournament. If this is the case, then it is immediately accepted, and is inserted according to the replacement rules. The only parameter that needs to be determined in advance is the tournament size, a parameter that would exist in a single objective optimisation anyway. Selection of this parameter requires a small amount of problem specific knowledge, and should vary between $Q = B/2$ (strong selective pressure) and $Q = B/6$ (weak selective pressure). The optimiser is not overly sensitive to this value, provided the user errs on the side of weak selective pressure (smaller tournaments) in the absence of better information. The egalitarian approach to the tournament (by selecting individuals at random) ensures good diversity amongst the selected individuals; no niching or forced separation of individuals has been found necessary. It can also be seen that in the event the fitness vectors have only one element (a single objective optimisation), this operator simplifies to the standard tournament selection operator (Goldberg 1989; Michalewicz 1992).

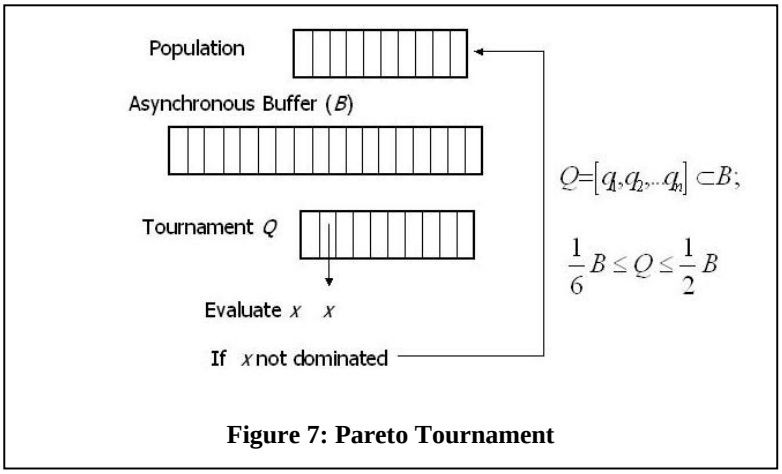

Figure 7: Pareto Tournament

5 AERO-STRUCTURAL ANALYSIS

5.1 INTRODUCTION

This section describes the aero-structural solver in detail. Sectio 5.1 describes the aero-structural program layout, section 5.2 details the validation of the aerodynamic solver while section 5.3 describes the structural model and analysis. Section 5.4 details the aero-structural analysis and results for two baseline geometries.

5.2 AERO-STRUCTURAL PROGRAM LAYOUT

A program to perform the aero-structural optimization was written in Matlab®. The aero structural solver program integrates two commercial analysis tools for Finite Element Analysis (FEA) and Computational Fluid Dynamics (CFD) namely MSC.Nastran®, developed by MSC Software, PANAIR, a high order Mornio class panel method developed by Boeing and, FRICTION to calculate the form and frictional drag about a candidate wing. The entire aero-structural program is controlled through a Matlab® script file. This allows for an easy coupling of the different required programs as one continuous Matlab® data structure can be utilized to define all the information passed between programs. A flow diagram of this process is illustrated in Figure 8. A description of the aerodynamic and structural analysis tools is given, followed by a general description of the validation cases.

The aero-structural program works in a very structured way as shown in Figure 8. On execution of the code, the workspace is cleared of any existing variables and any output files from previous program runs which may have existed in the working directory. The program loads in any user or optimiser specified inputs through the calling of the user generated input files.

Once loaded, the Aero-Structural program performs a number of geometry checks on the candidate wing and then creates the wing shape from the user specified inputs. From this output the FRICTION, PANAIR and MSC.Nastran® input files are created and executed. After running the PANAIR simulation, the aerodynamic loads are read in from the PANAIR output files and mapped to the MSC.Nastran® simulation.

Once again the candidate wing is tested but this time it is to see whether or not the wing violates any penalty function to do with the aerodynamics or structures. Thereafter an output file containing the simulation results is produced.

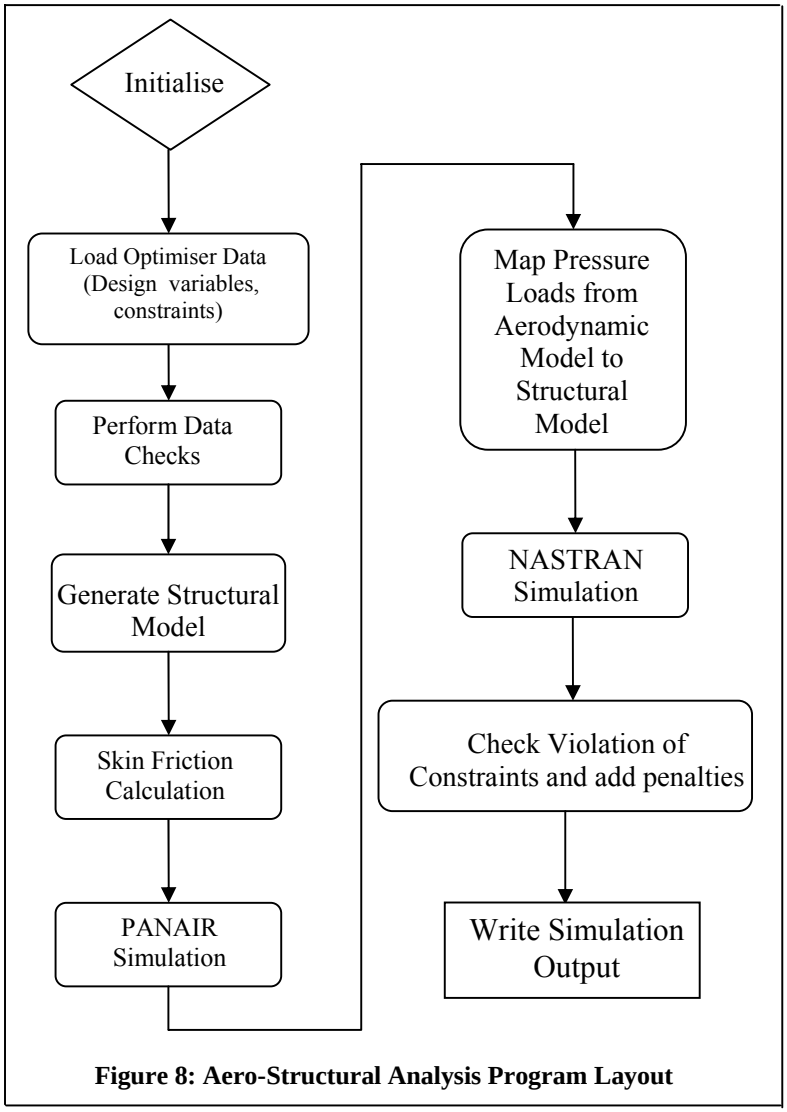

Figure 8: Aero-Structural Analysis Program Layout

If an unrecoverable error is encountered anywhere in the solution sequence, the aero-structural solver is able to recover and generate a simulation output file which indicates to the evolutionary optimiser that the solution failed.

5.1.1 INPUT FILES

The Aero-Structural solver loads in information describing the wing from two user defined sources. The first source is through the variables defined in the '*UserWing.m*' and "*UserAuxiliaryData.m*" files. This is the most common and simplest method used when only performing a single run of the Aero-Structural solver. When coupled to the Evolutionary Optimiser, a different method is used.

The loading in of Evolutionary Optimiser input variables to PANAIR is performed by a number of functions written in Matlab®. The functions have the ability to load in the variables. Four output files are used depending on the types of variables being passed to the aero-structural solver. Each file contains different information relating to the wing. The four different types of input files are used by the Aero-Structural Solver are:

- Planform data (*planformVariables.XX*)
- Auxiliary data (*auxiliaryVariables.XX*)
- Aerodynamics (*aerofoilsData.XX*)
- Structural data (*structuralVariables.XX*)

These files are simple comma separated value files describing each variable passed to the optimiser.

Planform data includes crank locations, sweep angles, etc. Auxiliary data handles the different flow conditions such as Mach number and angle of attack. Aerodynamics simply contains the different aerofoil shapes as *x* and *y* columns corresponding to the aerofoil sections at the root, tip and crank positions. The structural data has the thickness of the different elements making up the aircraft wing.

5.1.2 OUTPUT FILES

The Aero-Structural Solver creates two output files. The first file contains a simple indication as to whether or not the Aero-Structural Analysis Program simulation had terminated successfully, the second, if the termination was successful, contains the aerodynamic and structural results from the simulation.

To indicate whether or not the simulation had terminated successfully (there were no critical errors requiring Matlab® to unexpectedly return command to the command prompt), a convergence file '*convergence.txt*' is created with either a zero (0), (no errors and hence the results file was created) or a one (1) to indicate errors within the program.

If the aero-structural solver is able to run all the required simulations on a candidate wing, a results file is written. This results file has a simple header which is a legend into the remaining lines in the file. The legend describes what the value in the file corresponds to, be it the induced drag calculated by PANAIR, friction drag calculated by FRICTION, penalties the wing has been penalized with or the structural deflections. If the aero-structural is unable to calculate any value due to a recoverable error such as the MSC.Nastran® simulation failing, the affected results are indicated by a hash symbol (#).

5.1.3 AUTOMATIC WING GEOMETRY GENERATION

The aerodynamic and structural wing models are created though an automatic geometry modeller developed for this task ('*MatDef.m*'). The aerodynamic model is created first and provided the body from which the structural model is created.

After all the input data checks are performed, the aerodynamic model is built in sections. Each section is made up of the area between cranks as is shown in Figure 9. The first section constructed is between the root and intermediate crank and the second section is constructed between the intermediate and tip crank.

Matrix operations are used to define the initial layout of the section and take into account sweep and taper ratios. All sweep angles are defined relative to the global *XY* frame defined according to normal aircraft convention. The aerofoil shapes at the intermediate rib locations are determined through a linear interpolation of the aerofoils defined at each section boundary.

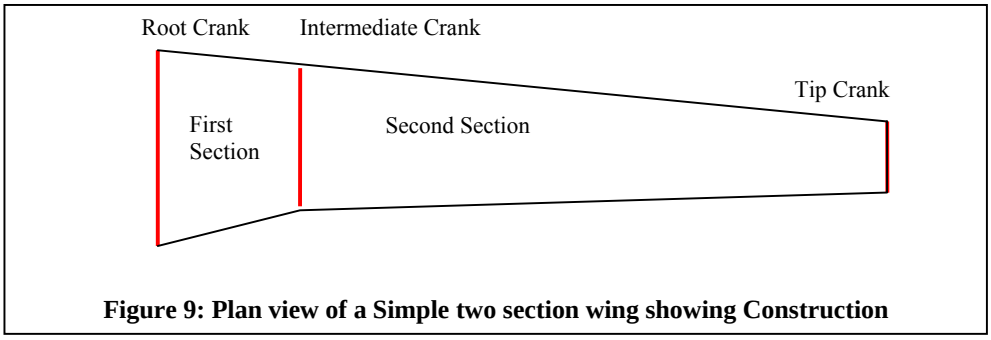

Figure 9: Plan view of a Simple two section wing showing Construction

Once all the sections have been created, the entire wing is defined through the amalgamation of all the computed sections.

As mentioned above, the structural model is extracted from the aerodynamic model. As all the cranks are defined according to the internal structure, this operation is easily performed.

Along with the external definition, when constructing the structural model, the automatic geometry modeller computes the location of all the Spar and Rib Caps.

5.1.4 Automatic Certification Of The Wing Geometry

Sometimes a random combination of number of cranks, chord ratios, sweep angles, etc or material properties can result in a physically unfeasible geometry. The Aero-Structural Analysis Program therefore has a number of internal checks to validate the data that is passed to it.

Structures

The material data defined in the '*MaterialProperties.m*' file is analysed to check if enough information is provided. Furthermore, the program determines which variable is missing data for certain crank locations and either replicates data, or if many variables are missing data, remove data from variables such that a common denominator is found.

Geometry

Two simple geometry checks are performed on the wing before any aerodynamic or structural analysis is performed. The first check ascertains whether or not the wing upper and lower surfaces intersect each other (Figure 10 a-Crossing), and the second check ascertains if the leading and trailing edges intersect (Figure 10 b–Switching). If either of these checks fails, the simulation is aborted.

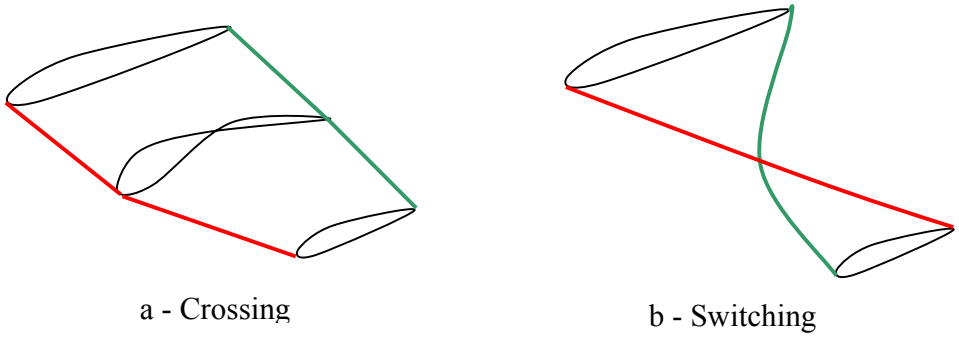

Figure 10: Geometry Checks performed by the Aero-Structural Analysis Program

Once both the data checks and basic geometry checks have been performed, The Aero-Structural Analysis Program checks to see if any of the data defining the internal layout of the wing will cause errors later in the simulation steps. Errors can be caused by a wing rib being referenced by two crank locations. This can be caused by the method in which the ribs are linearly spaced throughout the wing and the crank locations are rounded up or down to the nearest rib as in Figure 11. This above mentioned case can cause modelling problems and hence one of the sets of data defining one of the crank locations would have to be removed.

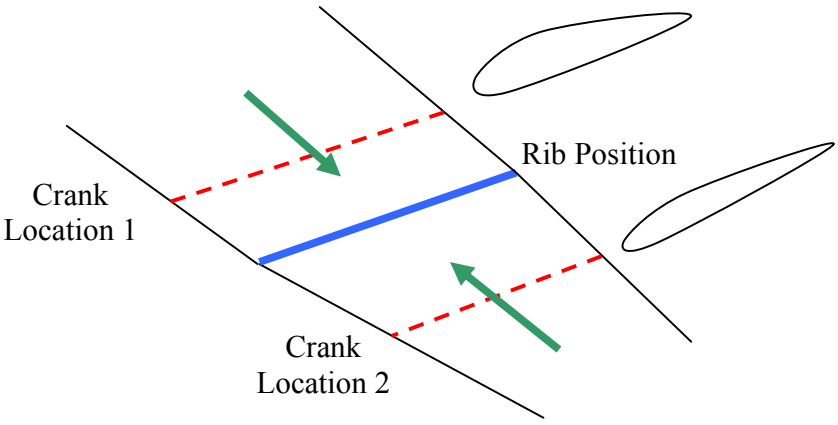

Figure 11: Errors relating to Internal Structure

This removal process is carried out by deleting the data defining the more outboard of the two or more data sets and retaining the inboard.

5.2 Aerodynamic Analysis

A proper selection and validation of analysis tools is required before coupling it with an optimisation process. A flow solver should meet some essential requirements such as: result accuracy, computational expense and robustness.

It is always desirable to use a high fidelity solver that can account for the flow complexities. The problem of using a full Navier-Stokes solver is the computational expense of the solution as one computation on a full 3 dimensional wing might take several hours on a supercomputer. Therefore, to reduce this expense it was necessary to find another high fidelity method which could yield accurate results at a minimum computational cost. It was for the above reason why the authors chose to use a high-order Morino class panel method code called PANAIR to solve for the flow properties about the arbitrary vehicle wing. PANAIR only calculates the Induced drag component produced by the wing as it travels through the air. Hence to correctly predict the total drag produced by the wing, both the Form and Friction components need to be calculated; for this task FRICTION (Mason 2001) was used.

5.2.1 High Order Panel Method (PANAIR)

The higher order panel method PANAIR was developed by Boeing as A502 to predict subsonic and supersonic linearised potential flows about an arbitrary geometry (Saaris 1992). PANAIR differs from earlier panel methods by employing a “higher order” panel method; that is, the singularity strengths are not constant on each panel. PANAIR has the ability to analyse arbitrary geometry, and this ability, along with the ease with which models could be created and results read through input and output files, greatly influenced the decision to select it as the flow solver to utilise in the simulations and coupling with the optimiser. To simplify the construction of PANAIR input files, MAKEWGS converts the set of data points

describing the external shape of the wing into the Langley Wire Frame Geometry Standard (WGS) (Craidon 1985) and a second program, PANIN, combines the MAKEWGS file with an auxiliary file to generate the complete PANAIR input file. The flow conditions contained in the auxiliary file are the altitude, angle of attack and reference data for the wing.

The output from PANAIR contains the calculated pressures and corresponding forces and moments about the simulated geometry. The outputted second order pressure coefficients were selected as they are the preferred ones for further analysis (Saaris 1992).

PANAIR seeks to solve the potential flow equation. This equation is a combination of the continuity equation, momentum and speed of sound equations, subject to certain conditions such as the flow being irrotational. After considerable mathematical rearrangement, these equations can be written as:

$$\left(1-M_\infty^2\right)\frac{\partial u}{\partial x}+\frac{\partial v}{\partial y}+\frac{\partial w}{\partial z}=M_\infty^2\left(1+\frac{\gamma-1}{2}M_\infty^2\right)\frac{2u'}{U_\infty}\frac{\partial u}{\partial x} \tag{1}$$

This equation can be written in terms of the perturbation velocities, (Eqn 2) .The right hand side term is often neglected as it is of second order in the perturbation components.

$$\left(1-M_\infty^2\right)\frac{\partial u'}{\partial x}+\frac{\partial v'}{\partial y}+\frac{\partial w'}{\partial z}=0 \tag{2}$$

By bringing in the velocity potential we have:

$$\begin{aligned} u' &= \frac{\partial \phi}{\partial x} \\ v' &= \frac{\partial \phi}{\partial y} \\ w' &= \frac{\partial \phi}{\partial z} \end{aligned} \tag{3}$$

Consequently,

$$\left(1-M_\infty^2\right)\phi_{xx}+\phi_{yy}+\phi_{zz}=0 \tag{4}$$

PANAIR solves these equations and uses a fully continuous quadratic doublet, and linear source distribution along both the span and chord-wise directions.

Complete derivation of Eqn 4 can be found in Bertin (Bertin 2002).

In PANAIR, for a panel solution to be found about an arbitrary configuration the wing or similar object must be closed, i.e. there are no gaps in the model. This means that for the simulations performed, the wing described has to be mirrored about the XZ plane such that it made a complete 'flying wing'. Although this model description would not yield the same results as if the wing were attached to a fuselage, it was concluded that for ease of simulation, this method would be chosen.

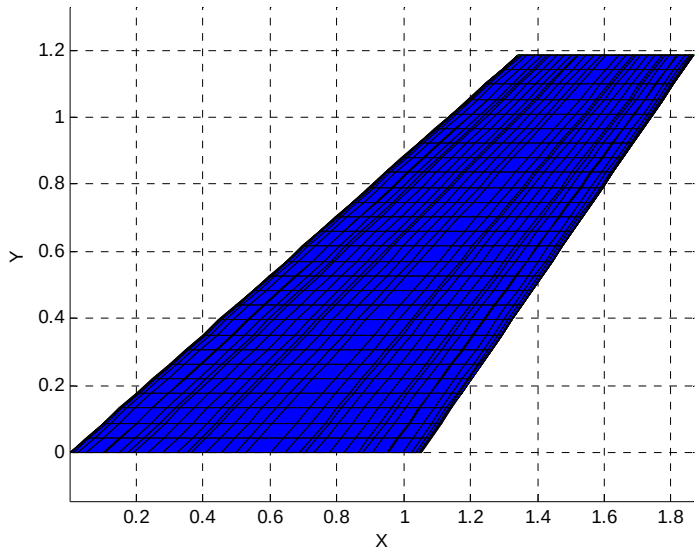

Figure 12: External Surface Elements Generated for PANAIR Calculations

Figure 12 shows the upper surface of the aerodynamic model of the wing. For all the simulations performed, the authors modelled the wings reflected about the *XZ* plane with a full outer skin along the upper and lower surfaces of the wing, and a straight wing tip. The wing tip panels are plotted in Figure 13.

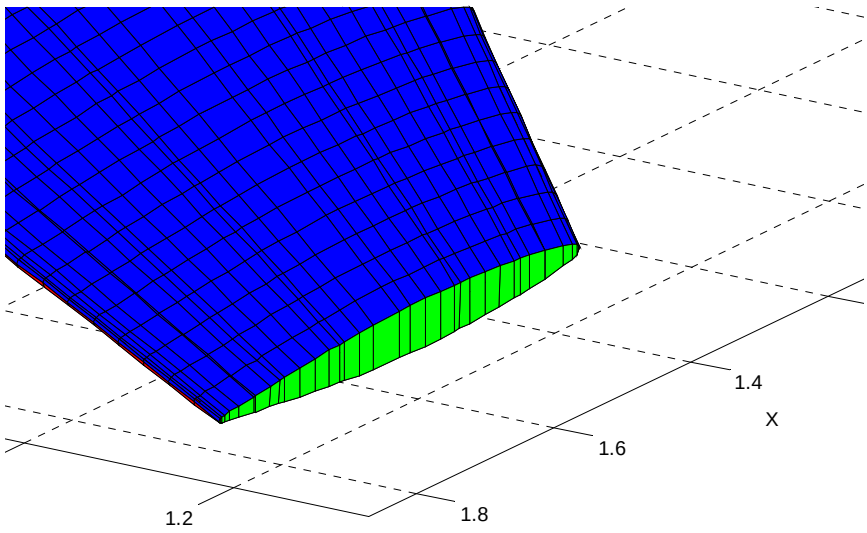

Figure 13: Wing Tip elements used in PANAIR model

A wake is automatically attached to the trailing edge of the wing by PANAIR.

5.2.2 VALIDATION OF PANAIR

Before coupling PANAIR with the optimiser, the program was validated against experimental wind tunnel data and results published by Margason, et al (Margason, Kjelgaard et al.). The test case considers the 45° swept back wing operating at $M_\infty = 0.6$ and at an angle of attack $\alpha = 6.3$ deg.

Along the leading and trailing edges, the panel sizes increased exponentially for the first ten percent of the chord, and then remained at a constant size for the remaining eighty percent. Through experimentation, this was found to yield the best result for the lowest computational cost.

Results

The CPU time for this aerodynamic computation was 12 minutes on a single Pentium 4 2.4 GHz processor.

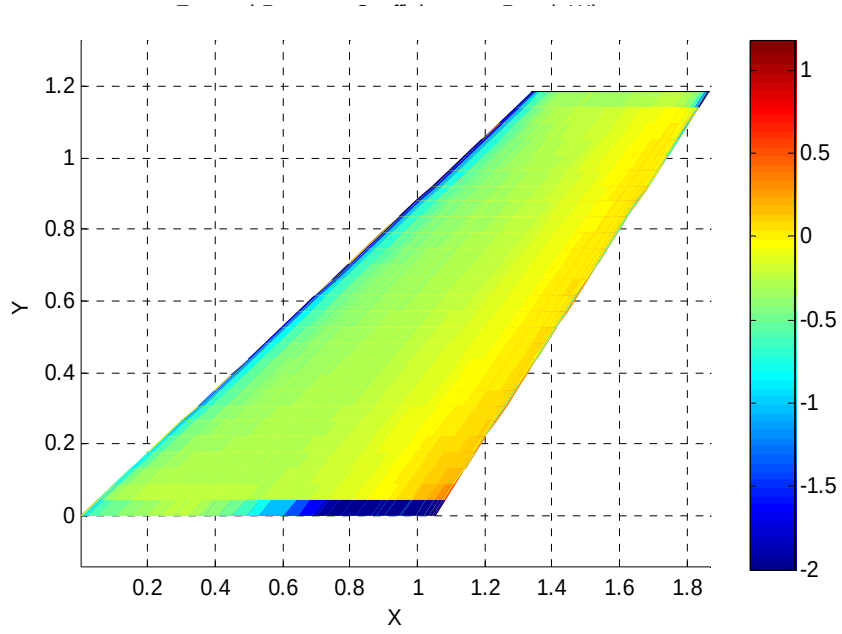

Figure 14: Pressure Coefficients about the Lower Surface of the Test Section

The graded coefficients of pressure distribution for the upper and lower surfaces are shown in Figures 14 and 15

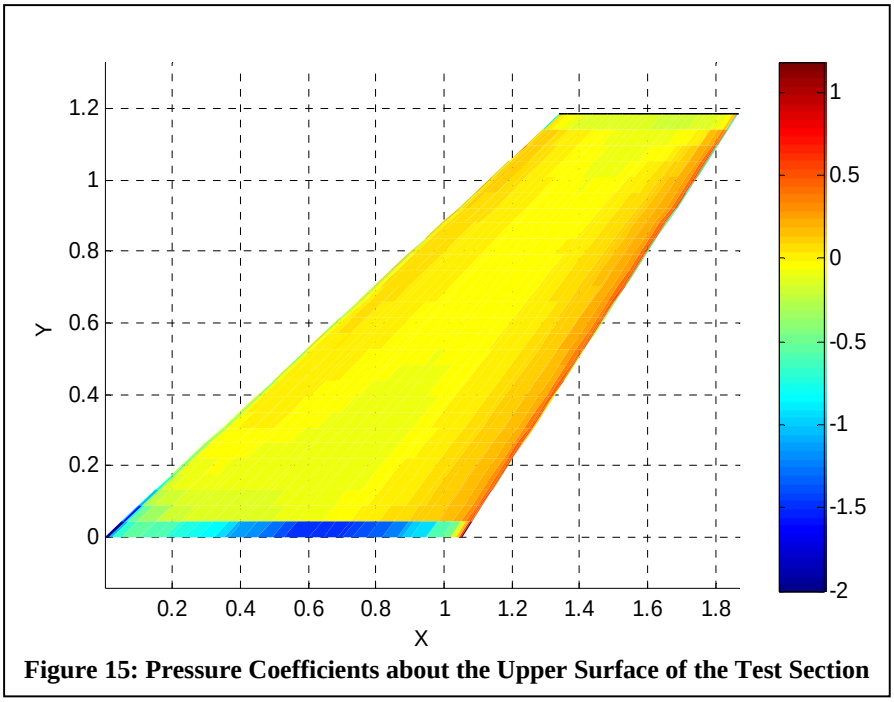

Figure 15: Pressure Coefficients about the Upper Surface of the Test Section

Figures 16 and 17 show the second order pressure coefficient distributions at two span-wise stations as calculated by PANAIR. The results from the fifty five percent span locations are shown in Figure 16. As indicated in this figure, the results attained are in close agreement with the experimental results reported in References (Kolbe and Boltz 1951) and (Margason, Kjelgaard et al.).

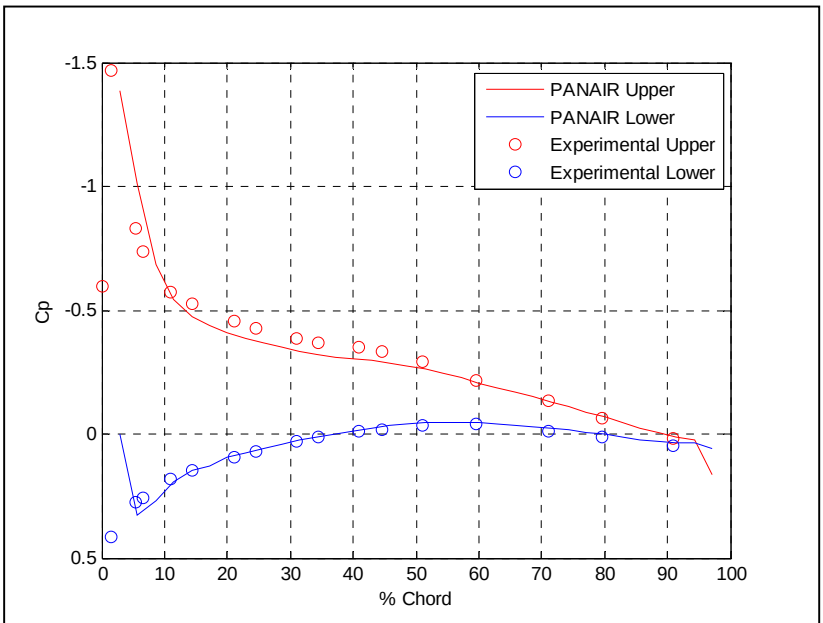

Figure 16: Pressure Distribution at 55% semi-span.

Figure 17 shows the results at 8 % span. The discrepancy between experimental and PANAIR results close to the wing root is due to a mismatch in the Kutta condition. This is due to the set up and execution of PANAIR where the Kutta condition is automatically imposed on the boundary with the trailing wing wake.

This resulted in an incorrect Kutta condition at the root chord and hence the condition of the upper pressures equalling the lower pressures, as should be found on the leading and trailing edges, was not correctly realised. Further along the wing, the Kutta condition is met as can be seen from Figure 16.

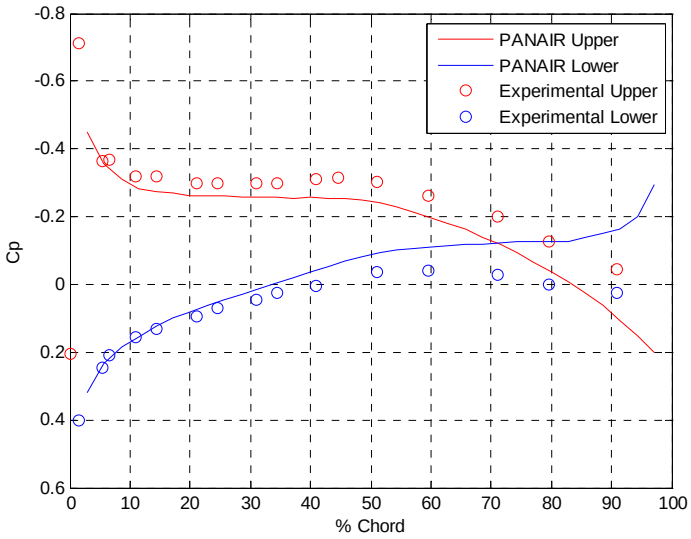

Figure 17: Pressure Distribution near Wing Root

Concluding the validation study, it is shown that the results obtained by PANAIR are in good agreement with experimental data. PANAIR has capabilities to provide accurate results for different arbitrary geometries and solve the aerodynamic characteristics on 3D wings. PANAIR provides some advantages over more complex Navier-Stokes solvers:

- good accuracy even considering the linearilised flow assumption
- a reduction in computational expense.

The computational time for a single PANAIR calculation varied between two and twelve minutes for an arbitrary wing on a Pentium 4, 2.4 GHz machine. The time taken was dependant on the number of discritised surface panels used to model each wing. In contrast, a full Navier Stokes solution takes in the order of several hours. Therefore, the aerodynamic solver has the capability to accurately model the flow about arbitrary geometries and is included in the aero structural algorithm and overall program coupling with the optimiser.

5.2.3 FRICTION

As mentioned in previous section, the program FRICTION is used to estimate the Form and Friction drag produced by the wing at the simulation conditions.

Form drag is drag due to the geometry of the wing being analysed and is influenced by the frontal area of the wing (*t/c* ratio).

Friction drag is drag due to the movement of air molecules along the wing surface which lead to the creation of boundary layers. If the boundary layer is laminar, momentum and energy are only mixed between neighbouring layers in the flow and on a microscopic level; hence the friction drag is small. As the boundary layer becomes turbulent and the mixing between sections of the boundary layer occurs on a macroscopic level, the friction drag can be many times larger than that for a laminar boundary layer.

FRICTION calculates the laminar boundary layer friction coefficient through the use of the standard Blasius formula (Eqn 5) with the inclusion of the Chapman-Rubesin constant C^*.

$$C_f = \frac{0.664\sqrt{C^*}}{\sqrt{\mathrm{Re}_x}} \tag{5}$$

The turbulent boundary layer is calculated through the use of the van Driest II method. For a full details on the method employed when calculating the turbulent boundary layer, refer to Bertin (Bertin 2002).

Assumptions

In the simulation process it is assumed that fifty percent of the wing was turbulent, and the remainder laminar. This was set as an assumption and kept for all simulations as smooth graphite epoxy has a very low roughness value, even though this value would vary between simulated wings in real life. The value of fifty percent chord was selected after consulting pictures of ribbon experiments performed on numerous aircraft wings (Bertin 2002).

5.3 STRUCTURAL ANALYSIS

The structural analysis is conducted using MSC.Nastran®, a modular Finite Element Analysis (FEA) software package written by MSC.Software®. MSC.Nastran® has modules for heat transfer, dynamics, spot welding, aero-elasticity, and nonlinear analyses.

In this work, the operation of MSC.Nastran® was done through the use of the Bulk Data File (BDF) input method. For the simulations SOL 106 was used which defines the Nonlinear Static analysis. This method was chosen over SOL 101, Linear Static as it was expected that some of the wing geometries defined would undergo large deflections and or large strains. It was therefore necessary to correctly determine structural forces formed and hence the Nonlinear Static solution method, as described in Section 5.3.3, was chosen.

5.3.1 STRUCTURAL MODEL AND CONSTRAINTS

For the structural analysis, a simplified finite element model constructed from a varying number of ribs and spars was used. The majority of the structural model was assembled using shell elements with the spar and rib caps modelled as rod elements. The number of nodes and elements and hence degrees of freedom (DOF) varied depending on the internal wing structure. A sample finite element model is illustrated in Figure 18 and 19.

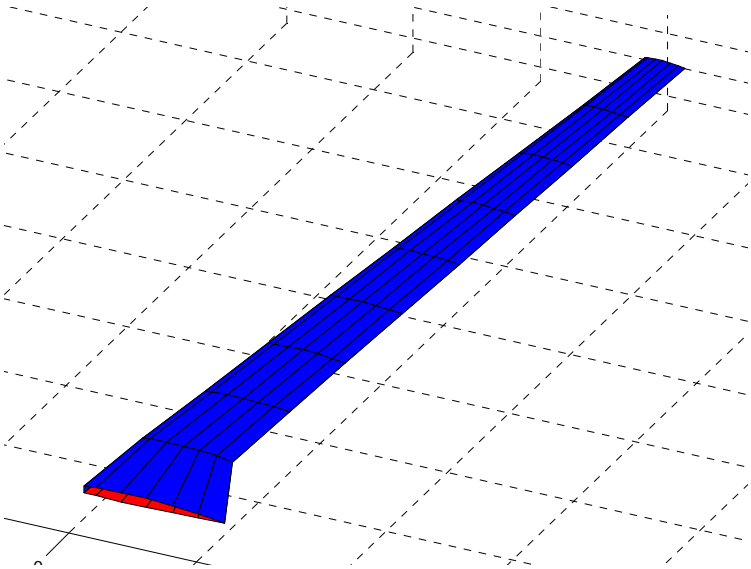

Figure 18: Structural finite element model used in MSC.Nastran (Upper surface panels – blue, Lower surface panels– red)

The different components making up each candidate wing, namely spars, ribs, wing skin and spar and rib caps, are described in more detail below.

Spars

The Spars were linearly distributed over the chord depending on their number. This greatly reduced the number of variables in the simulation, but did not necessarily yield the optimal result for any given number of spars.

The thicknesses of the Spars were modelled to decrease according to a parabolic function as a function of the span. This modelling method allowed the optimizer the ability to define thicknesses that varied at a constant rate down the span to Spar thickness which varied parabolically increasing the scope of the optimization solution.

Each spar was broken down into sections. The sections were defined as the distance between consecutive ribs and this allowed for a minimum of MSC.Nastran® structural elements to be used when defining the overall structure as shown in Figure 19.

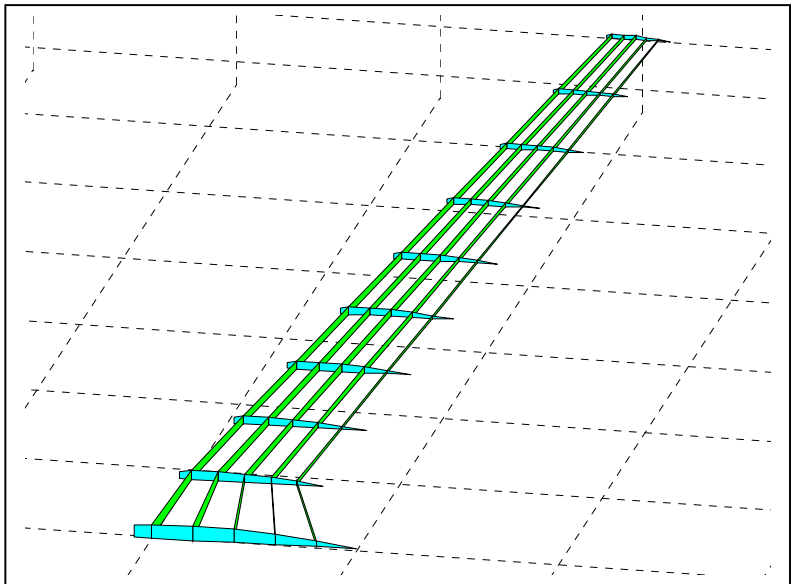

Figure 19: Wing Spars (Green) and Ribs (Light Blue)

As per recommendations by Marisarla (Marisarla 2005), the number of spar element sections never decreased below 8. This allowed for the correct modelling of nonlinear element bending with sufficient accuracy.

Ribs

As with the Spars, the Ribs were also broken down into sections. The sections were defined from the leading edge to the first spar, between consecutive spars if they existed and then from the trailing edge spar to the wing trailing edge.

The Rib thickness was also varied according to a parabolic function in a similar manner as to the Spar thicknesses.

As the rounded shape of the leading edge provides additional torsional support in the structure, the leading edge section of each rib was modelled using a quadrilateral element as in Figure 20. Furthermore, the trailing edge section was modelled using a triangular element to retain the correct structural modelling as shown in Figure 21.

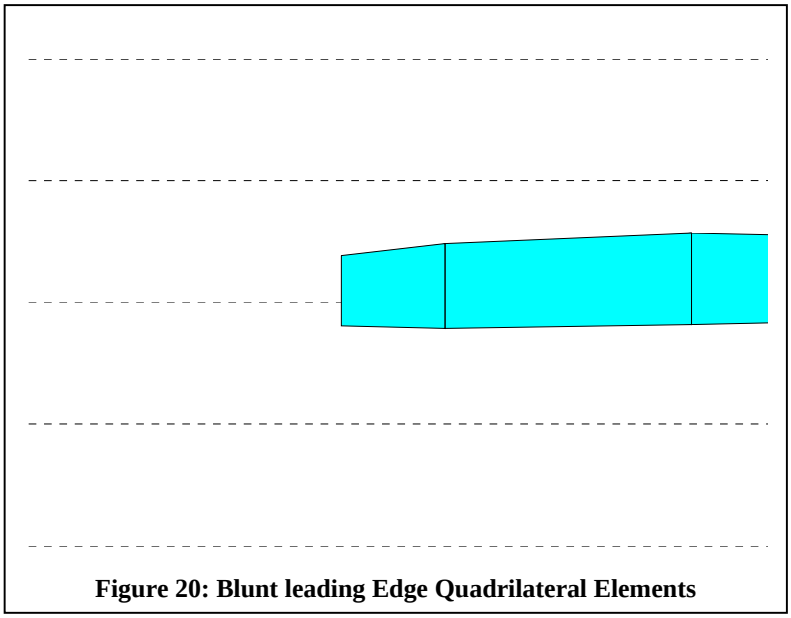

Figure 20: Blunt leading Edge Quadrilateral Elements

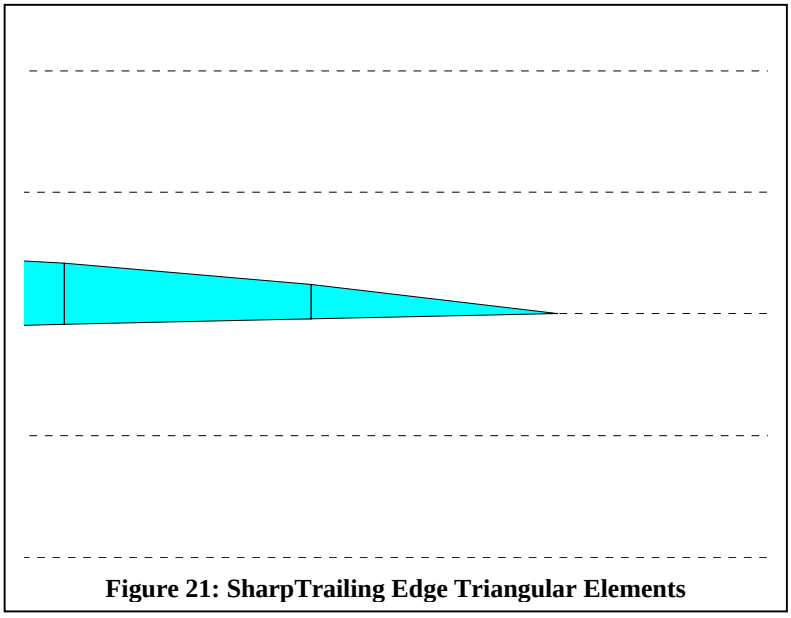

Figure 21: SharpTrailing Edge Triangular Elements

Wing skin

The wing skin was defined by quadrilateral element sections. These sections covered both the upper and lower surface of the wing and were primarily used as a means of accurately placing the pressure loads onto the internal wing structure. Each section therefore extended between neighbouring spars and ribs, and in the case of the blunt wing leading edge, between rib points as in Figure 22.

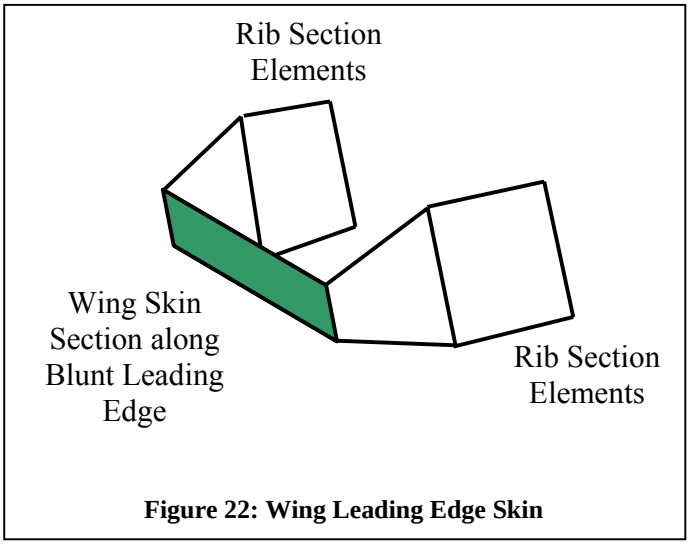

Figure 22: Wing Leading Edge Skin

As the wing skin thickness varies from wing root to wing tip and from the wing leading edge to the wing trailing edge, so the wing skin thickness in the MSC.Nastran® structural model had the ability to have a varying wing skin thickness as well. This variation was a simple linear function for both the variation along the span and chord.

Spar and Rib Caps

Spar and rib caps significantly add to the structural rigidity of the wing and hence were modelled as lumped thicknesses at the junction between spars and ribs with the wing skin as rod elements. As with the rib and spar thicknesses, the rib and spar caps thicknesses had the ability to taper from the root to the tip.

5.3.2 INPUT FILE FROM STRUCTURAL MODEL

MSC.Nastran® works using a Bulk Data input file which defines the type of solver and structural model. Some details and considerations for a typical BDF file in the simulation are:

Bulk Data

Before the definition of any of the Element Properties, etc, a number of parameters were set up for each run. The most important were the ones affecting nodal constraint and solution definition.

As the simulation being performed was a nonlinear static one, the requirement to constrain nodes which underwent large rotations was relaxed.

The Nonlinear Static solution method was selected. MSC.Nastran® simulations were run with fifty load steps. This allowed the program ample chance to find a simulation solution within a minimum time frame. If a larger number were chosen, MSC.Nastran® would most probably find most simulation solutions, but the cost would be in the increase in computational time required to perform all the structural simulations at this small load step size.

The other feature of interest in the nonlinear parameter setup was the convergence criteria used. As the solutions being found were for coarse structural models defining rough design analysis, the convergence criteria were relaxed. This was backed up through referring to the ‘Quick Reference Guide’ for MSC.Nastran® (MSC.Software 2005).

Element Properties

The Spars, Ribs and Wing Skins were modelled using shell elements. Considerable research was conducted into different modelling techniques which have been used when defining the above mentioned structural elements (Marisarla 2005), (Venter and Sobieszczanski-Sobieski 2004). It was decided that shell elements would be used to define the structural members through the PSHELL command. For these structural elements this would not only allow bending and shear within each of the elements, but would also account for the coupling properties such as Poisson's Ratio which would not be accounted for if only shear elements were used.

The drawback of using rod elements to describe the lumped rib and spar caps, described in later sections, is that rod elements have a constant cross sectional area. Furthermore, each rod element with a different cross sectional area needs to have a separate entry describing the properties attributed to that element. This was done through the PROD input deck.

Quadrilateral Elements

CQUAD4 input decks were used to define skin panels, wing spars and wing ribs which had varying thickness at all four corners of the quadrilateral elements. This allowed for better structural modelling compared to the use of a constant thickness throughout all the defined element sections.

Furthermore, CQUAD4 elements define plane strain plate elements and hence this feature was beneficial to the structural simulation.

One example of a CQUAD element definition is as follows:

```
CQUAD4        31       1     498     816     812     494
                         0.00058 0.00044  0.0004 0.00052
```

This method of CQUAD description allowed for the definition of edge thicknesses at node points along the element.

For a full breakdown of the CQUAD4 and subsequent input decks, please refer to the MSC.Nastran® reference manuals available from MSC.Software®.

Triangular Elements

CTRI3 elements were used to model the trailing edge elements defining the wing ribs. As with the CQUAD4 entries, the use of CTRI3 elements allowed for the specification of different element thicknesses at each of the node points. This allowed for refined structural calculations.

An example of a CTRI3 element definition is as follows:

```
CTRIA3       252       1    1379    3340    1909
                         0.00132 0.00132 0.00132
```

The same definition type was used with the CQUAD elements as was used with the CTRI3 elements in that it allowed the authors the ability to define the edge thicknesses at each of the node points.

Rod Elements

CROD elements were used to model lumped spar and rib caps; the desirable feature being that they are only able to carry tension and compression loads and hence do not alter the torsional properties of the wing section.

An example of a CROD element definition is as follows:

```
CROD,266,4,266,478
```

This entry simply defines the rod element according to the nodes located at each end of the element.

Materials

For all the simulations performed, only one material was used. Due to time constraints the material was defined as an isotropic graphite epoxy material which had constant material properties under tension, compression and shear. This resulted in a material with a Poisson's Ratio of 0.3, Young's Modulus of 1.53E11 and a density of 1310 kg/m^3. The material was defined through the MAT1 input deck and referenced by all elements.

An example of MAT1 describing the Graphite Epoxy composite used with both the High and Medium Altitude Long Endurance vehicles is as follows:

```
MAT1*   1     153000000000.0                    0.30             *M1
*M1     1310.01
```

Due to the large values used when describing the Young's Modulus of the material, the long field format was used.

Nodes

This section referenced the node number to the corresponding *x*, *y* and *z* location. The node numbers were used when defining the CQUAD4, CTRI3 and CROD elements.

Loads

Two loads were applied to each candidate wing structure. The second order pressure coefficients calculated by PANAIR and converted to pressures were applied to the upper and lower wing skin panels, and a gravity load was added to model the deflection and strains due to the mass of the structure.

The gravity load was required as the mass of the structure would create a downward acting force, and hence a moment about the X axis, which would then counteract the lifting force and moment generated by the applied pressures. Therefore the gravity load would decrease the deflection of the wing and give a more realistic indication of the initial deflection under the applied aerodynamic loads.

The pressure load was defined through the use of the PLOAD2 input deck. This input deck defined the magnitude of the pressures acting perpendicular to the surface defining a wing skin panel. Due to some pressures being larger than eight characters in length; the authors chose to use the large field format.

```
PLOAD2* 2          -2917.363       54                          *P54
*P54
```

From the above example code, one can see that the long field format was used as the applied pressures on each of the wing skin panels in column three could become very large about the leading edges.

Node Constraints

For simplicity it was decided that all the nodes along the wing root would be constrained. Although this would not happen in the case of a wing installed into the fuselage of an aircraft, for simulation purposes and to ease the comparisons made between results, the entire wing root was fixed in all displacements and rotations.

If the fuselage was included in the simulation environment, the wing spars would simply be extended to the fuselage centre line and the nodes defining the ends of the spars fixed in both displacements and rotations. This would be the correct method of simulating the node fixities for the wing as the fuselage would counter some of the forces and moments generated by the wing.

5.3.3 USE OF MSC.NASTRAN® FOR ANALYSING HIGH ASPECT RATIO WINGS

As it was unknown to what amount each candidate wing would deflect under the calculated aerodynamic loading, it was necessary to use a generic and robust method when solving for wing deflection. Furthermore, the deflection solution would need to be accurate if it were to be included in determining the overall Pareto front members and if the variables used to define the wing were to be passed to a higher level in the optimiser structure. It was therefore decided that a linear static solution (Eqn 6), calculated in MSC.Nastran® would not provide accurate results as this method would only solve the candidate wing using small deflection theory. The choice of solution method was also made after conclusions drawn by Marisarla (Marisarla 2005).

$$KQ = F \tag{6}$$

As some of the candidate wings could deflect an amount greater than a linear theory could accurately model, the non-linear solution method was chosen. The limit to linear theory is roughly taken in the case of a cantilever beam to be deflections of the same order of magnitude as the beam thickness. The change to a nonlinear solution method only required changes to the MSC.Nastran® input file.

For the Nonlinear Static solution, the applied loads are broken down into a number of sub loads. These loads are then applied in steps and the solution energy and deflection iterated until convergence for that load step, and the solution sequence continued until the entire load has been applied to the structure. MSC.Nastran® has the ability to bisect the current load step if it is unable to find a solution with the current step size. If, even after a number of user specified load step bisections, MSC.Nastran® is unable to find a solution, the program terminates with a failure message.

Further information on the nonlinear solution method used by MSC.Nastran can be found in (Komzsik 2001).

A draw back to using this method was that since the load was incrementally increased and iterated for deflection and energy balance, the solution time was longer increasing the computational cost per iteration.

5.4 AERO-STRUCTURAL ANALYSIS OF BASELINE DESIGNS

To illustrate the use of the aero- structural analysis we apply the method to two test cases related to UAV wing design; a Medium Altitude Long Endurance (MALE) research UAV similar to the Altair UAV wing and a High Altitude Long Endurance (HALE) UAVs similar to the Global Hawk wing.

5.4.1 MEDIUM ALTITUDE LONG ENDURANCE (MALE) UAV

Problem Formulation

A detailed analysis of a wing for a medium altitude research UAV application similar to the Altair UAV was considered. The operating conditions and data are based on details specified by NASA (NASA 2004). The aircraft maximum gross weight is approximately 3175 *kg*, has a wingspan of approximately 12.542 *m*, a mean chord of approximately 1.244 *m*, and a planform shape with 2.25° sweep between the root and second crank (Figure 23 and Table 1).

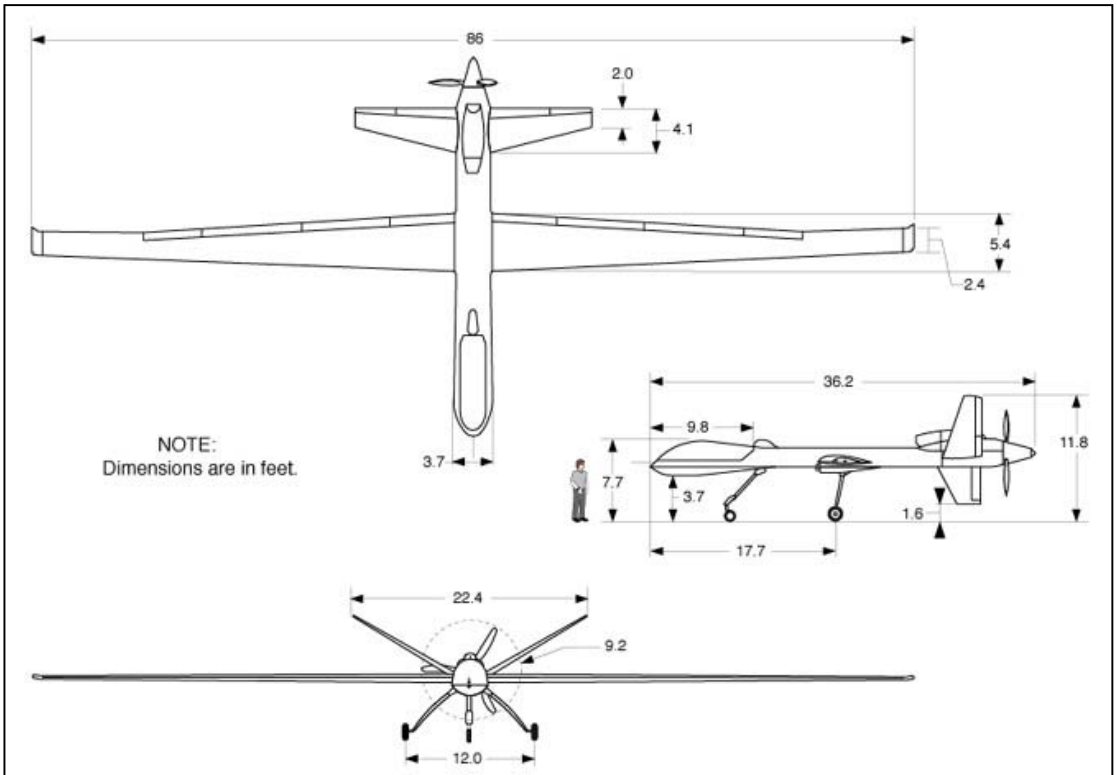

Figure 23: Design Variables for Altair (NASA 2004)

An assumption was made that the aircraft operated at 210 KIAS (108.10 m/s) at a cruise altitude of 41,600*ft*.

It was assumed that the wing uses the NACA4415 aerofoil at all spar locations as information on the actual aerofoils used was unavailable. Table 2 summarises some of the flight properties for the aircraft. These conditions assume an aircraft at mid weight-cruise during an extended cruise phase at intermediate altitude.

Characteristics, Units	
Maximum Altitude, *(m)*	15850
Cruise Altitude (80%MaxAlti), *(m)*	12680
Density @ Max Altitude, (*kg/m^3*)	0.16492
Density @Cruise Altitude, (*kg/m^3*)	0.27830
Air Speed, *(m/s)*	108.10
Speed of Sound @ Max Altitude, *(m/s)*	295.073
Speed of Sound @Cruise, *(m/s)*	295.073
Mach @Max Altitude	$M_\infty = 0.3663$
Mach @Cruise	$M_\infty = 0.3663$
Gross Weight, (*kg*)	3175

Table 1: Flight Conditions for Altair

Minimum Required Lift Coefficient

The following equation was used to calculate the required coefficient of lift at a number of flight conditions (Eqn 7).

$$C_L = \frac{W \times 9.81}{\frac{1}{2} \times \rho \times V^2 \times S} \quad (7)$$

The results after using Eqn 7 are summarised in Table 2.

Flight Condition	Required C_L
Max Gross Take Off at Maximum Altitude	1.1066
Beginning Cruise after T/O and Climb (5% fuel consumption)	0.6417
Middle of Cruise (50% fuel left)	0.5152
right before Landing (10% fuel left → reserve)	0.4028

Table 2: Required Altair C_L at different Flight Conditions

Simulations were performed at an angle of attack of 4° which yielded a calculated C_L greater than 0.64. This is equivalent to operating the Altair UAV at the beginning of the cruise condition as tabulated in Table 2.

Aerodynamics Model

The PANAIR and FRICTION codes were used for the aerodynamic analysis and are described in Section 5.2. In total, 1224 aerodynamic panels were used to discretise the Altair MALE model. Figure 24 shows the external planform shape.

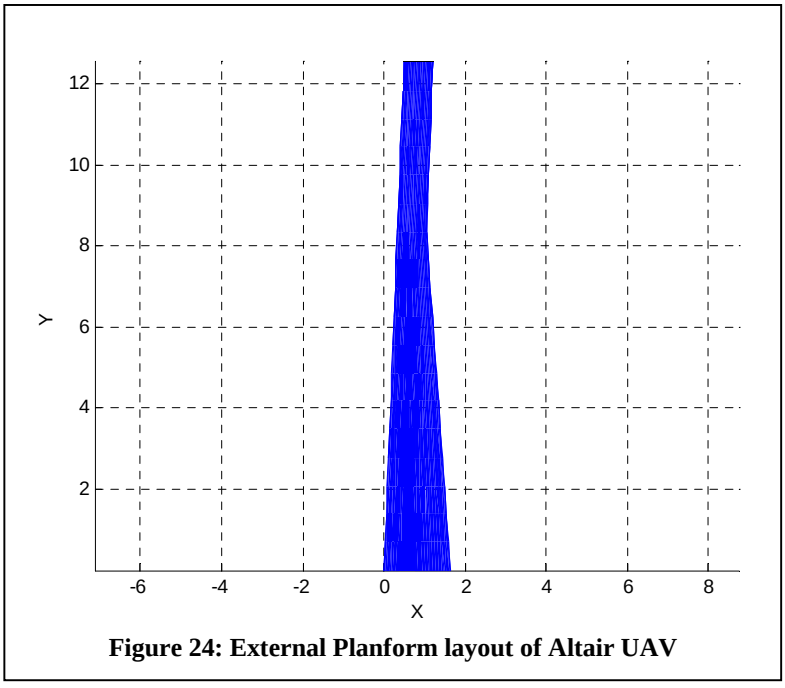

Figure 24: External Planform layout of Altair UAV

Figure 25 shows the linear (mid chord section) and exponential (leading and trailing edges) layout of the quadrilateral panels comprising the upper surface of the aerodynamics model.

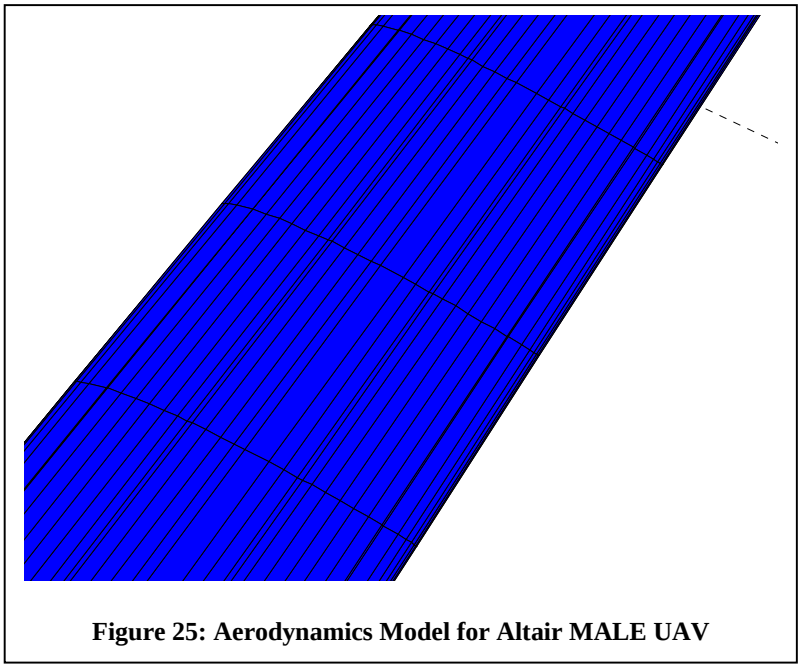

Figure 25: Aerodynamics Model for Altair MALE UAV

Structural Model

The structural model is described by the values displayed in Table 3 and shown in Figure 26.

Variable	*Value*
Number of spars	2
Number of ribs	10
Materials	
Wing skin	Graphite/epoxy
Spars	Graphite/epoxy
Ribs	Graphite/epoxy
Thicknesses	
Wing skin (m)	0.0001
Spars (m)	0.08
Ribs (m)	0.005
Thickness Ratios	
Wing Skin (Tip)	0.1
Wing Skin (Trailing Edge)	0.1
Spars	0.05
Ribs	0.25
Areas	
Spar Cap (m^2)	0.00375
Rib Cap (m^2)	0.0015
Material Properties	
Youngs Modulus (Pa)	1.53E11
Poissons Ratio	0.3
Density (kg/m^3)	1310

Table 3: Structural Variable Values for Altair UAV

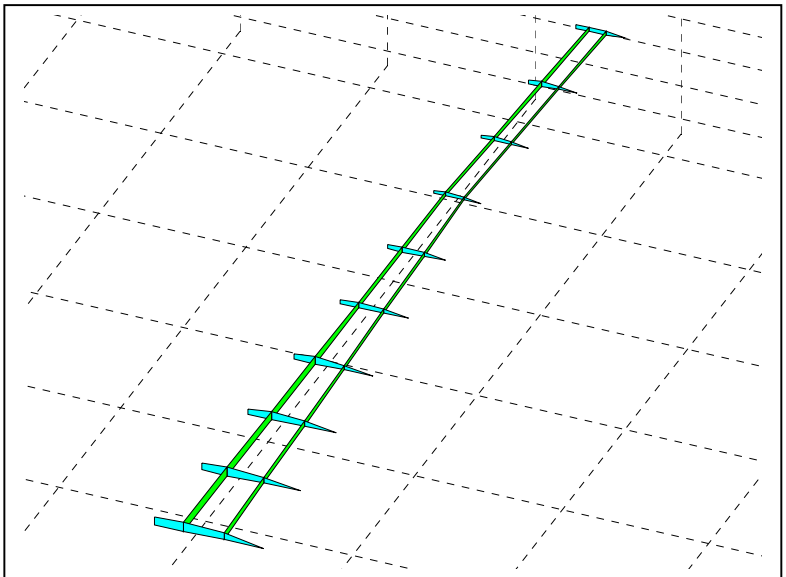

Figure 26: Internal Structural Model for the Altair UAV

Results

Aerodynamic analysis

Figures 27 and 28 show the wing span pressure coefficient distribution. The overall Altair wing aerodynamic characteristics for the above defined configuration are listed in Table 4.

The wing was found to weigh 220.9 *kg* which is in close agreement with the value estimated from Raymer (Raymer 1999).

L/D	23.9
C_L	0.66478
C_D	0.028
C_m	-0.1768
Deflection	12.06%

Table 4: Altair Wing Aerodynamic and Deflection Characteristics

Figure 27 shows the pressure distribution over the upper wing surface and Figure 28 that of the lower surface.

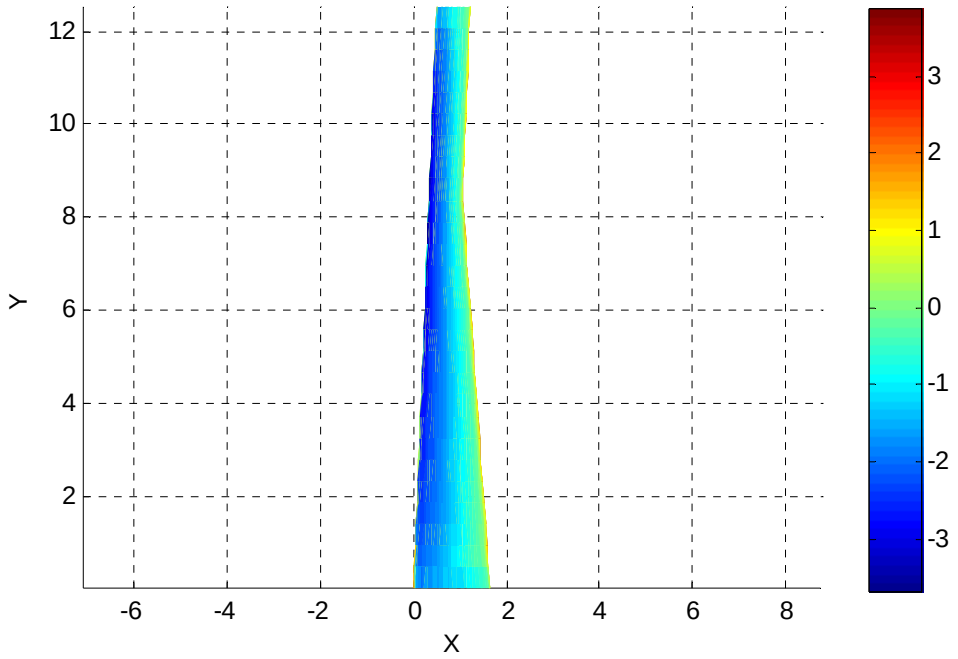

Figure 27: Pressure distribution along Altair Wing Top surface

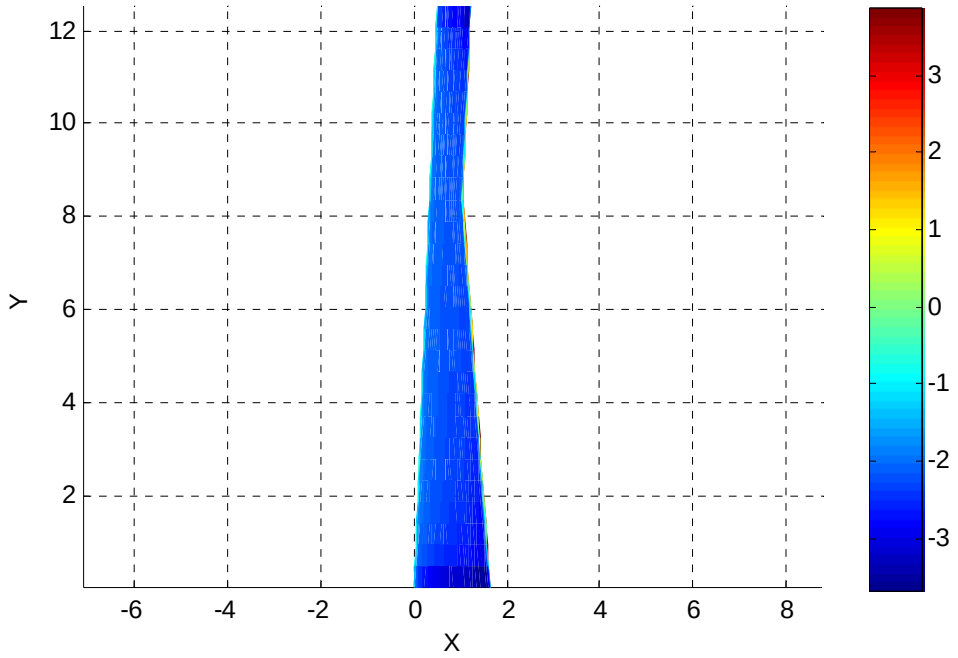

Figure 28: Pressure distribution along Altair Wing Bottom surface,

Performing a Mach sweep where the angle of attack for the vehicle was kept constant yielded the results in Figure 29 for the calculated induced component of the total C_D value.

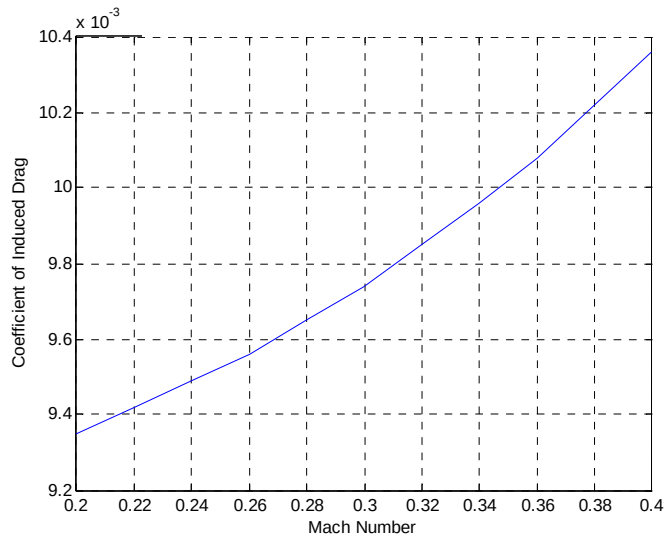

Figure 29: C_D results for Altair Mach Sweep between 0.2 and 0.4

Performing the same calculations for the coefficient of lift yielded the results shown in Figure 30.

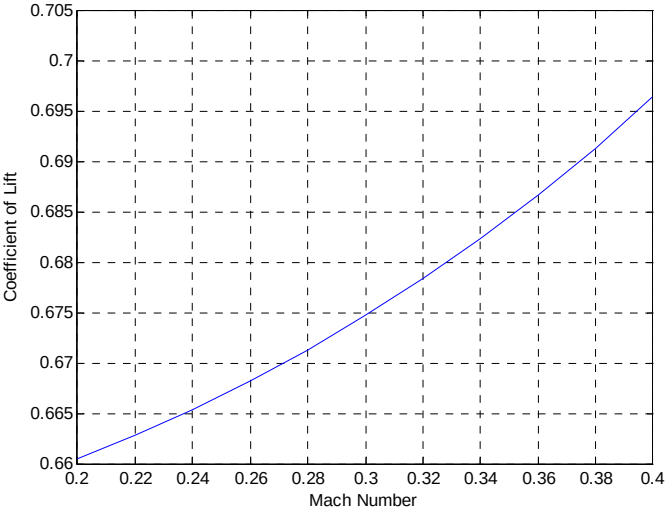

Figure 30: C_L results for Altair Mach Sweep between 0.2 and 0.4

Structural Analysis

Figures 31 and 32 show the displacement and strain results respectively after applying the pressure values calculated using PANAIR.

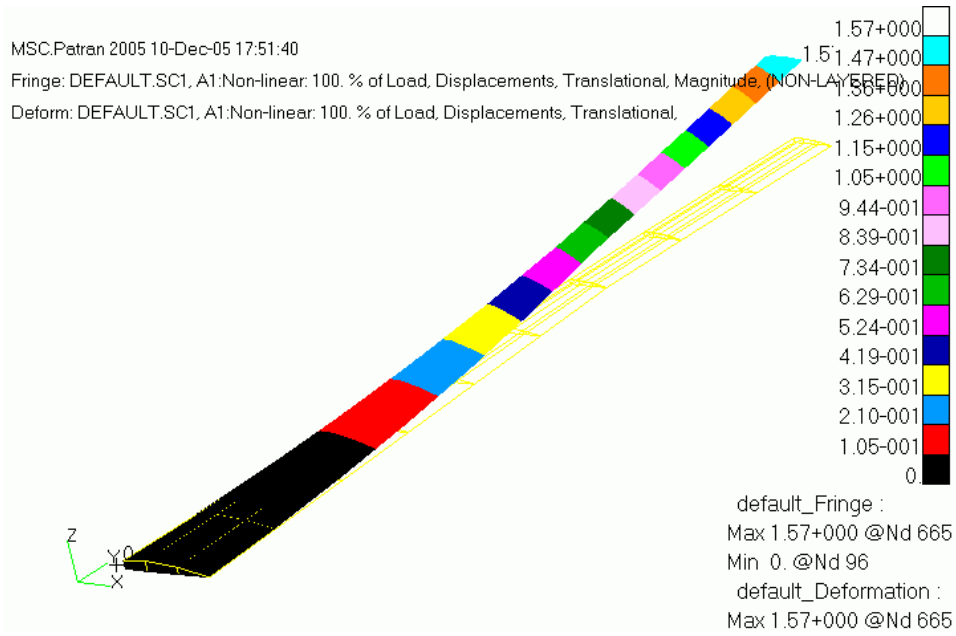

Figure 31: Non-linear Displacement for Altair UAV wing under 2.5g load case

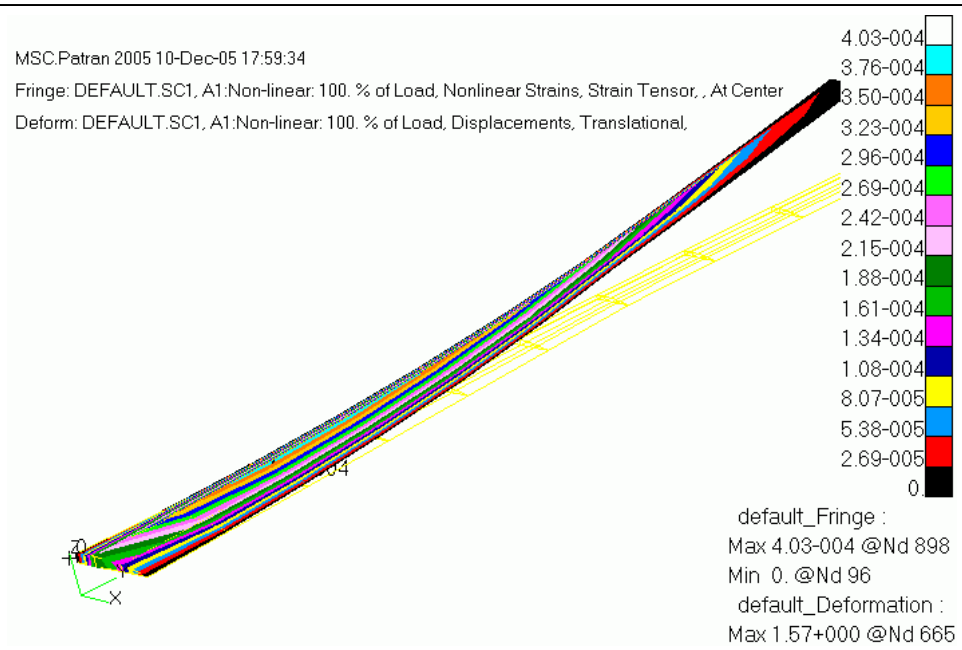

Figure 32: Non-linear Strain for Altair UAV wing under 2.5g load case

The calculations above resulted in the definition of the benchmark for the Altair MALE UAV redesign to be considered in Section 7.1.

5.4.2 HIGH ALTITUDE LONG ENDURANCE (HALE) UAV WING

Problem Formulation

As with the Altair MAVE UAV a detailed analysis was performed on a UAV similar to the Global Hawk HALE. The operating conditions and data are based on the information provided in Air Force Technology (www.airforce-technology.com 2004). The aircraft maximum gross weight is approximately 12,100 *kg*, has a wingspan of approximately 17.7 *m*, a mean chord of approximately 1.72 *m*, and a planform shape with 5.9° sweep between the root and tip (Figure 33). The assumption was made that the aircraft operated at 334 KIAS (176.56 *m/s*) at a cruise altitude of *15850 m*.

From Selig (Selig 2002), the Global Hawk makes use of the NASA LRN 1015 aerofoil section throughout the wing.

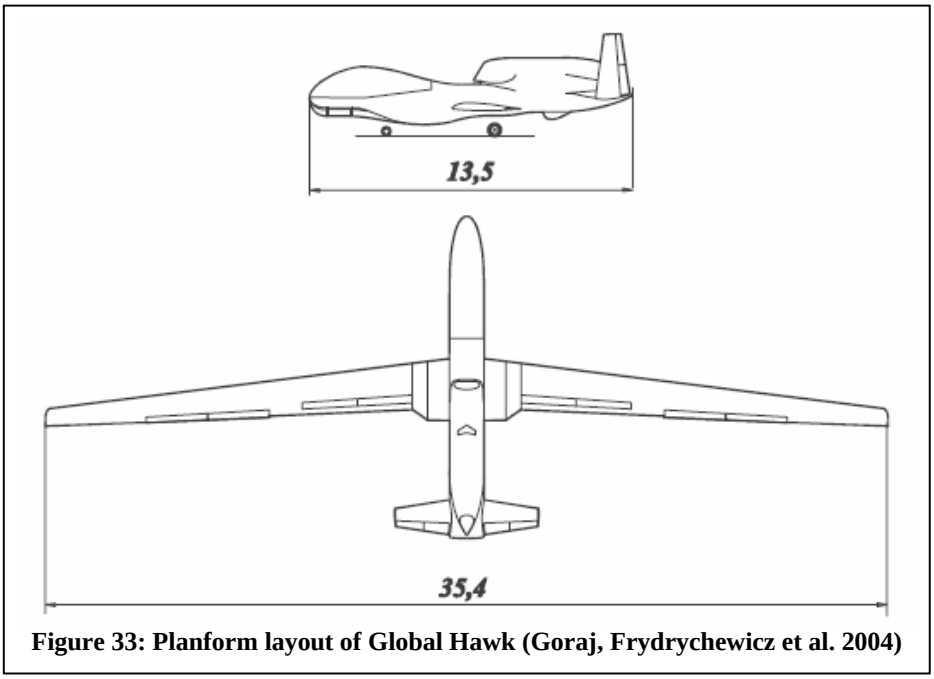

Figure 33: Planform layout of Global Hawk (Goraj, Frydrychewicz et al. 2004)

The Global Hawk flight conditions are summarised in Table 5.

Characteristics, Units	
Maximum Altitude, *(m)*	19812
Cruise Altitude (80%MaxAlti), *(m)*	15850
Density @ Max Altitude, (*kg/m^3*)	0.08761
Density @Cruise Altitude, (*kg/m^3*)	0.16938
Air Speed, *(m/s)*	176.566
Speed of Sound @ Max Altitude, *(m/s)*	295.073
Speed of Sound @Cruise, *(m/s)*	295.073
Mach @Max Altitude	$M_\infty = 0.5983$
Mach @Cruise	$M_\infty = 0.5983$
Gross Weight, (*kg*)	11,600

Table 5: Flight Conditions for the Global Hawk

Minimum Required Lift Coefficient

Eqn 7 was used to calculate the required coefficient of lift at each flight condition indicated in Table 5. The results after using Eqn 7 are summarised in Table 6.

Flight Condition	**Required C_L**
Max Gross Take Off at Maximum Altitude	1.7341
Beginning Cruise after T/O and Climb (5% fuel consumption)	0.8962
Middle of Cruise (50% fuel left)	0.6718
right before Landing (10% fuel left → reserve)	0.4723

Table 6: Required Altair C_L at different Flight Conditions

Simulations were performed at an angle of attack of 4.75° which yielded a calculated C_L greater than 0.8962. This is equivalent to operating the Global Hawk UAV at the beginning of the cruise condition as tabulated in Table 6.

Aerodynamics Model

The PANAIR and FRICTION codes were used for the aerodynamic analysis and are described in Section 5.2. In total, 1980 aerodynamic panels were used to discritise the Global Hawk HALE benchmark model. Figure 34 shows the linear (mid chord section) and exponential (leading and trailing edges) layout of the quadrilateral panels comprising a portion of the upper surface of the aerodynamics model. This is the same model layout as was used with the Altair benchmark in Section 5.4.1.

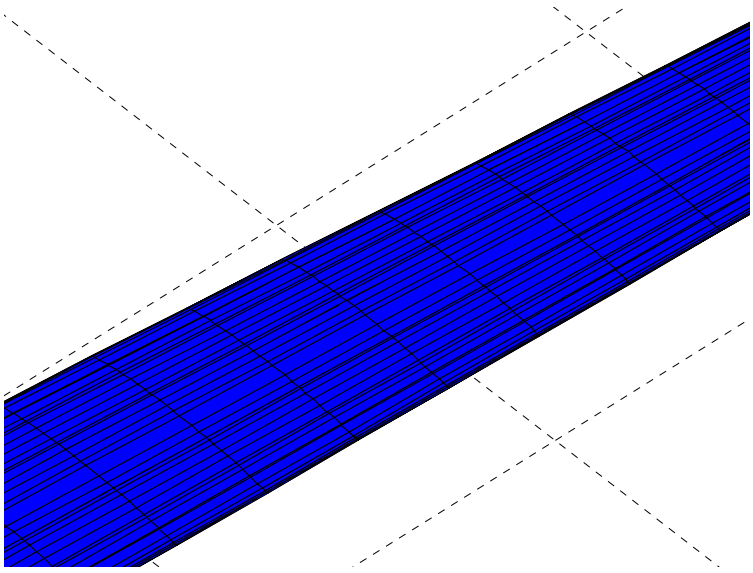

Figure 34: Aerodynamics Model for Global Hawk HALE UAV

Structural Model

The structural model is described by the values displayed in Table 7 and shown in Figure 36. Figure 35 shows the internal structure of the wing and Figure 36 the external panels.

Variable	*Value*
Number of spars	5
Number of ribs	10
Materials	
Wing skin	Graphite/epoxy
Spars	Graphite/epoxy
Ribs	Graphite/epoxy
Thicknesses	
Wing skin (m)	0.01
Spars (m)	0.08
Ribs (m)	0.0015
Thickness Ratios	
Wing Skin (Tip)	0.01
Wing Skin (Trailing Edge)	0.01
Spars	0.01
Ribs	0.01
Areas	
Spar Cap (m^2)	0.01
Rib Cap (m^2)	0.0005
Material Properties	
Youngs Modulus (Pa)	1.53E11
Poissons Ratio	0.3
Density (kg/m^3)	1310

Table 7: Structural Variable Values for Global Hawk UAV

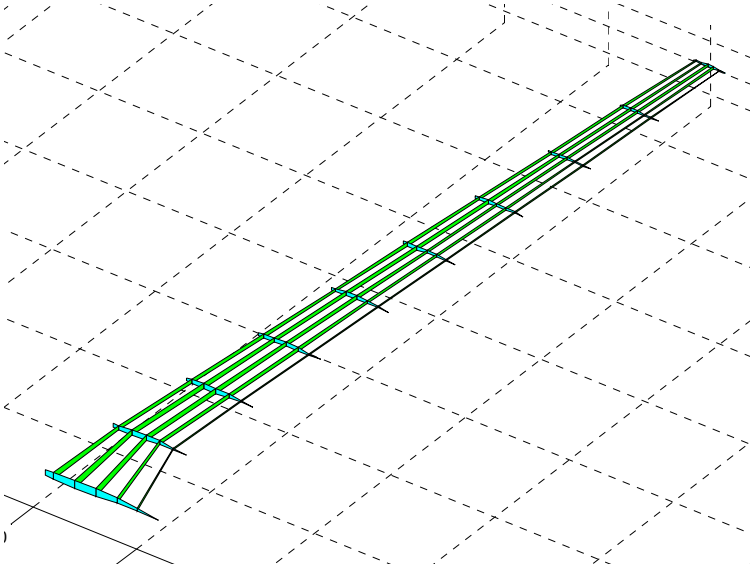

Figure 35: Internal Structural Model for the Global Hawk UAV

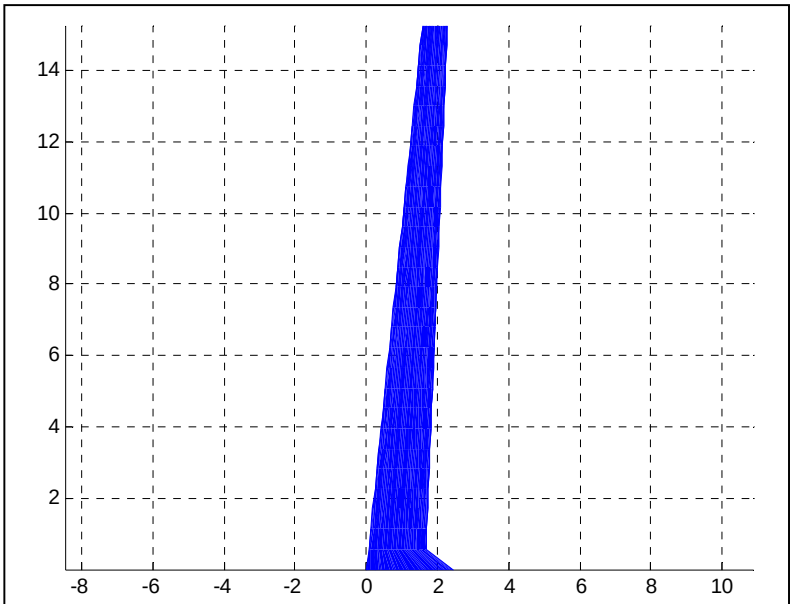

Figure 36: External Planform layout of Global Hawk UAV

Results

Aerodynamic analysis

The overall Global Hawk wing aerodynamic characteristics for the above defined configuration are listed in Table 8. Figures 37 and 38 show the wing span pressure coefficient distribution.

L/D	31.729
C_L	0.905
C_D	0.02849
C_m	-0.208
Deflection	16.7%

Table 8: Global Hawk Wing Aerodynamic and Deflection Characteristics

The wing was found to weigh 1138.15 *kg* which is in close agreement with the value calculated through the use of Raymer (Raymer 1999).

Figure 37 shows the pressure distribution over the upper wing surface and Figure 38 that of the lower surface.

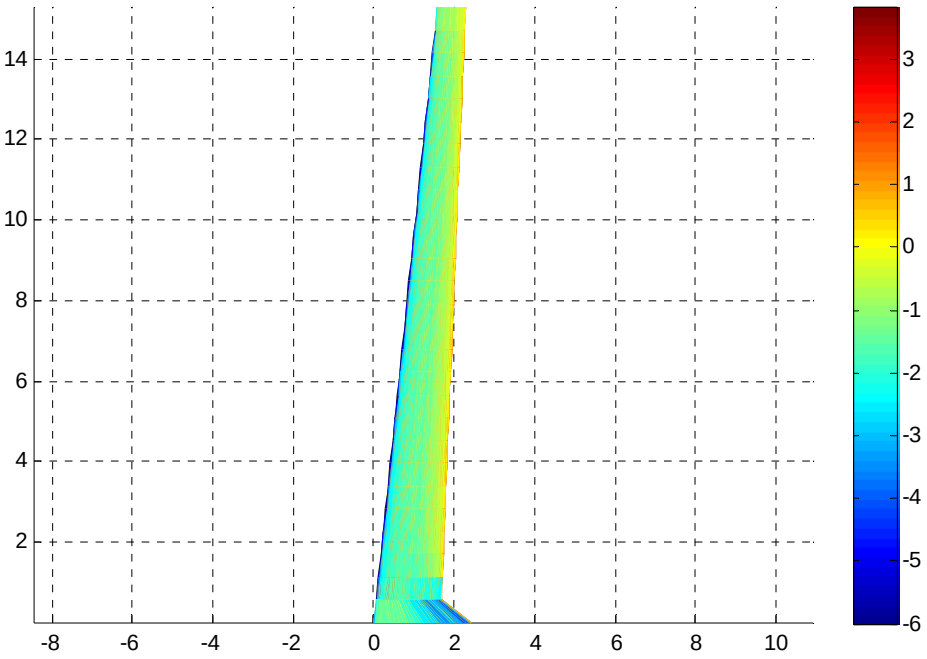

Figure 37: Pressure distribution along Global Hawk Wing Top surface

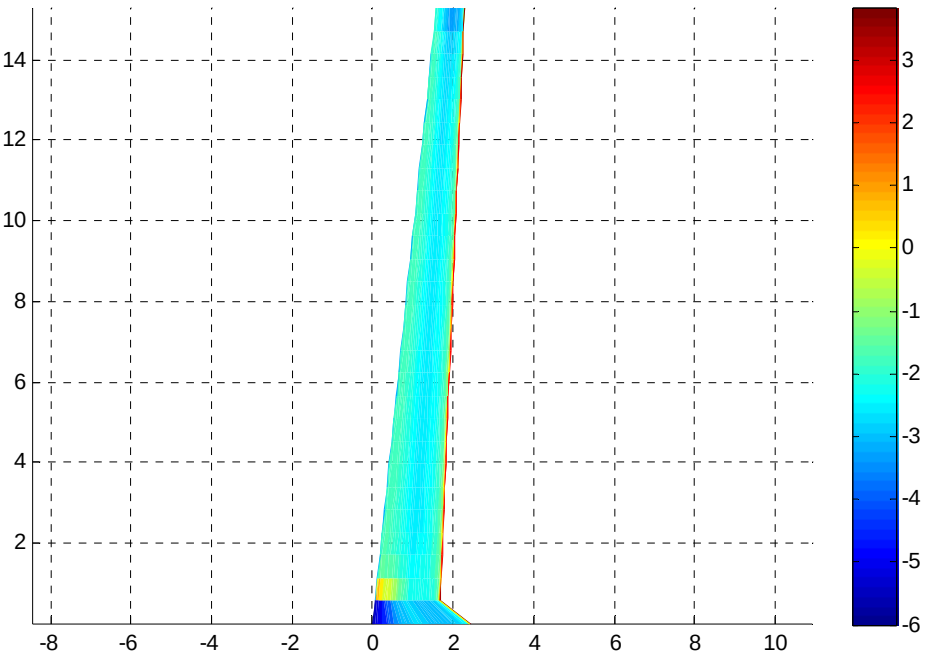

Figure 38: Pressure distribution along Global Hawk Wing Bottom surface

Performing a Mach sweep where the angle of attack for the vehicle was kept constant yielded the results in Figure 39 for the calculated induced component of the total C_D value.

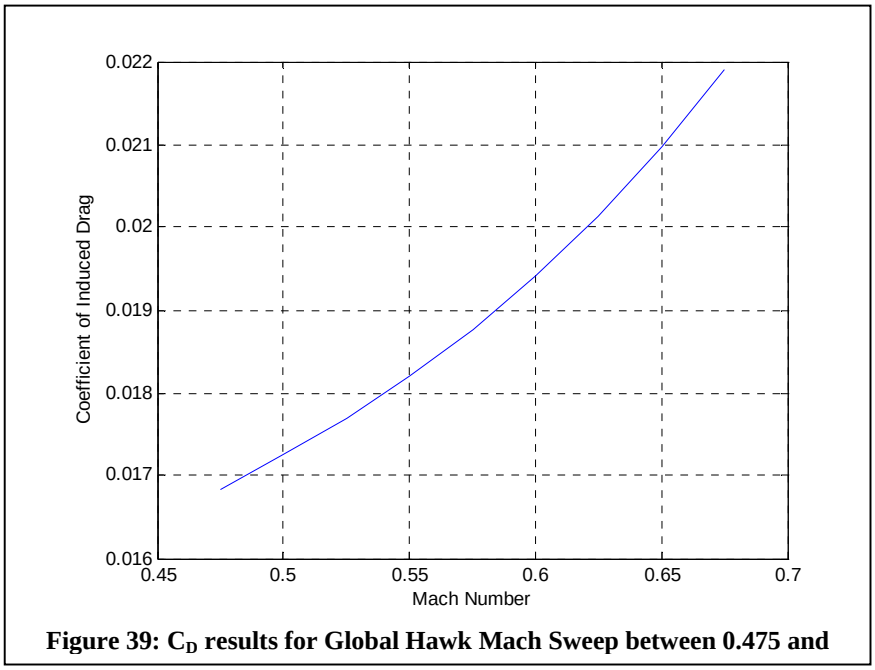

Figure 39: C_D results for Global Hawk Mach Sweep between 0.475 and

Performing the same calculations for the coefficient of lift yielded the results shown in Figure 40.

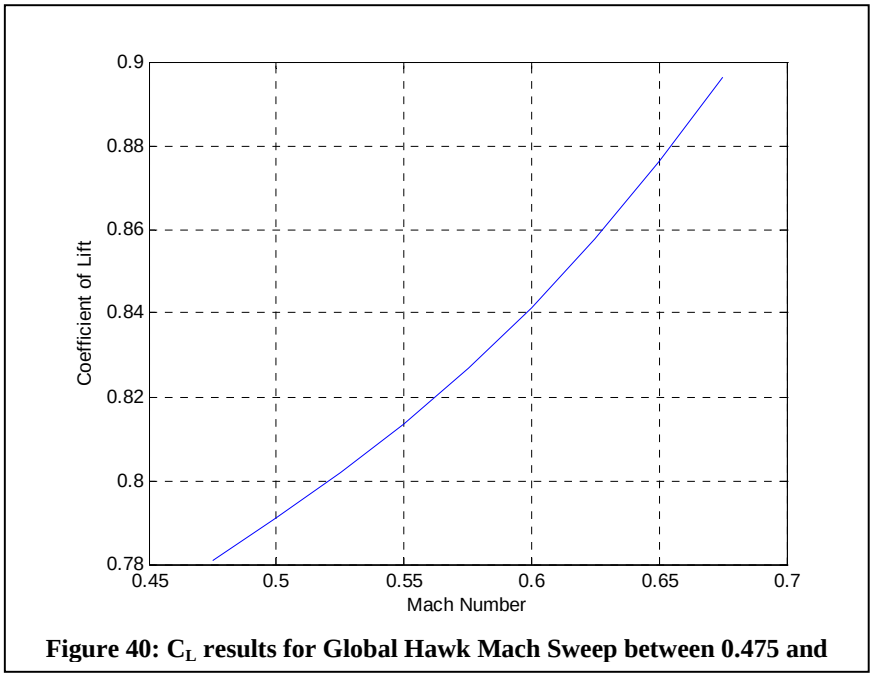

Figure 40: C_L results for Global Hawk Mach Sweep between 0.475 and

Structural Analysis

Figures 41 and 42 show the displacement and strain results respectively after applying the pressure values calculated using PANAIR.

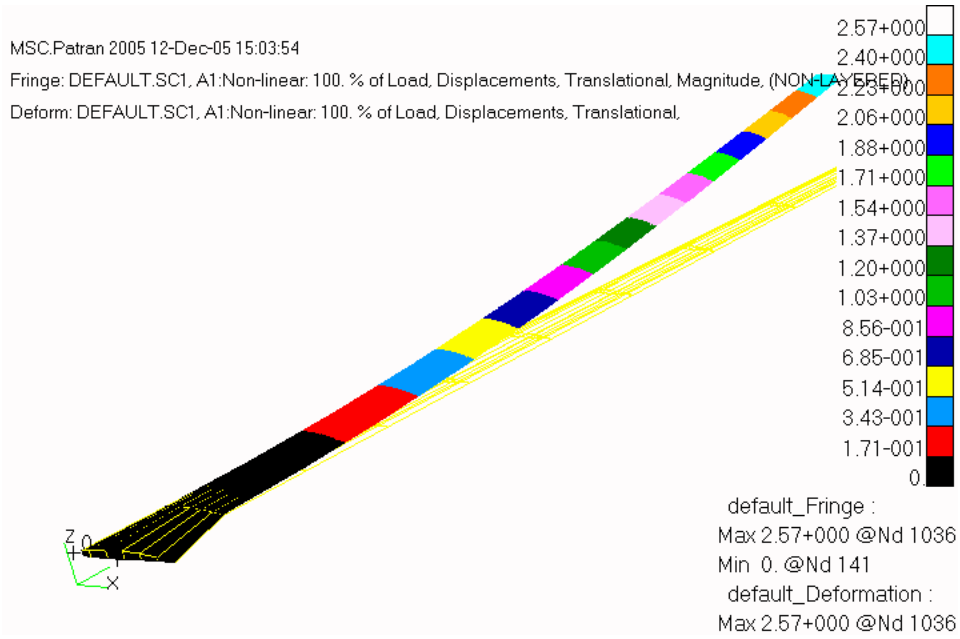

Figure 41: Non-linear Displacement for Global Hawk UAV wing under 2.5g load case.

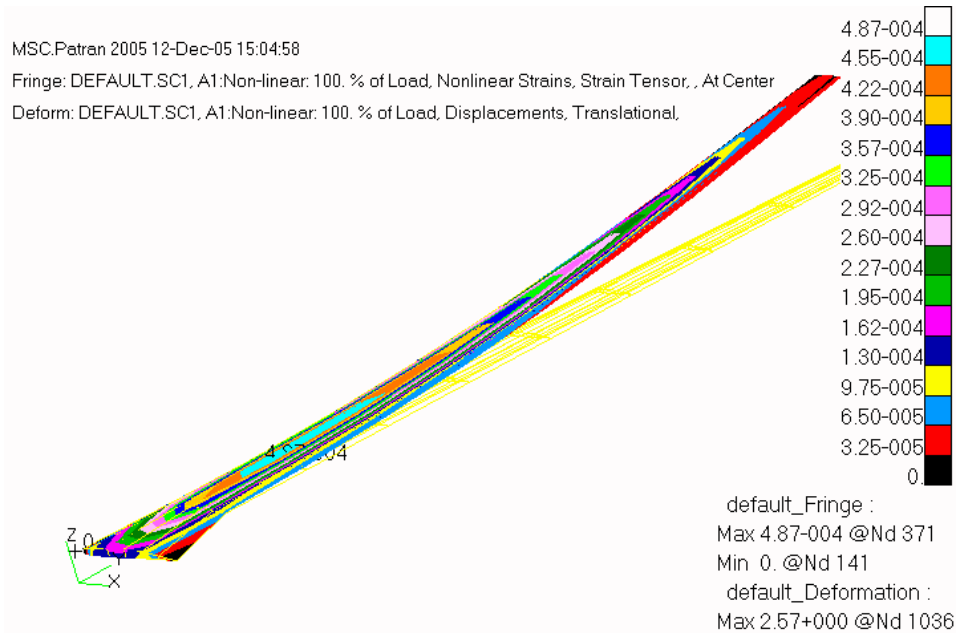

Figure 42: Non-linear Strain for Global Hawk UAV wing under 2.5g load case

The calculations above resulted in the definition of the benchmark for the Global Hawk HALE UAV redesign to be considered in Section 7.2

6 AERO-STRUCTURAL OPTIMISATION

In a general form, the aero-structural optimisation process follows the flow diagram in Figure 43. The Aero-Structural Solver computes the flow dynamics for the planform and structural variables defined by the Evolutionary Optimiser and create the four output files described in Section 5.1.2.

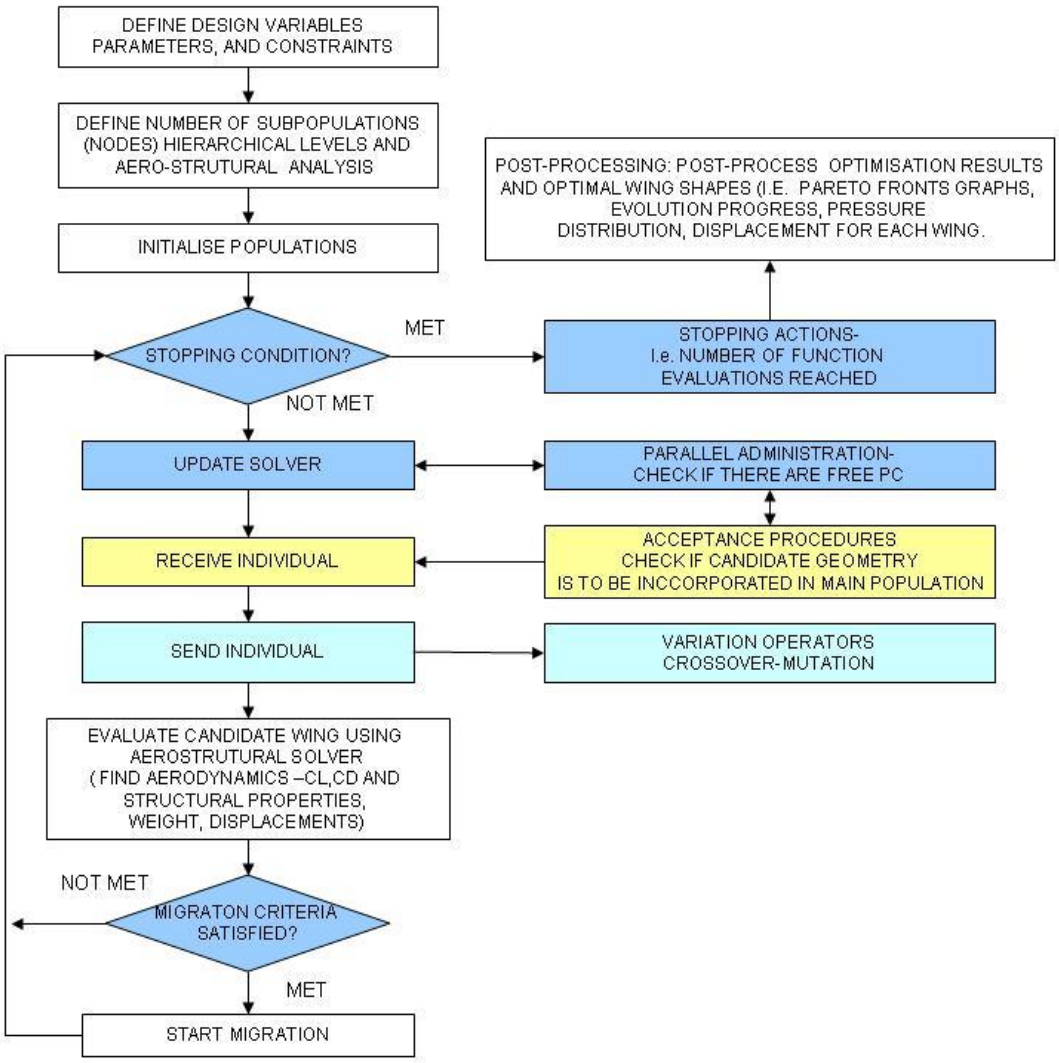

Figure 43: Aero-structural optimisation flow chart

In Figure 43, the Evolutionary Optimiser uses a hierarchical approach with three levels, on the bottom level a coarse analysis is performed to direct the exploration, at the top level a more precise model, that better describes the physics involved, is used and at an intermediate level, a compromised balance between the top and bottom layers is used. Initially the system will specify the design variables, constraints and parameters and will generate a random sub population of individuals at each layer. It then defines the number of sub populations (nodes) and number of hierarchical levels which for simplicity is equal to the number of analyses being performed. Once these initial populations are generated, the algorithm will initialise all the required populations through repeated calls to the Aero-Structural Solver and go through a

series of steps. The scheduler first determines whether the given stopping conditions have been met, and if so, the evolutionary loop is exited and the entire process is stopped. If no stopping conditions are met, the scheduler updates the asynchronous solver so that further progress can be made. The scheduler determines whether or not candidate solutions which have been solved are ready for incorporation into the population. If such solutions exist, the incorporation routine is called and available candidates, which now have had a fitness assigned (evaluated by the Aero-Structural Solver), are processed; it receives the individual, ages the population and buffer, performs Pareto tournament selection, deletes the oldest from the buffer and if the acceptance is true, it is inserted in the population which was subsequently sorted. It then updates the CMA parameters. Finally the scheduler determines whether it is possible to generate more candidates by polling the asynchronous solver. If this is possible, then the generation routine is called and individuals are generated via the evolutionary operators through recombination and mutation via CMA always checking the upper and lower bounds. During evaluation, the optimiser will take output analyses and parameters to guarantee the satisfaction of constraints and compute the overall fitness function. If the problem is multi objective, the algorithm will find the non-dominated individuals and will calculate the Pareto fronts.

As MSC.Nastran® runs on the availability of licenses on a master server, the Aero-Structural Solver was written such that the code checks to see whether or not a license file exists when attempting to analyse a candidate wing with MSC.Nastran®. If a license does not exist as all the licenses are currently being used by other analyses, the program waits for a license to become available and does not simply discard the simulation.

This ability to wait for licenses, therefore allows the Evolutionary Optimiser to be run on more machines than there are MSC.Nastran® licenses. This is beneficial as only a fraction of the total time taken to solve each candidate wing solution is taken calculating the structural solution. Therefore, if only the same numbers of computers as MSC.Nastran® licenses are run, there will be instances when MSC.Nastran® licenses are idle. This ability to wait for licenses therefore is beneficial.

6.1 HANDLING OF CONSTRAINTS

Constraints are handled using penalty functions which are broken up into two different parts. The first part penalized the aerodynamics of the wing, and the second the structure. It was found to be beneficial to separate the penalties as it meant that if the optimizer generates a candidate solution which resulted in a light and rigid structure, while the aerodynamics were far from optimum, the structure could still exist within the Pareto set and have its variable values passed onto further generations of candidate solutions. The same consideration applied to the aerodynamics of a candidate wing. If the aerodynamics were found to be near optimal while the wing deflection large with failed structural components due to high strain values, it would slow down the optimizer if the solution were merely discarded.

Therefore, by programming the penalty function to only penalize those components which failed, the overall efficiency of the optimizer was increased.

To further assist the EA when evaluating potential non-dominated solutions, an exponential penalty function is used. This forces penalised wings into regions outside the Pareto front, or off to one extreme favouring only one of the fitness functions. This meant that only wings which were not penalised, or penalised slightly, existed close to the Pareto front. This would not be seen with the use of a linear penalty function as a wing which was penalised for defecting 50% could be seen as a wing with the same weight as a 200% wing.

6.1.1 AERODYNAMICS

Aerodynamic moment

In order to keep the control system of the vehicle relatively unchanged, the authors decided to impose penalties on the tested wing if the aerodynamic moment generated by the wing was greater than the original benchmark tests performed.

The wing was linearly penalized by increasing the fitness value defined by the inverse of the lift to drag ratio for every percent over the aerodynamic moment benchmark value calculated.

Coefficient of Lift

If the optimizer were to design a wing with aerodynamics such that the inverse of the lift to drag ratio was minimized, and only the aerodynamic moment penalized, the code might evolve a wing which would produce too little lift when placed in the required flight regime. Furthermore, if one were then to alter the angle of attack for the aerofoil to attain the required Coefficient of Lift, the total drag for the aerofoil would change and hence there lies a possibility that the aerofoil would cease to be the optimal configuration.

The authors therefore decided to penalize a candidate wing if the lift created was below a set amount. This amount was usually set at ninety percent of the required lift at the start of the cruise phase of the aircraft. As with the Aerodynamic moment penalty, the Coefficient of Lift penalty was added to the fitness function defined by the inverse of the lift to drag ratio at a rate for every percent under the required value. If the Coefficient of Lift calculated for the wing was above the required value, no penalty was imposed.

6.1.2 STRUCTURE

Aerofoil Thickness

The thickness of an aerofoil shape has implications not just for the aerodynamics of the vehicle. If a very thin aerofoil section is designed it might produce excellent aerodynamic results when built and tested, but there would be a very large drawback in that the space between the upper and lower surfaces of the wing would be very small resulting in a cramped and tight working environment. This small working environment would affect the internal layout of the wing and the ease of component inspection.

Therefore the thickness of each aerofoil must exceed a value of 12% ($t/c \geq 0.12$). If the Evolutionary Optimiser produced a candidate aerofoil which had a smaller thickness value, the aerofoil would be penalised by equally penalising both the aerodynamic and structural values via a linear penalty method. In addition, aerofoil sections generated by the Evolutionary Optimiser which had thicknesses outside some bounds, usually between 10% and 15%, were rejected immediately before any analysis was performed with them.

Buckling of Wing Skin Panels

Thin sheets of material under compression and or shear loads are subject to buckling. When a sheet of material buckles under the applied load, the magnitude of the strength with which the sheet of material is able to withstand reduces significantly.

An accurate method of predicting whether or not any of the elements within a candidate wing would be subject to buckling would be to perform a buckling analysis in MSC.Nastran®. The additional computational overhead would be rather large increasing the time required to determine the fitness of each candidate wing. This would further extend the time required by HAPMOEA to find a global optimal solution given the simulation bounds. It therefore became appropriate to find another method to determine whether or not any elements within a candidate wing would buckle. As the Spars and Ribs were of considerable thicknesses compared to the wing skin, and also since the loads and moments carried by these two structural elements lay in plane with the elements as in Figure 44*a*, the possibility of any of the sections making up the Spars and Ribs buckling would be very small compared to the possibility of the skin panel sections buckling. This is due to the fact that the applied loads and moments across the Skin sections lie out of plane as in Figure 44*b*.

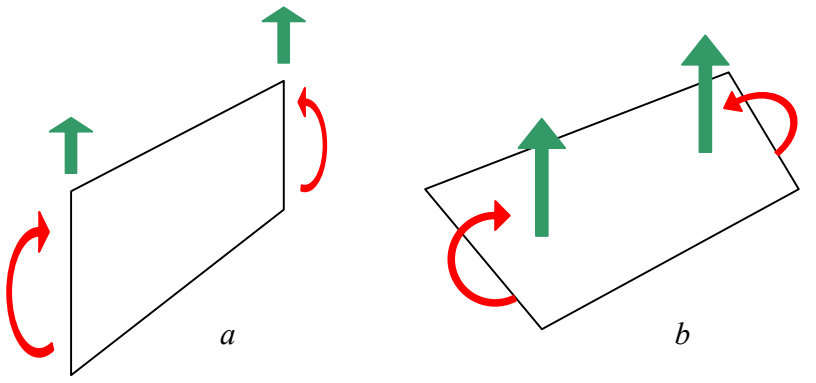

Figure 44: In and Out of Plane Section Loading

Following the method followed by Venter and Sobieszczanski-Sobieski (Venter and Sobieszczanski-Sobieski 2004), simple analytical expressions were used to test whether or not the stresses in the Wing Skin sections were large enough to cause buckling. These local buckling expressions are described by Eqn. 8.

$$\begin{aligned} &\frac{\sigma_1}{\sigma_{cr}} - 1 \le 0 \\ &\frac{\tau_1}{\tau_{cr}} - 1 \le 0 \\ &\frac{\sigma_1}{\sigma_{cr}} + \left(\frac{\tau_{12}}{\tau_{cr}}\right)^2 - 1 \le 0 \end{aligned} \tag{8}$$

Where:

$$\sigma_1 = \frac{N_1}{2t}, \sigma_{cr} = \frac{3.6kE}{\left(\frac{b}{t}\right)^2}$$

$$\tau_{12} = \frac{N_{12}}{2t}, \tau_{cr} = \frac{4.85kE}{\left(\frac{b}{t}\right)^2}$$

and b is the width of each Wing Skin section and k was an additional safety factor to guard against delamination of the plies making up the carbon graphite composite material. The safety factor was set at four for all the optimisations.

Tip Twist

As the wing bends, the pressures generated by the wing would change and hence the forces within the wing would also change. If the wing tip twisted, there is a possibility that the wing would greatly increase the drag created by the wing, and also increase the moment about the Z axis. As a full aero-elastic analysis was not part of the simulation runs, any further increase in the angle at which the wing would make with the freestream flow would be disadvantageous to the computation as the final wing position and internal forces could not be computed.

It was therefore necessary to penalize wings in which after the structural simulation using MSC.Nastran®, the wing tip angle of attack was greater than a user set value from the initial wing setting angle. This penalty took the form of mass added to the structure at the rate for each additional degree.

Deflection

As no full aeroelastic analysis was performed on each candidate wing, the final aerodynamic and structural solution was not known. Therefore the assumption was made that if the initial deflection of the wing was small, the wing would have a smaller chance of aerodynamic divergence if the aerodynamic and structural simulations were performed on the deflected wing was made. Although this might not be the case for certain wings, it was simple and easy to implement and placed a far smaller overhead on the computational cost compared to the analysis of the mass matrix for each candidate wing.

The wing was therefore allowed to deflect a set percentage of the span for a 2.5*g* load case before a penalty value was added to the fitness value. As with the Tip Twist condition, the penalty took the form of additional mass and was added per percent deflection over twenty percent.

Failure of Internal Component Panels

In this aero-structural analysis the testing of structural members for failure was performed through the use of the maximum strain theory. This was done as stress varies between plies and orientations in a composite material, while strain varies linearly through the thickness. This same method was employed in Venter and Sobieszczanski-Sobieski (Venter and Sobieszczanski-Sobieski 2004).

If any components making up the internal structure within the wing, spars, ribs, skin, etc failed due to excessive strains, the wing was heavily penalized by the addition of extra wing mass. This mass was increased at a rate of ten percent for each panel making up a component which failed. Hence, if ten CQUAD4 components making up a spar failed, the mass of the wing structure was increased one hundred percent.

6.1.3 COMBINED PENALTIES

If a wing was analysed and the penalties were very large against a user set maximum, instead of only penalising one of the fitness functions, both fitness functions would be penalised according to the maximum penalty associated with either of the calculated values. This forces the solution to be dominated and hence the genetic information is not passed on to any further generations of candidate wing solutions.

7 AERO-STRUCTURAL OPTIMISATION TEST-CASES

This section considers the application of the optimisation methodology for two test cases related to UAV design. The first test case is for a Medium Altitude Long Endurance (MALE) UAV and the second for a High Altitude Long Endurance (HALE) UAV.

7.1 MEDIUM ALTITUDE LONG ENDURANCE (MALE) UAV DESIGN AND OPTIMISATION

This first test case considers the multidisciplinary, multi-objective design optimisation of a MALE UAV Wing similar to the Altair MALE Unmanned Aerial Vehicle (UAV) considered in Section 5.4.1. The two objectives are the maximisation of the lift to drag ratio (L/D), and the minimisation of wing weight. The cruise Mach number and altitude are 0.3663 and 12680 *m* respectively and the wing area is set to 29.21 m^2.

7.1.1 DESIGN VARIABLES AND CONSTRAINTS.

The wing geometry is represented by three aerofoil sections with sixteen variables for each section, eight variables that describe the wing planform and eleven variables to describe the internal structure.

The aerofoil geometry is represented by the combination of a mean line and thickness distribution, which is a very common procedure in classical aerodynamics (Abott and Doenhoff 1980). Both lines are represented by Bézier curves with leading and trailing edge points fixed at (0.0,0.0) and (1.0,0.0) respectively, and a variable number of intermediate control points whose *x*-positions are fixed in advance and whose *y*-heights form the problem unknowns. In this case 6 free control points on the mean line and 10 free control points on the thickness distribution are taken.

The wing planform design variables are indicated in Figures 45 and 46 and their upper and lower bounds are represented in Table 9. In total 67 design variables are used for the MALE UAV wing optimisation.

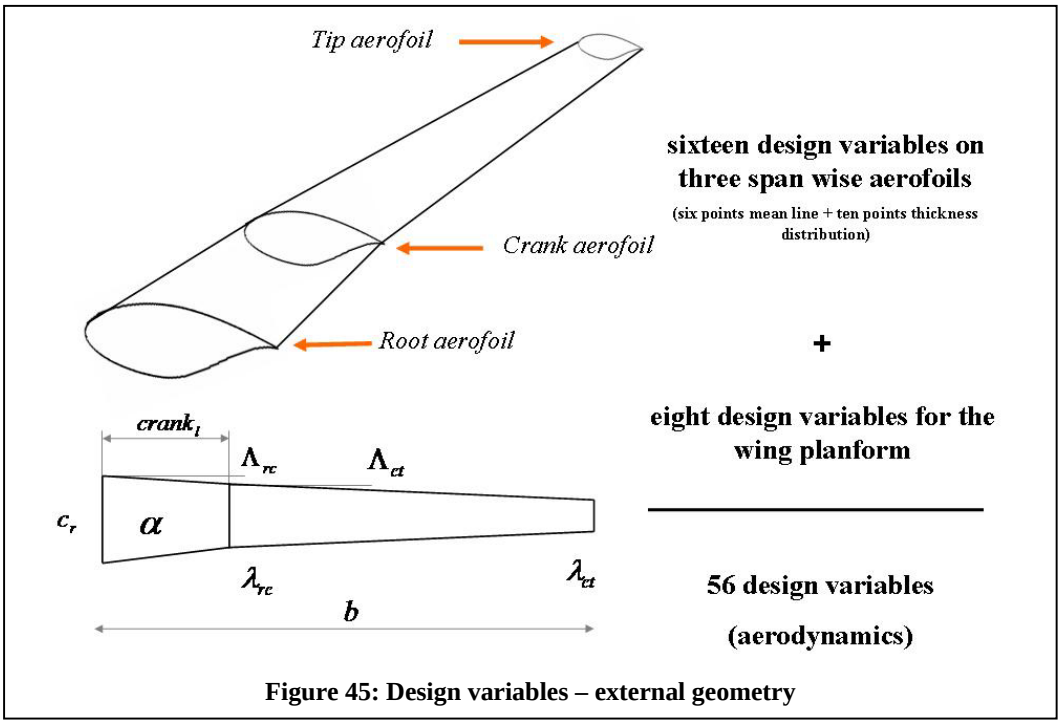

Figure 45: Design variables – external geometry

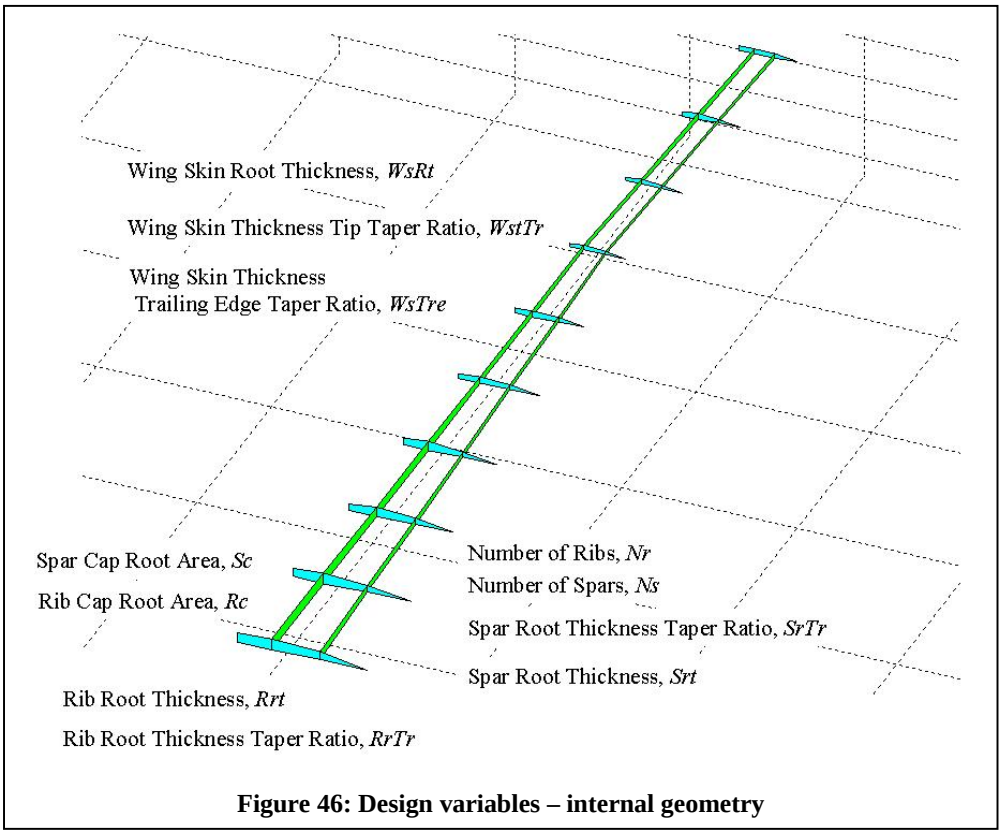

Figure 46: Design variables – internal geometry

Description	**Benchmark**	**Lower Bound**	**Upper Bound**
Angle of Attack, α *(deg)*	4	0	6
Wing Semi Span, *b (m)*	12.542	8.2	18.5
Root Chord, c_r *(m)*	1.646	1.6	1.7
Wing Inboard Leading Edge Sweep, $\Lambda_{rc,}$ *(rad)*	0.039	0	5
Wing Outboard Leading Edge Sweep, Λ_{ct} *(rad)*	0.039	0	5
Chord Ratio at Break, $\lambda_{rc,}$	0.444	0.35	0.65
Chord Ratio at Tip, λ_{ct}	0.444	0.35	0.65
Crank Location, $crank_l$	0.731	0.5	0.8
Number of Spars, *Ns*	2	1	3
Number of Ribs. *Nr*	10	8	12
Rib Root Thickness, *Rrt (m)*	0.005	0.003	0.0065
Rib Root Thickness Taper Ratio, *RrTr*	0.25	0.15	0.3
Spar Root Thickness, *Srt (m)*	0.08	0.05	0.09
Spar Root Thickness Taper Ratio, *SrTr*	0.05	0.01	0.2
Wing Skin Root Thickness, *WsRt (m)*	0.001	0.0005	0.002
Wing Skin Thickness Tip Taper Ratio, *WstTr*	0.1	0.05	0.15
Wing Skin Thickness Trailing Taper Ratio, *WsTre*	0.1	0.05	0.15
Spar Cap Root Area, *Sc* (m^2)	0.00375	0.0025	0.04
Rib Cap Root Area, *Rc*(m^2)	0.0015	0.001	0.002

Table 9: Structural and Planform Design Variables for the MALE UAV wing

7.1.2 DESIGN CONSTRAINTS AND PENALTIES

There are several constraints which must be satisfied for each candidate wing namely:

- The pitching moment must not be greater than -0.1768.
- The calculated coefficient of lift must be greater than 0.64.
- The thickness of each aerofoil must exceed 12% ($t/c \geq 0.12$).
- No internal or external structural sections can buckle or fail due to excessive strains.
- The wing tip may not twist more than one degree.
- The wing may not deflect more than twenty percent of the span.

All the above mentioned constraints are applied by penalising either, or both fitness values via an exponential penalty method as described in Section 6.1. In addition, any aerofoil generated outside the thickness bounds of 10% to 15% are rejected immediately before any analysis is performed on the wing. The above data is summarised in Table 10.

Description	Values
Allowable Strain	0.00333
Allowed wing tip twist in degrees	1
Allowed wing deflection as a percentage span	20
Allowed wing moment (benchmark)	-0.1768
Minimum lift to be generated by the wing	0.64
Wing Mass per degree twist of wing tip	0.1
Wing Mass per deflection percent over 20	0.1
Wing Mass per failed panel	0.1
Additional C_D per over allowable aerodynamic moment	0.001
Additional C_D per less than the required minimum C_L	0.005
Penalise both fitness functions above a Drag ratio of	0.1
Penalise both fitness functions above a Mass ratio of	0.1

Table 10: Constraint and Penalty Values

7.1.3 FITNESS FUNCTIONS

The two fitness functions to be optimised are defined as Eqn 9 and Eqn 10:

$$\min(f_1): \quad f_1 = \frac{1}{(L/D)} + penalty \tag{9}$$

$$\min(f_2): \quad f_2 = W + penalty \tag{10}$$

Eqn 9 relates to the aerodynamics of the candidate wing. The Evolutionary Optimiser seeks to minimise the inverse of the lift to drag ratio with the addition of penalties which are described in Section 6.1.

Eqn 10 relates to the structural aspects of the candidate wing. This function has the units of mass and seeks to minimise the calculated structural mass of the wing. Penalties are also added to Eqn 10 which are described in Section 6.1

For both Eqns 9 and 10, the penalties are calculated based on the constraints specified in Section 7.1.2.

7.1.4 AERO-STRUCTURAL ANALYSIS

The aerodynamic and structural characteristics of the wing configurations are evaluated using the Aero-Structural Solver described in Section 5.1.

7.1.5 IMPLEMENTATION

The solution to this problem has been calculated using two approaches; the first one uses a traditional EA method with a single population model based upon a fine meshed aerodynamic model of each candidate wing. Between 1904 and 2992 aerodynamic panels were used to define the candidate wings using a fine mesh structure. The second method uses a hierarchical topology of mesh resolutions comprising three levels. The same aerodynamic resolution as was used in the single population experiments was used for the top level, a more coarse mesh model used in an intermediate aerodynamic level (between 1428 and 2244 aerodynamic panels), and a coarse mesh (between 952 and 1496 aerodynamic panels) used in the lowest model to explore the design search space.

This resulted in the coarse mesh solutions requiring roughly 4 minutes to solve for the aerodynamic pressures about a candidate wing, and 15 minutes for a fine mesh. And intermediate wing took roughly 10 minutes on a single 2.4 GHz machine.

Three P4, 2.4 GHz machines were used in the calculation and the population size for this problem was set to 30 in all levels. This was set for both the single and hierarchical solutions.

For both solution approaches, the single population and the hierarchical method, the structural model panel density was kept as a function of the internal geometry and was not based upon the level of model complexity. For a description of the method used, please refer to Section 5.3.

7.1.6 RESULTS

The algorithm was run for 500 function evaluations and took 36 hours to compute on a cluster of three machines. Figure 47 shows the Pareto fronts obtained by using the two approaches. The Pareto members selected for further investigation are also indicated. By inspecting Figure 47 it can be seen that the use of a multi-fidelity (hierarchical) approach gives an overall lower front as compared to a single model approach. Both approaches give results which lie to the left of the benchmark value for the MALE wing.

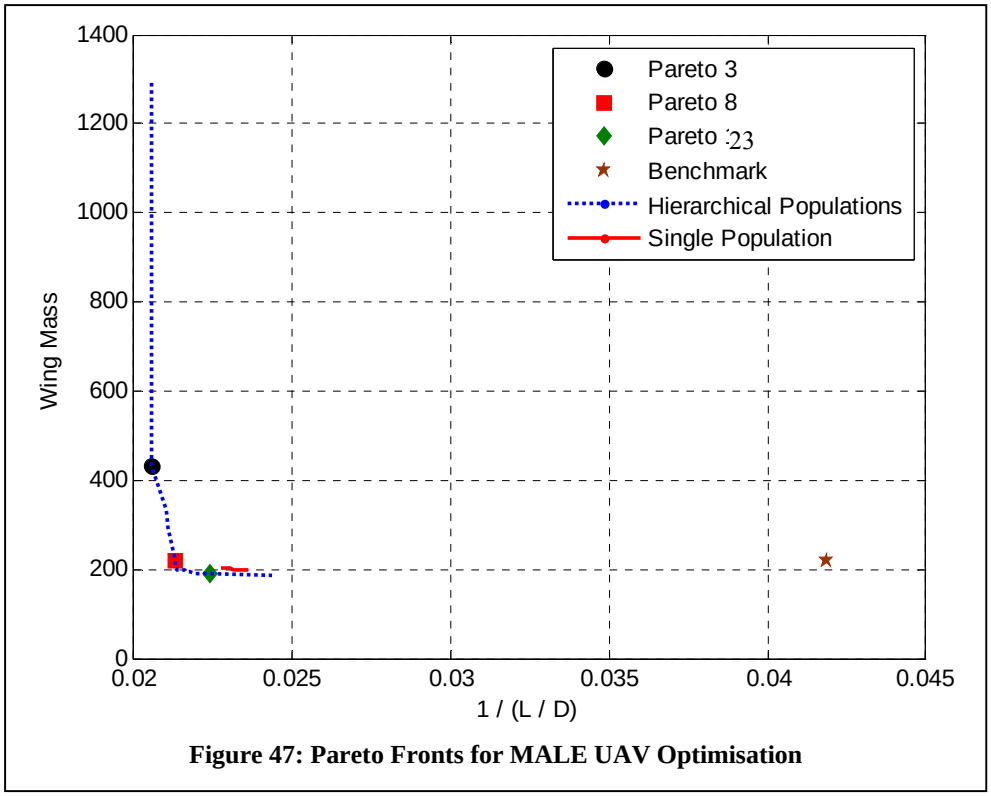

Figure 47: Pareto Fronts for MALE UAV Optimisation

The algorithm progress for the hierarchical approach is shown in Figure 48. The fitness for all levels decreases with time and it can be seen that after 350 evaluations, the fitness of each level reaches a steady state value indicating an optimum solution given the constrains imposed.

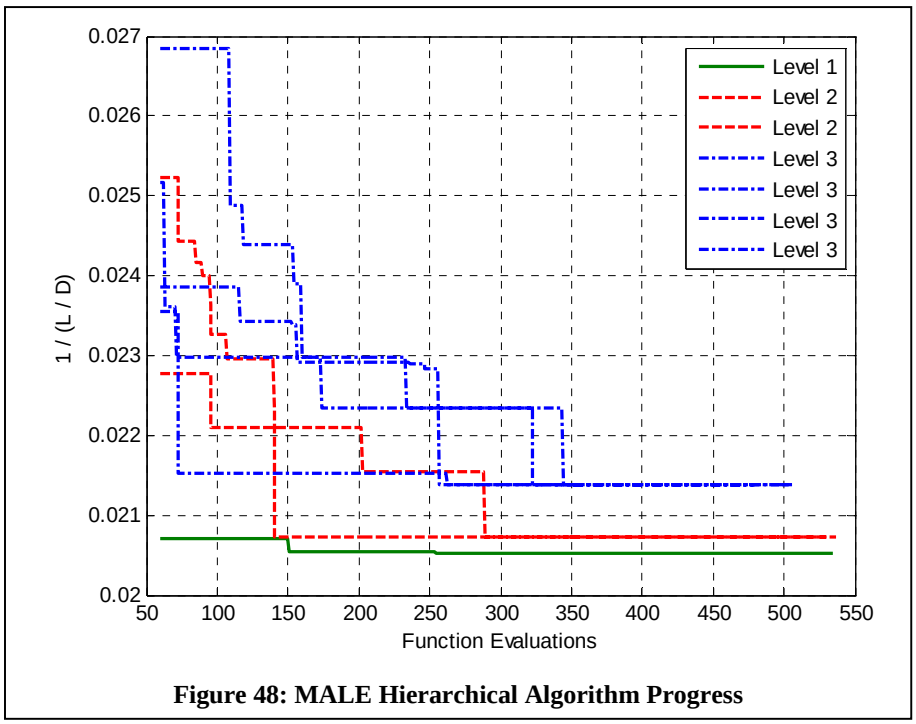

Figure 48: MALE Hierarchical Algorithm Progress

The optimisation was run for a second time but with only one population to test the validity of the hierarchical procedure employed by the HAPMOEA algorithm. The results are shown in Figure 49.

The algorithm progress shown in Figure 49 relates to the Pareto front shown as a solid red line on Figure 47.

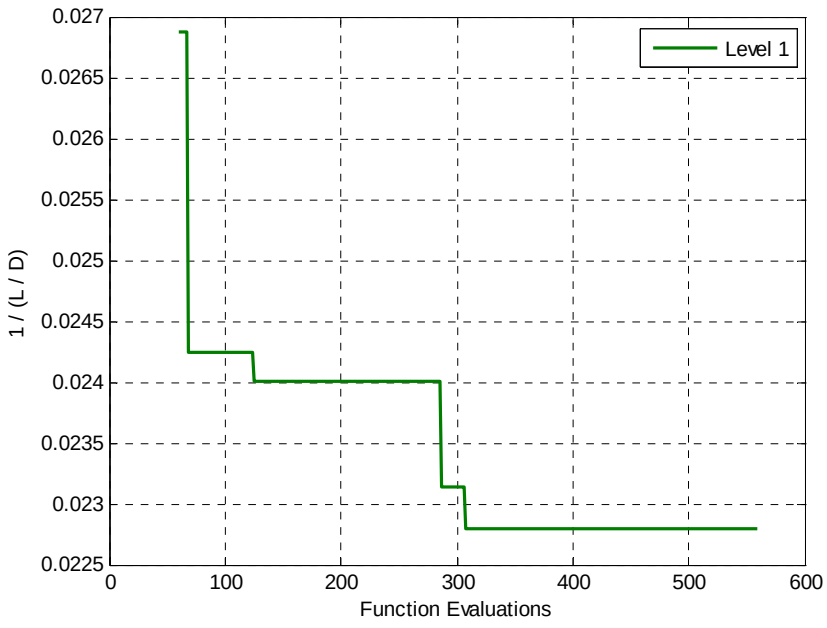

Figure 49 MALE Single Population Algorithm Progress

From Figures 47 to 49 it can be seen that the performance for the Hierarchical scheme was higher than that of the single population scheme over the same number of function evaluations of the Level 1 node. The hierarchical approach therefore yields better solutions for the same number of function evaluations of the Level 1 node.

Three wings are taken for further evaluation (Pareto members 3, 8 and 23) from the hierarchical optimisation strategy results to illustrate the two objective extremes and a compromise between the two results. According to the optimiser, Pareto 3 has the best aerodynamics, Pareto 23 the best structural response to the aerodynamic loading and 8 lies between the two solutions.

Table 11 summarises and compares the values for the design variables and the objective functions for these three geometries against the benchmark.

Description	**Benchmark**	**PM 3**	**PM 8**	**PM 23**
Angle of Attack, *α (deg)*	4	4.055	3.957	5.16798
Wing Semi Span, *b (m)*	12.542	13.871	13.385	12.4694
Root Chord, c_r *(m)*	1.646	1.638	1.641	1.66618
Wing Inboard Leading Edge Sweep, $\Lambda_{rc,}$ *(rad)*	0.039	0.0871	0.0694	0.0801
Wing Outboard Leading Edge Sweep, Λ_{ct} *(rad)*	0.039	0.0255	0.0486	0.0105
Chord Ratio at Break, $\lambda_{rc,}$	0.444	0.422	0.448	0.427
Chord Ratio at Tip, λ_{ct}	0.444	0.475	0.388	0.477
Crank Location, $crank_l$	0.731	0.583	0.667	0.787
Number of Spars, *Ns*	2	1	2	2
Number of Ribs. *Ns*	10	11	10	9
Rib Root Thickness, *Rrt (m)*	0.005	0.00351	0.00465	0.00435
Rib Root Thickness Taper Ratio, *RrTr*	0.25	0.182	0.287	0.243
Spar Root Thickness, *Srt (m)*	0.08	0.0805	0.0576	0.0571
Spar Root Thickness Taper Ratio, *SrTr*	0.05	0.131	0.154	0.019
Wing Skin Root Thickness, *WsRt (m)*	0.001	0.000885	0.000953	0.00199
Wing Skin Thickness Tip Taper Ratio, *WstTr*	0.1	0.122	0.1	0.0541
Wing Skin Thickness Trailing Taper Ratio, *WsTre*	0.1	0.106	0.0608	0.108
Spar Cap Root Area, *Sc* (m^2)	0.00375	0.00908	0.00314	0.00314
Rib Cap Root Area, *Rc*(m^2)	0.0015	0.00123	0.00175	0.00105

Table 11: Summary and comparison of design variables for MALE UAV

Figure 50 shows a top view of the wings selected for further analysis and Figures 51 to 53 compare the baseline aerofoils and the aerofoil sections of each Pareto member at the root, crank and tip.

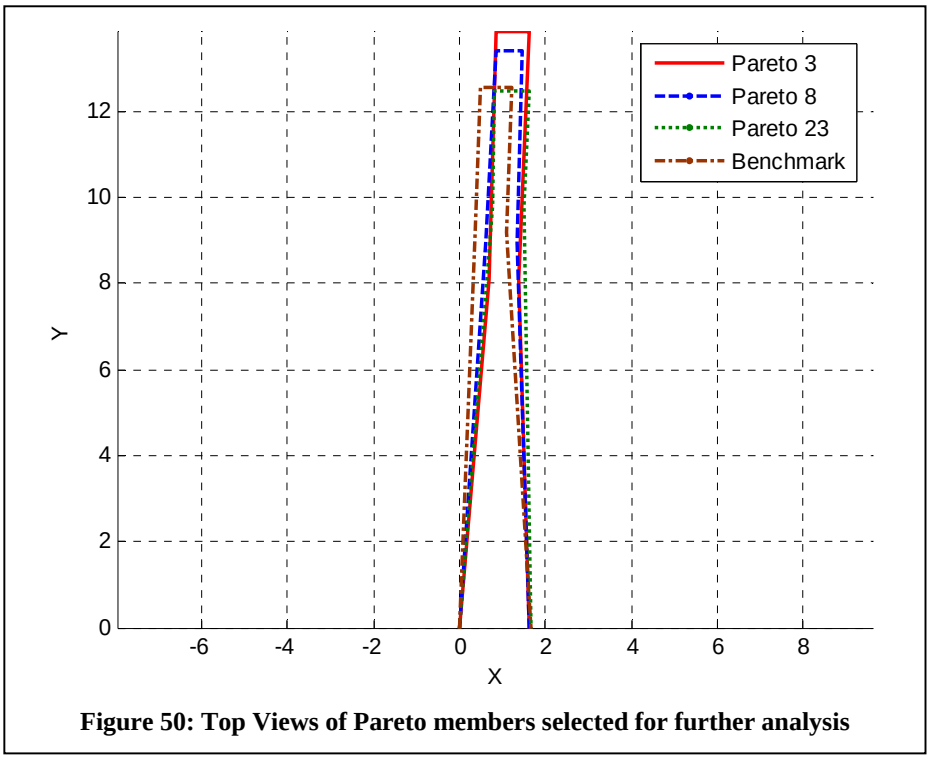

Figure 50: Top Views of Pareto members selected for further analysis

On inspecting Figure 50, the optimiser found that the original layout of the wing favoured the structural constraints more than the aerodynamics and changed the wing span and crank location between the different Pareto members to achieve better aerodynamics.

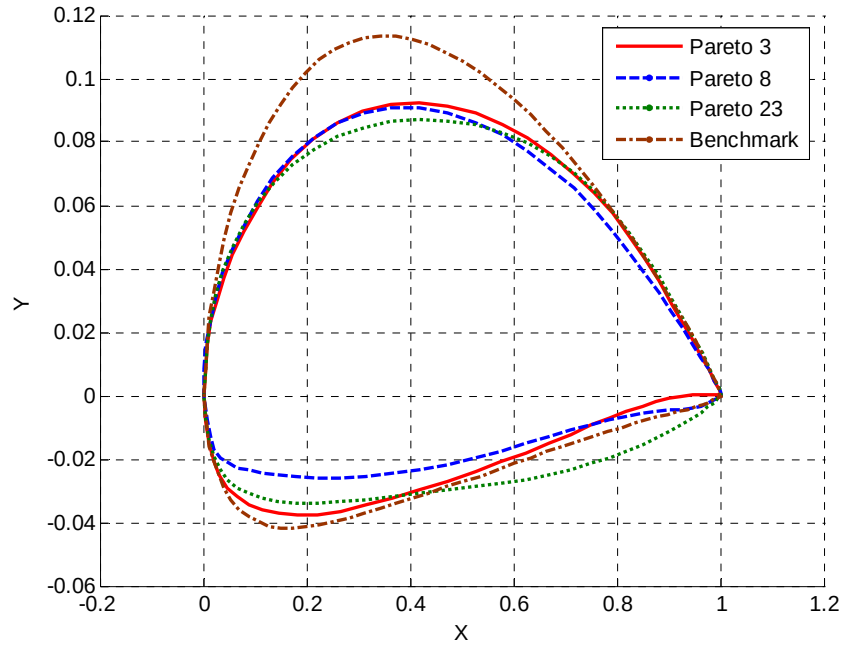

Figure 51: Selected MALE Pareto member Root Aerofoil Sections

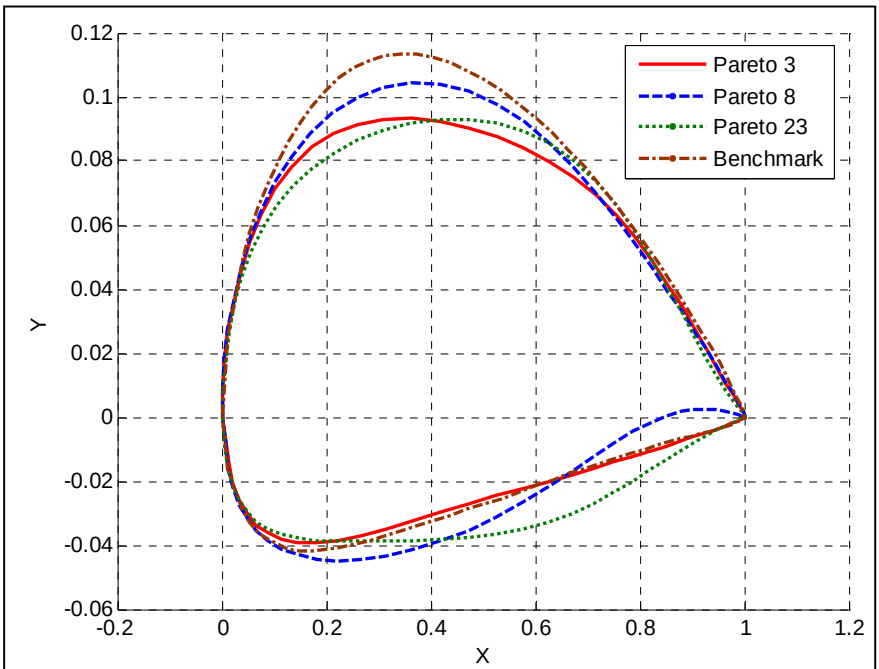

Figure 52: Selected MALE Pareto member Break Aerofoil Sections

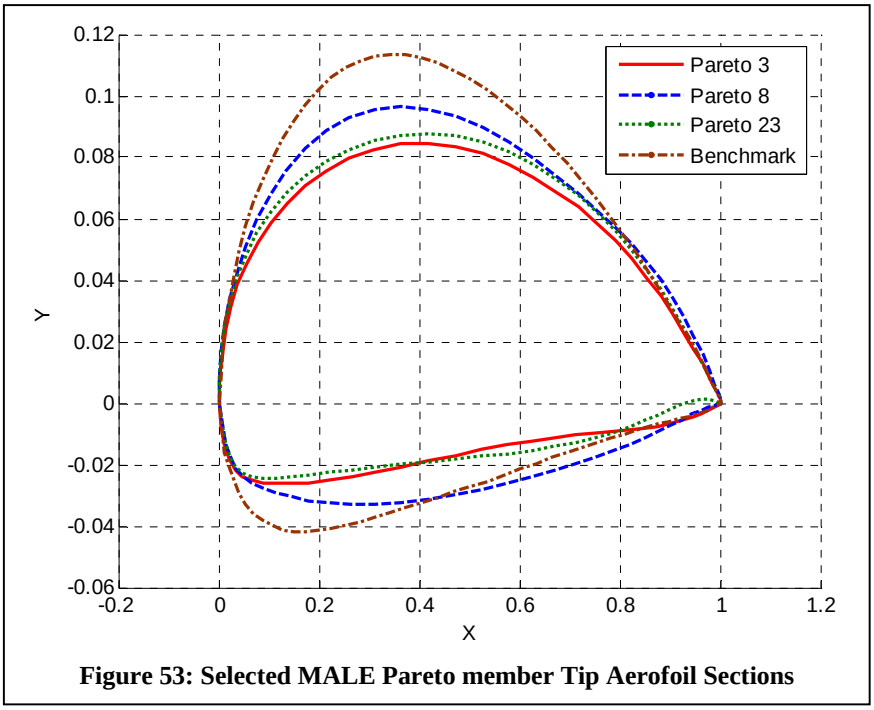

Figure 53: Selected MALE Pareto member Tip Aerofoil Sections

It can be seen that classical aerodynamic shapes have been evolved, even considering that the optimisation was started completely from random and the evolution algorithm had no problem specific knowledge of appropriate solution types.

Of interest is that all the aerofoil sections generated by the HAPMOEA code and shown in Figures 51 to 53 have a lower *t/c* ratio than that of the benchmark aerofoil section. There are only slight differences between the root aerofoil sections describing the Pareto members selected in Figure 51.

A Mach number sweep was performed at a constant angle of attack for the selected Pareto members and the results are displayed in Figure 54 for coefficient of drag and Figure 55 for coefficient of lift. The benchmark wing is included for comparison.

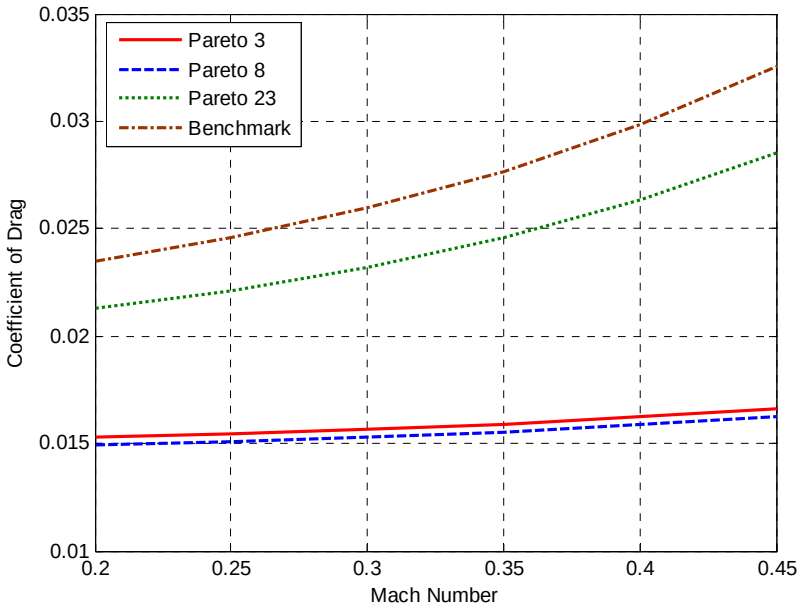

Figure 54: Coefficient of Drag vs. Mach number for selected MALE Pareto members and Benchmark

Over the range of Mach numbers investigated, the Pareto members have lower drag coefficient than the benchmark wing. The Pareto members three and eight operate at an almost constant drag value over the range of Mach numbers.

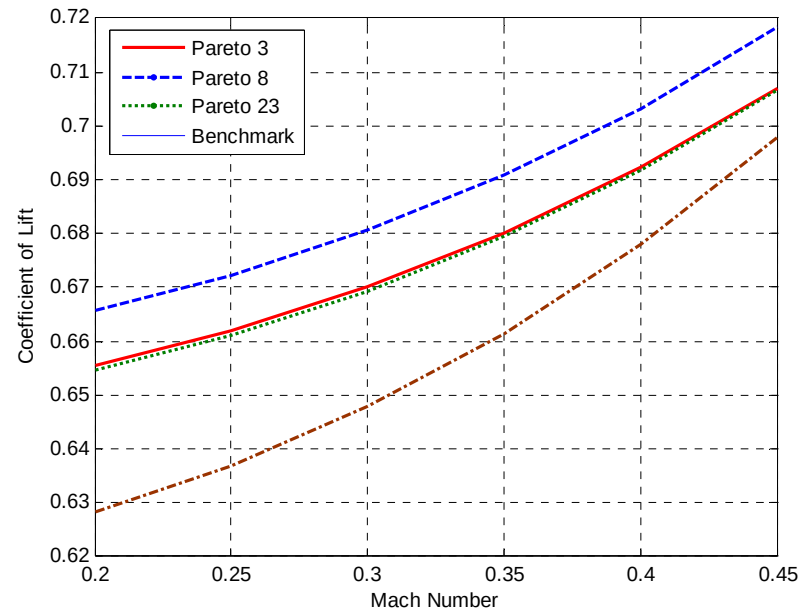

Figure 55: Coefficient of Lift vs. Mach number for selected MALE Pareto members and Benchmark

As the Lift penalty function described in Section 6.1.1 only penalised candidate wing which produced a lift coefficient lower than the required value to maintain the cruise altitude and velocity, the selected Pareto

member wings all produce more than the required lift. This extra lift value is small through compared to the overall required force, being roughly 0.02 for Pareto member eight compared to the benchmark.

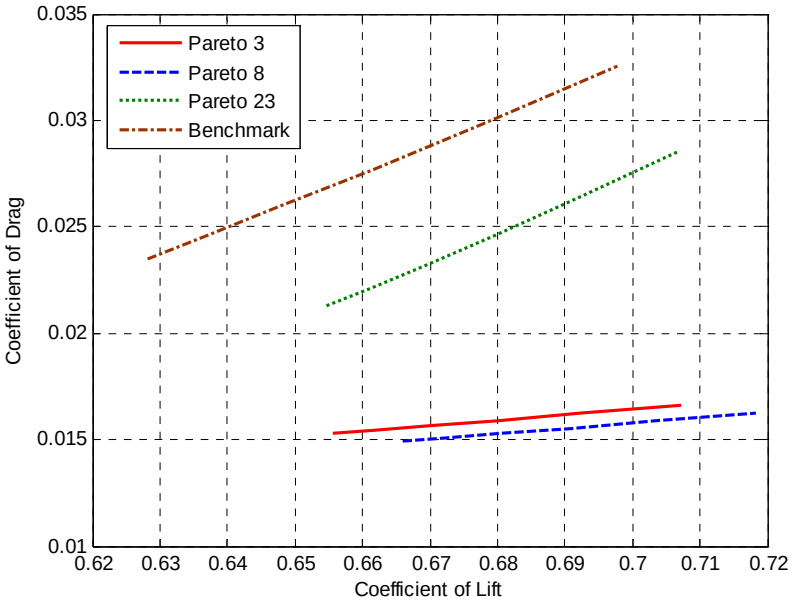

Figure 56: Coefficient of Lift vs. Coefficient of Drag for selected MALE Pareto members and Benchmark.

When the Coefficient of Lift is plotted versus the Coefficient of Drag for the selected Pareto members and the benchmark MALE wing in Figure 56, one can see that the performance of all the wings belonging to the Pareto front is higher than that of the benchmark wing. The required Coefficient of Lift of 0.64 is met at a lower Coefficient of Drag with all the selected Pareto member wings.

The selected MALE UAV Pareto member are further analysed by performing an Angle of Attack sweep between three and six degrees and displayed in Figures 57 and 58. For all the analyses performed, the Mach number was kept constant at 0.3663, the operating velocity of the benchmark vehicle.

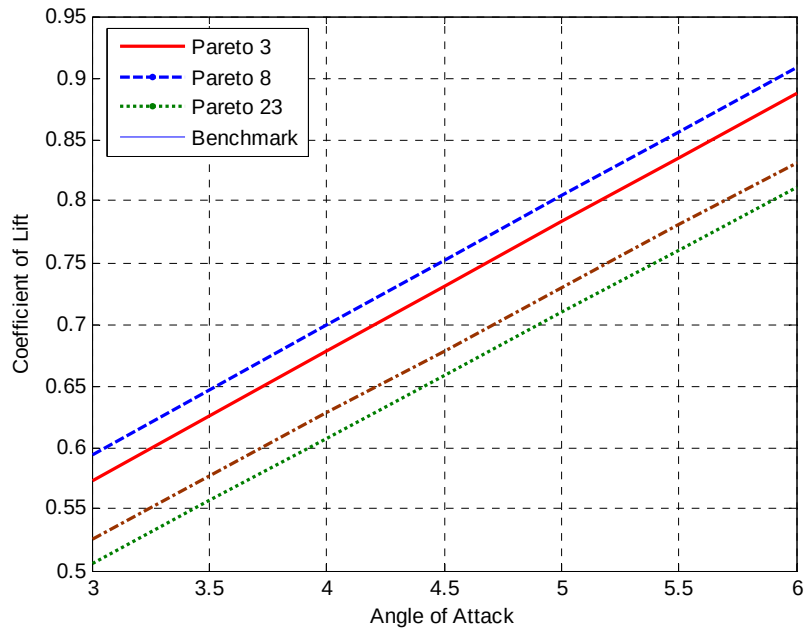

Figure 57: Coefficient of Lift vs. Angle of Attack for selected MALE Pareto members and Benchmark

For all the wings tested, the Coefficient of Lift shown in Figure 57 varied in almost a linear fashion over the angles tested. Furthermore, all the wings behaved in a similar fashion in that the gradients of the Lift slopes are all very similar.

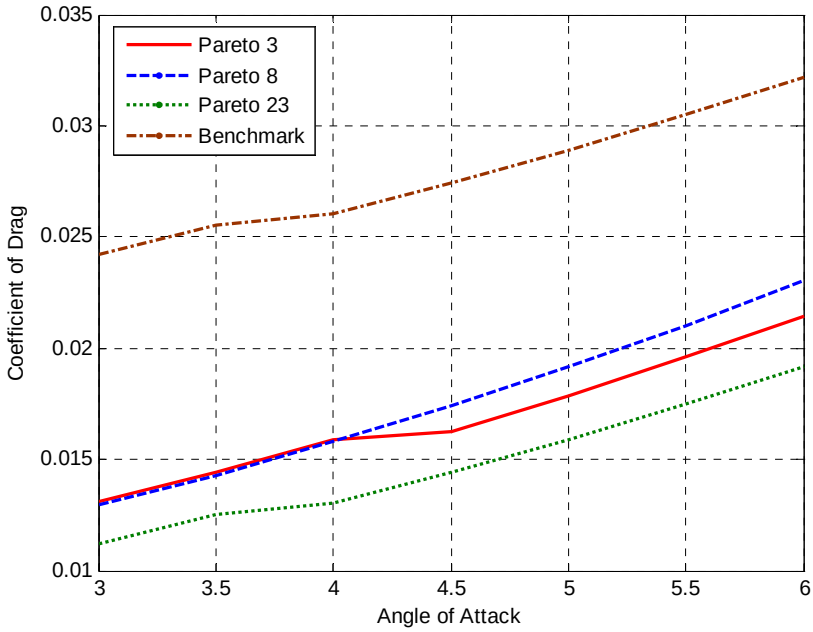

Figure 58: Coefficient of Drag vs. Angle of Attack for selected MALE Pareto members and Benchmark

As with the Mach sweep performed and displayed in Figure 54, the selected Pareto members displayed and tested in Figure 58 have a lower Coefficient of Drag over all tested angles of attack. Between the angles of three and four, Pareto 23 and the bench exhibit the same reduction in drag. Pareto eight does not exhibit a similar drop over the angle range covered while Pareto three exhibits the reduction between four and four and a half degrees.

Figures 59 and 60 plot the second order pressure coefficients for the selected Pareto wings.

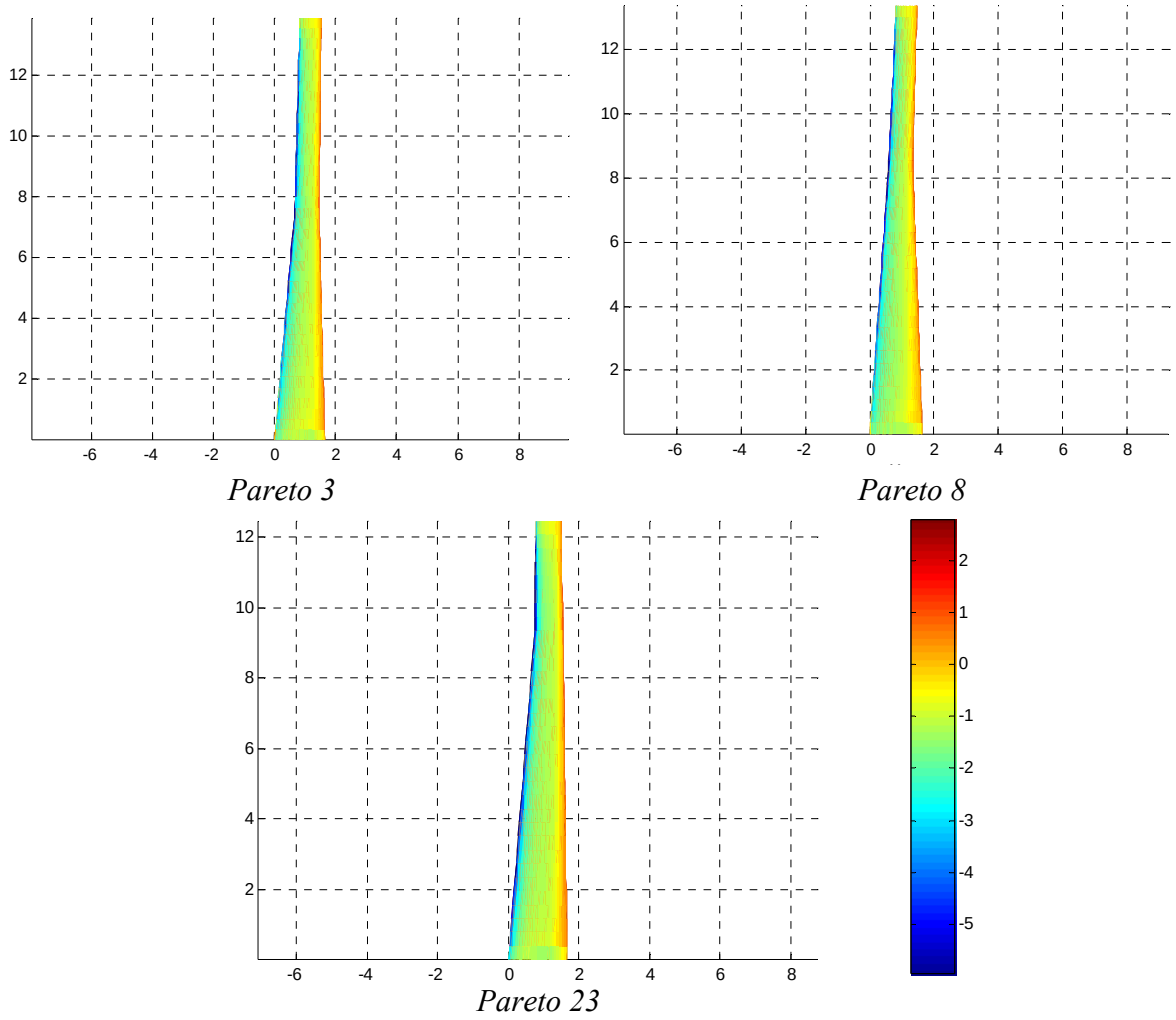

Figure 59: External Pressure Coefficients for selected MALE Pareto Members – Upper Surface

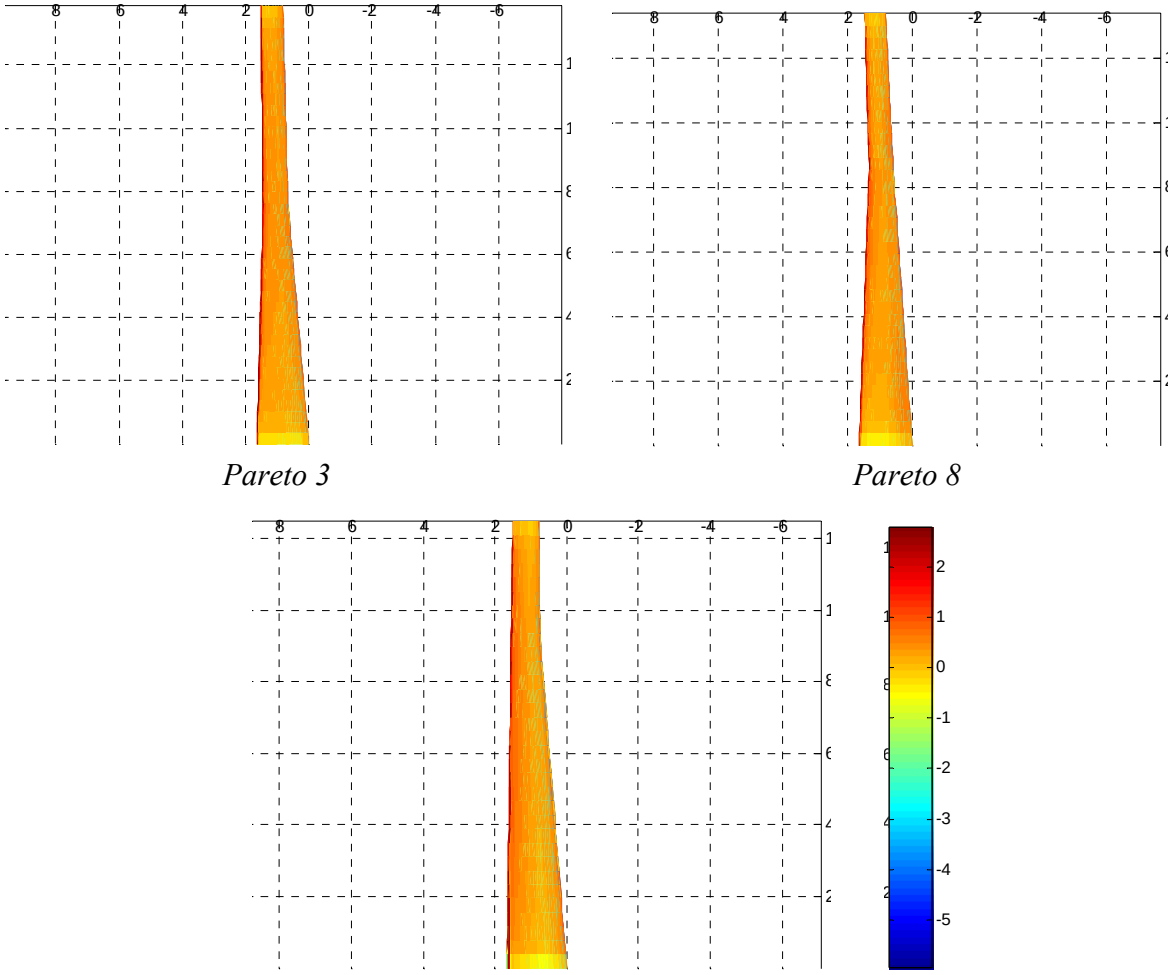

Figure 60: External Pressure Coefficients for selected MALE Pareto Members – Lower Surface

In comparison with the MALE UAV benchmark wing pressure coefficients displayed in Figures 27 and 28, the wings selected from the Pareto set produce higher pressures along the leading edge of the wings. The maximum coefficient of pressure for the benchmark wing is negative three while the Pareto members all produce coefficients of pressure as high as negative five. This could be due to the smaller *t/c* ratio of the Pareto aerofoils evident in Figures 51 to 53. The pressures generated along the lower surface of the Pareto wings are also smaller in magnitude than that of the benchmark.

A larger resultant lift force is therefore created by the Pareto member wings and this is in good agreement with the high performance of the wings noted when the Coefficients of Lift and Drag were plotted in Figure 56.

Figures 61 to 63 show the deflected Pareto wings. The original wing position and internal structure is shown as a wire frame for comparison.

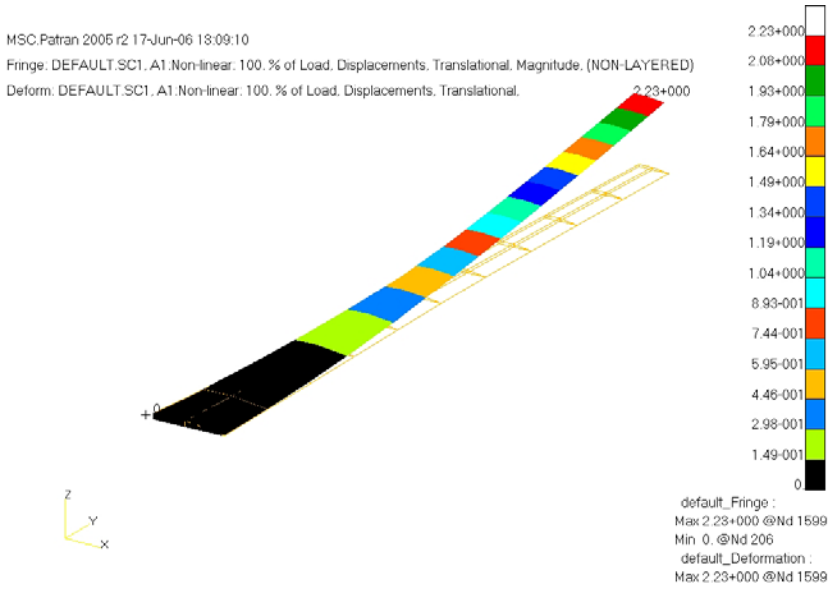

Figure 61: MALE Pareto 3 Displacement

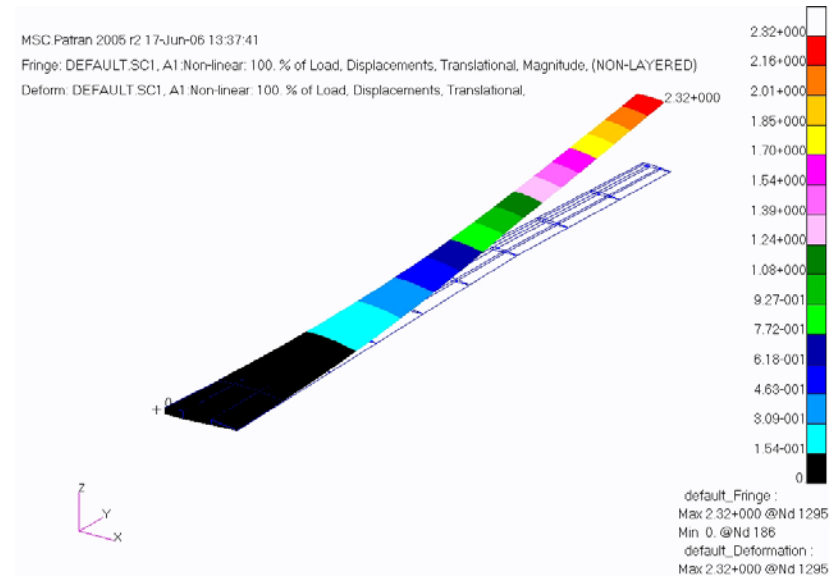

Figure 62: MALE Pareto 8 Displacement

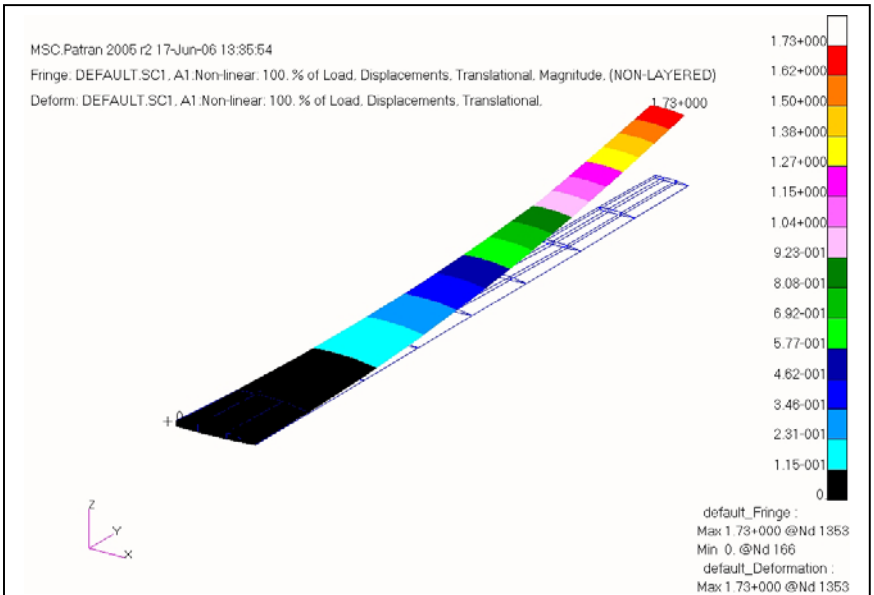

Figure 63: MALE Pareto 23 Displacement

All the MALE wings deflect nonlinearly. From the Figures above it can be seen that the deflection at the wing tips is greater than the thickness of the aerofoil sections and hence wing spars. The nonlinear analysis solutions, selected for the MSC.Nastran® structural calculations, was therefore necessary as the deflections encountered are too large for a Linear Static analysis and if used, would have yielded incorrect results.

An analysis of the strains produced by the aerodynamic forces is shown in Figures 64 to 66.

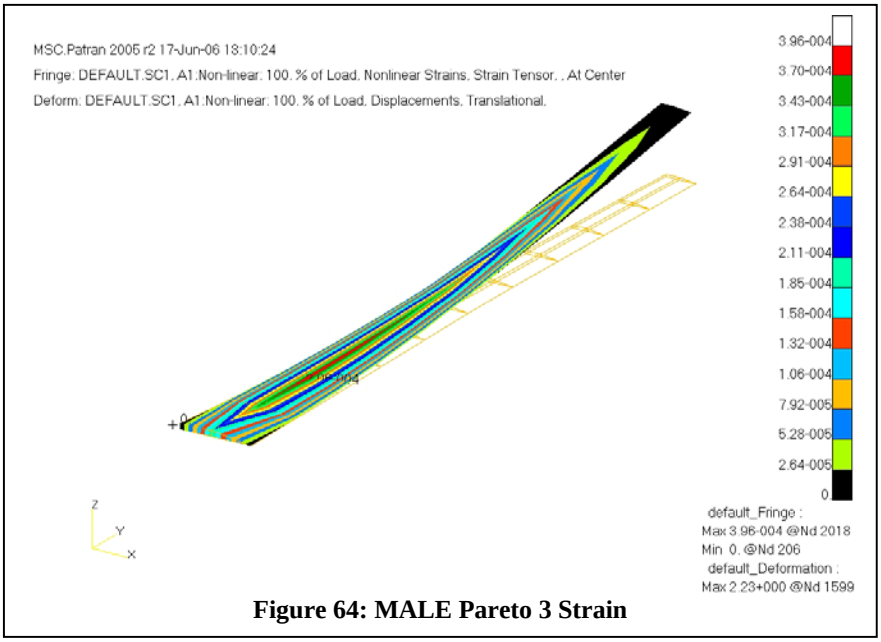

Figure 64: MALE Pareto 3 Strain

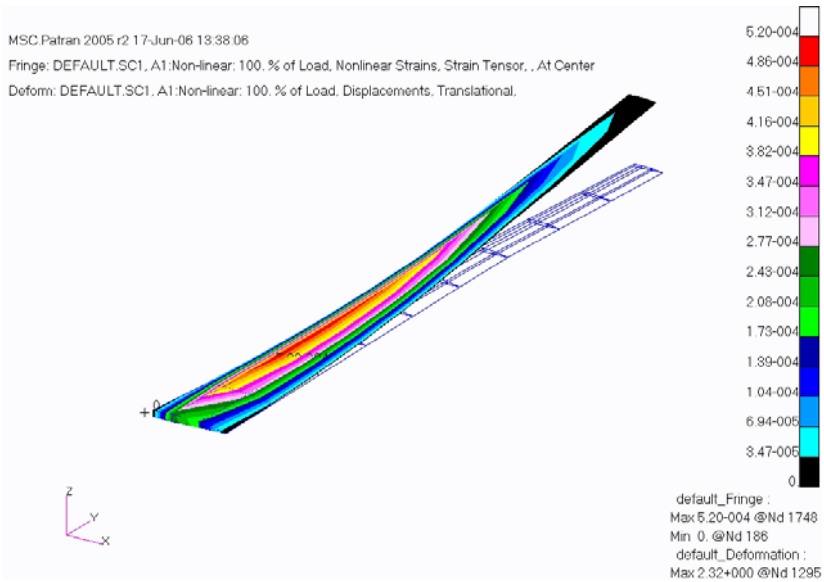

Figure 65: MALE Pareto 8 Strain

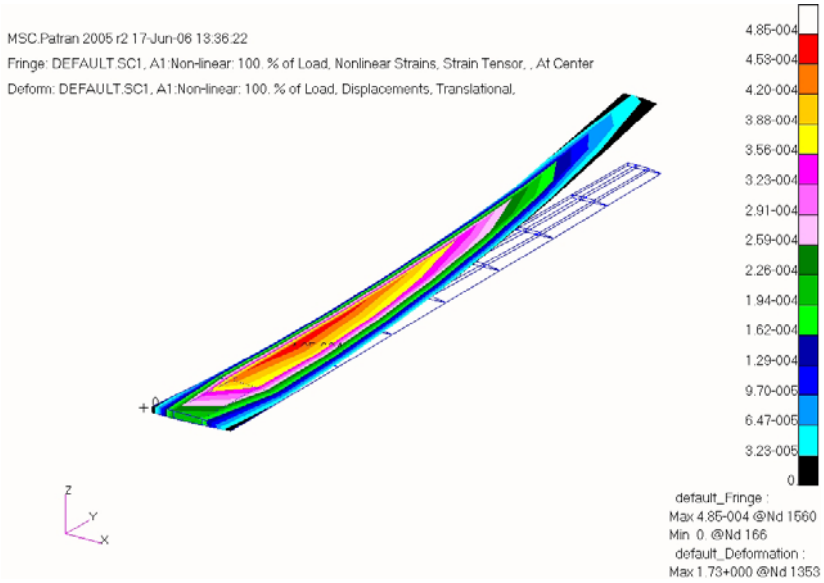

Figure 66: MALE Pareto 23 Strain

The aerodynamic load generated by the aerofoil sections cause the candidate wings to want to rotate about the wing root (X axis). As the wings were fixed in all directions and all rotations at the wing root, the maximum strain does not occur at the wing root but rather a distance from the root, where the rotation occurs.

	Pareto 3	Pareto 8	Pareto 23	Benchmark
Deflection (%)	16	17.3	13.8	12.5
Maximum Strain	0.000396	0.00052	0.000485	0.000403
Mass (kg)	233.735	217.873	185.1	220.9
L/D	43.367	44.4	44.25	23.9
Mass Penalty (kg)	40	0	0	0
Drag Penalty	0.0027	0	0	0

Table 12: Summary of Displacement, Strain and Mass for Selected MALE Pareto members and the Benchmark

A summary of each of the Pareto and benchmark wing overall characteristics is shown in Table 12 for comparison.

It can be noted from Table 12 that all the Pareto member wings out-performed the benchmark wing on L/D ratio with Pareto members 8 and 23 had weights which were lower than that of the benchmark wing when the penalty values were included in the overall wing mass. All the wings had strain values which were below the maximum allowable strain defined in Table 10.

7.2 HIGH ALTITUDE LONG ENDURANCE (HALE) UAV WING DESIGN AND OPTIMISATION

In the second case, the detailed analysis and optimisation of a wing for a high altitude long endurance (HALE) UAV application is considered. This is a multi-objective problem where the goal is to maximise the lift-to-dag ratio and minimise wing weight. The operating conditions and data for the baseline wing are based on reference (NORTHROP-GRUMMAN 2006)The aircraft has a wingspan of approximately 17 *m*, a mean chord of approximately 2.43 *m,* a wing area of *50.19* m^2 and a plan form shape with 5.9 *deg* sweep. A breakdown of the benchmark wing can be found in Table 13.

The aircraft is assumed to operate at $M_\infty = 0.5983$ at a cruise altitude of 15840 *m*. It is also assumed that this UAV uses a single aerofoil, the LRN1015 aerofoil, as the only wing section aerofoil along the wing span.

7.2.1 DESIGN VARIABLES AND CONSTRAINTS.

Similar to the previous test case, the wing geometry is represented by three aerofoil sections consisting of sixteen variables each, eight variables that describe the wing planform and eleven variables to describe the internal structure. Once again, 6 free control points on the mean line and 10 free control points on the thickness distribution were used to describe each of the aerofoil sections.

The benchmark, upper and lower bounds for the design variables are indicated in Table 13.

Description	**Benchmark**	**Lower Bound**	**Upper Bound**
Angle of Attack, α *(deg)*	5.75	0	6
Root Chord, c_r *(m)*	2.432	2.375	2.5
Wing Inboard Leading Edge Sweep, $\Lambda_{rc,}$ *(rad)*	0.102972	0	0.1745
Wing Outboard Leading Edge Sweep, Λ_{ct} *(rad)*	0.102972	0	0.1745
Chord Ratio at Break, $\lambda_{rc,}$	0.78	0.55	0.9
Chord Ratio at Tip, λ_{ct}	0.287	0.2	0.8
Crank Location, $crank_l$	0.0881	0.06	0.6
Number of Spars, *Ns*	5	3	7
Number of Ribs. *Ns*	16	12	18
Rib Root Thickness, *Rrt (m)*	0.0015	0.001	0.005
Rib Root Thickness Taper Ratio, *RrTr*	0.05	0.01	0.15
Spar Root Thickness, *Srt (m)*	0.09	0.045	0.091
Spar Root Thickness Taper Ratio, *SrTr*	0.05	0.01	0.15
Wing Skin Root Thickness, *WsRt (m)*	0.001	0.0001	0.05
Wing Skin Thickness Tip Taper Ratio, *WstTr*	0.01	0.0095	0.15
Wing Skin Thickness Trailing Taper Ratio, *WsTre*	0.01	0.0095	0.15
Spar Cap Root Area, *Sc* (m^2)	0.012	0.004	0.0125
Rib Cap Root Area, *Rc*(m^2)	0.0005	0.00045	0.002

Table 13: Structural and Planform Design Variables for the HALE UAV wing

7.2.2 DESIGN CONSTRAINTS AND PENALTIES

The constraints which must be satisfied for each candidate wing are indicated in Table 14 along with the rates with which wings which fail the constraints are penalised.

Description	**Values Allowed**
Allowable Strain	0.00333
Allowed wing tip twist in degrees	1
Allowed wing deflection as a percentage span	20
Allowed wing moment (benchmark)	-0.3041
Minimum lift to be generated by the wing	0.89
Wing Mass per degree twist Penalty Values	0.1
Wing Mass per degree over 20 span	0.1
Wing Mass per failed panel	0.1
Additional *Cd* per over allowable	0.001
Additional *Cd* per less than the required minimum	0.005
Penalise both fitness functions above a Drag ratio of	0.1
Penalise both fitness functions above a Mass ratio of	0.1

Table 14: Constraints and Penalty Rates

All the above mentioned constraints are applied by penalising either fitness values via a linear penalty method as described in Section 6.1. In addition, any aerofoil generated outside the thickness bounds of 10% to 15% are rejected immediately before any analysis is performed on the wing.

7.2.3 FITNESS FUNCTIONS

The two fitness functions to be optimised are defined as Eqn 11 and Eqn 12:

$$\min(f_1): \quad f_1 = \frac{1}{(L/D)} + penalty \tag{11}$$

$$\min(f_2): \quad f_2 = W + penalty \tag{12}$$

Eqn 11 relates to the aerodynamics of the candidate wing. The Evolutionary Optimiser seeks to minimise the inverse of the lift to drag ratio with the addition of penalties which are described in Section 6.1.

Eqn 12 relates to the structural aspects of the candidate wing. This function has the units of mass and seeks to minimise the calculated mass of the wing. Penalties are also added to Eqn 12 which are described in Section 6.1

For both Eqns 11 and 12, the penalties are calculated based on the constraints specified in Section 7.1.2.

7.2.4 AERO-STRUCTURAL ANALYSIS

The aerodynamic and structural characteristics of the wing configurations are evaluated using the Aero-Structural Solver described in Section 5.1 and represented in Figure 67.

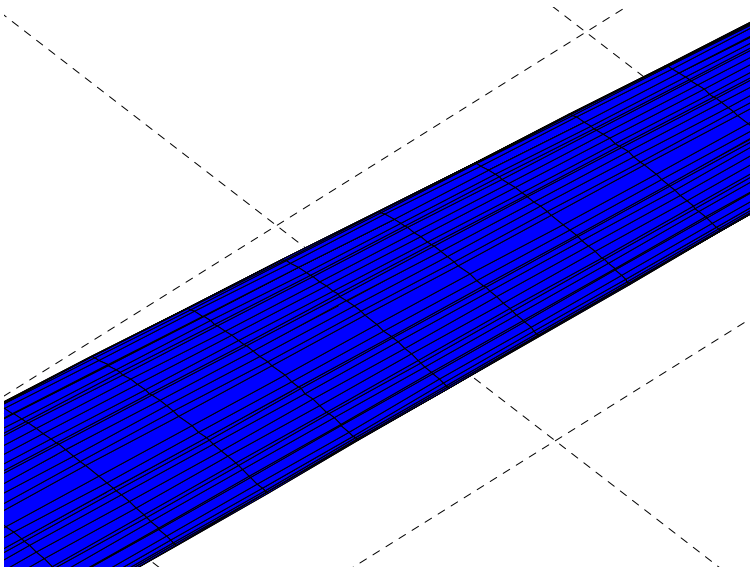

Figure 67: Aerodynamics Model for HALE UAV

7.2.5 IMPLEMENTATION

A single optimisation was performed for the HALE UAV wing. This optimisation used a hierarchical approach with three levels and seven populations. The top level (Level 1) used a fine mesh of between 2992 and 4624 aerodynamic panels to calculate the pressures about the candidate wings. A more coarse mesh model was used in the intermediate aerodynamic level (between 2244 and 3468 aerodynamic panels), and a coarse mesh (between 1496 and 2312 aerodynamic panels) used in the lowest mode to explore the design search space.

Three P4, 2.4 GHz machines were used in the calculation and the population size for this problem was set to 30 in all levels and for both the single and hierarchical solutions.

The structural model panel density was kept as a function of the internal geometry and was not based upon the level of model complexity.

7.2.6 RESULTS

The algorithm was run for 300 function evaluations and took in average three days to compute on a cluster of three, 2.4 GHz machines. Figure 68 compares some of the members of the Pareto front and the baseline geometry. Figure 69 shows the algorithm progress for objective one, each step in the figure roughly corresponds to migration step- good information from the bottom levels have been seeded to the upper levels. Figures 71 to 73 compare the aerofoils at root break and tip for each of the members of the Pareto front and the aerofoil for the baseline geometry. Table 15 indicates the final values of design variables and objective functions for the baseline geometry and some members of the Pareto front.

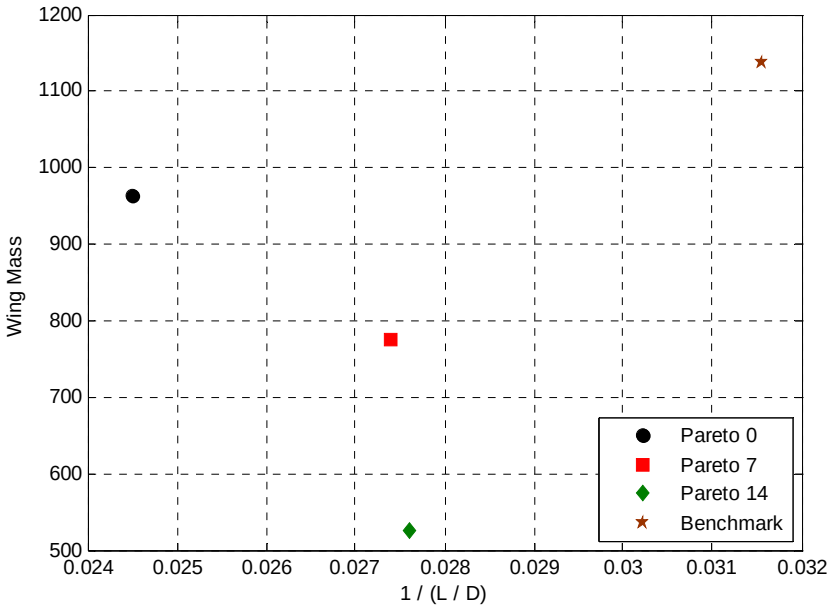

Figure 68: Pareto Selected HALE Members and Benchmark

The Pareto selected HALE members are shown against the benchmark mass and inverse of the L/D ratio in Figure 68. From the above Figure, the selected Pareto members outperform the benchmark wing.

The algorithm progress for the HALE UAV wing optimisation is shown in Figure 69. It can be seen that the Level 1 fitness decreases with function evaluations performed.

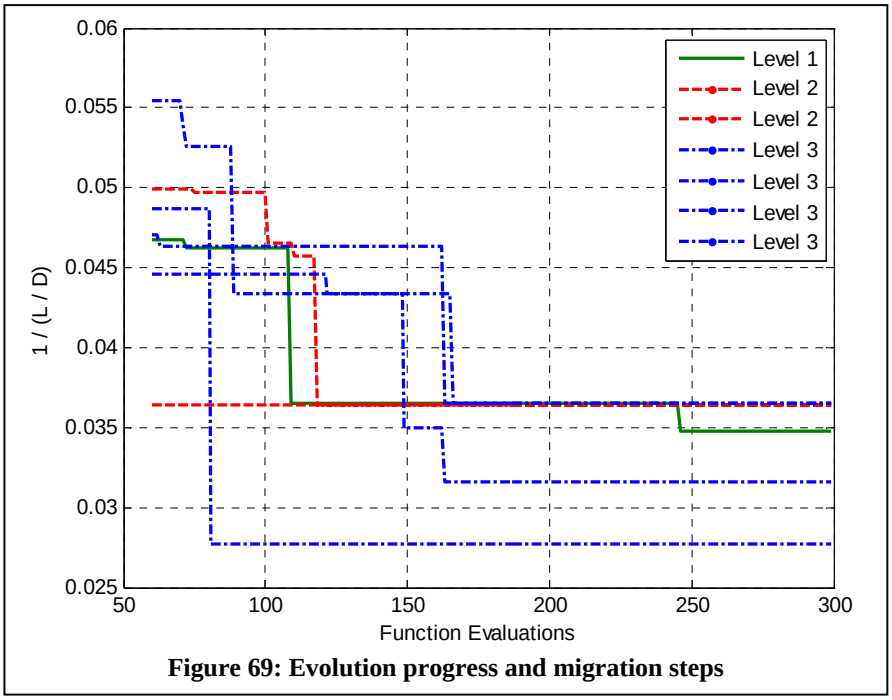

Figure 69: Evolution progress and migration steps

Table 15 summarises and compares the values for the design variables for the three selected geometries against the benchmark.

Description	**Benchmark**	**PM 0**	**PM 7**	**PM 14**
Angle of Attack, α *(deg)*	5.75	5.427	5.716	5.428
Wing Semi Span, *b (m)*	16.941	17.768	16.586	16.199
Root Chord, c_r *(m)*	2.432	2.403	2.401	2.389
Wing Inboard Leading Edge Sweep, $\Lambda_{rc,}$ *(rad)*	0.103	0.111	0.0769	0.0996
Wing Outboard Leading Edge Sweep, Λ_{ct} *(rad)*	0.103	0.0141	0.0799	0.0165
Chord Ratio at Break, $\lambda_{rc,}$	0.78	0.744	0.804	0.845
Chord Ratio at Tip, λ_{ct}	0.287	0.255	0.283	0.255
Crank Location, $crank_l$	0.0881	0.124	0.117	0.14
Number of Spars, *Ns*	5	4	3	3
Number of Ribs. *Ns*	16	14	15	15
Rib Root Thickness, *Rrt (m)*	0.0015	0.00122	0.0024	0.0013
Rib Root Thickness Taper Ratio, *RrTr*	0.05	0.023	0.0215	0.03
Spar Root Thickness, *Srt (m)*	0.09	0.0906	0.091	0.0904
Spar Root Thickness Taper Ratio, *SrTr*	0.05	0.128	0.133	0.12
Wing Skin Root Thickness, *WsRt (m)*	0.001	0.000975	0.0103	0.00119
Wing Skin Thickness Tip Taper Ratio, *WstTr*	0.01	0.0645	0.0962	0.0942
Wing Skin Thickness Trailing Taper Ratio, *WsTre*	0.01	0.0569	0.0391	0.0501
Spar Cap Root Area, *Sc* (m^2)	0.012	0.008	0.00655	0.00508
Rib Cap Root Area, *Rc*(m^2)	0.0005	0.000867	0.00131	0.00102

Table 15: Summary and Comparison of HALE UAV

Planform Shapes

Figure 70 shows the planform shapes for the selected HALE Pareto members along with the Benchmark. From the Figure one is able to see that all the wings have a high aspect ratio and that the reference area was kept constant.

The evolutionary optimiser produced wings which seemed to favour wings with a lower leading edge sweep angle. The crank location between the Pareto members and the Benchmark wing are all at a rather consistent point in the wing.

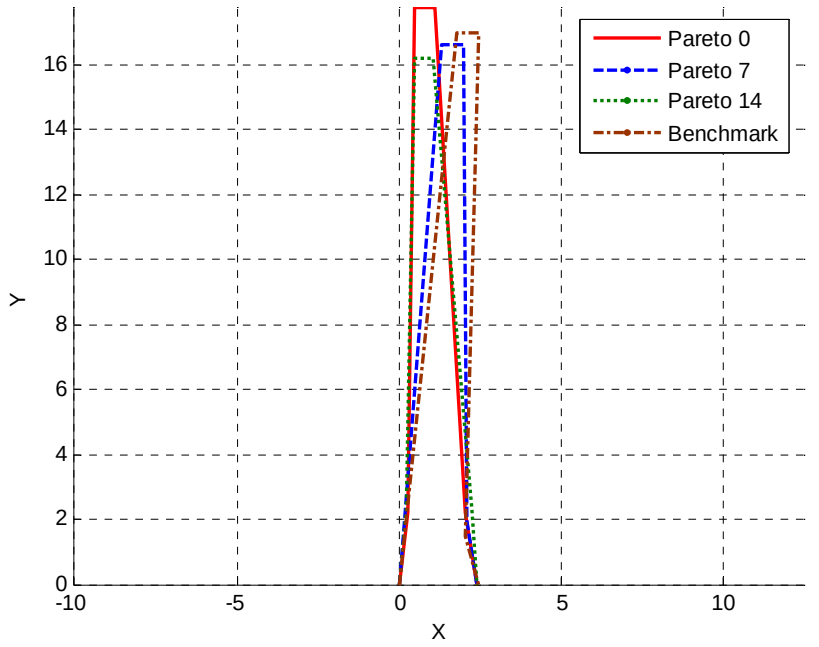

Figure 70: HALE Pareto and Benchmark planform shapes

Aerofoil Sections

The evolutionary optimiser determined a number of different aerofoil sections when constructing Pareto members. The root, crank and tip aerofoil sections are shown below for Pareto members 0, 7 and 14 along with the Benchmark LRN 1015 aerofoil section.

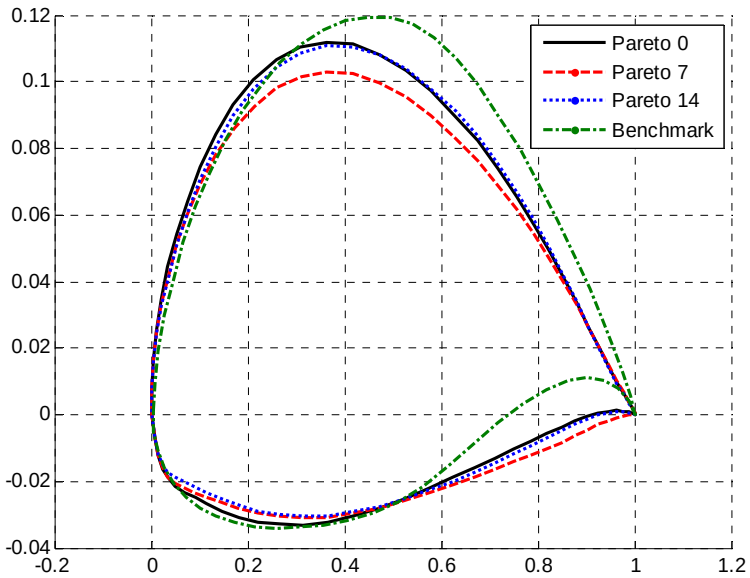

Figure 71: Comparison of Root aerofoil geometries for selected Pareto Members and baseline

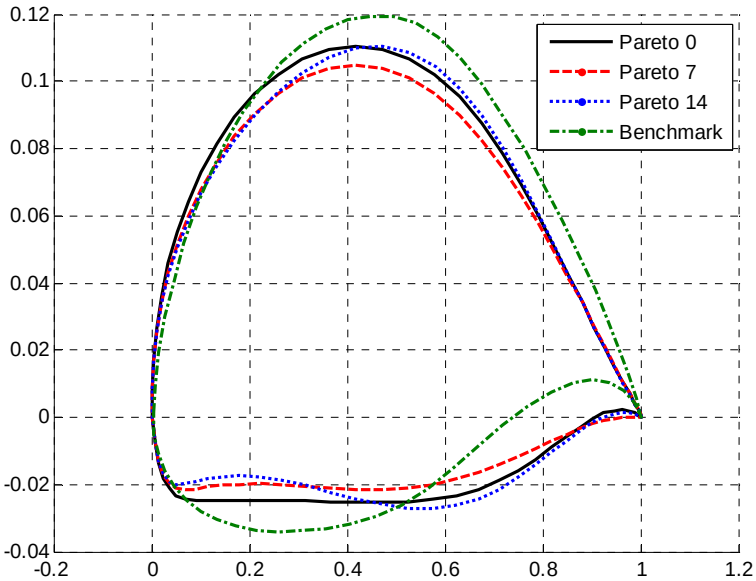

Figure 72: Comparison of Crank aerofoil geometries for selected Pareto Members and baseline

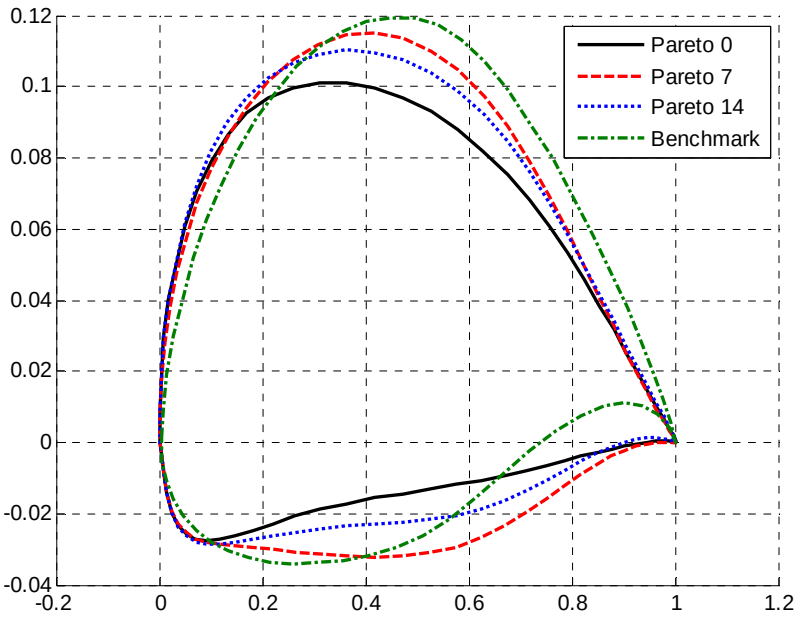

Figure 73: Comparison of Tip aerofoil geometries for selected Pareto Members and baseline

From the above Figures 71 to 73, one can see the large variation in aerofoil shapes. The variations though seem to have a common trend as at the trailing edges, all the aerofoils rise above the leading and trailing edges and then descent to the trailing edge. The high variation in aerofoil shapes is consistent with the variation in planform shapes shown in Figure 70 as each variation requires different aerodynamic characteristics in an attempt to meet the requirements of the penalty functions.

Also of interest as with the sweep angles in Figure 70, the Pareto aerofoil shapes have a lower upper surface height compared to the benchmark aerofoil.

It must be noted that the Pareto member aerofoil sections all have a lower *t/c* ratio compared to that of the benchmark aerofoil shape.

The diverse range of aerofoil shapes further confirms that the use of a Pareto front when evaluating the HALE UAV wing problem was a success at there are large variations in geometry.

Mach Sweep

A Mach number sweep was performed for the selected Pareto members and the results are displayed in Figure 74 for coefficient of drag and Figure 75 for coefficient of lift.

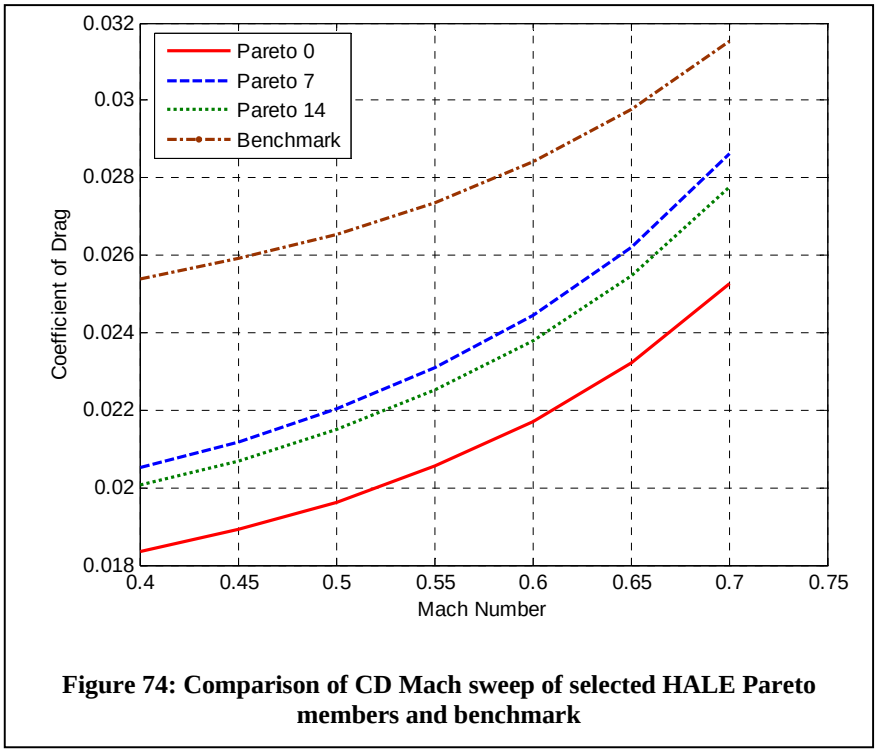

Figure 74: Comparison of CD Mach sweep of selected HALE Pareto members and benchmark

The Pareto member wings produce less drag than the benchmark wing over the range of Mach numbers investigated. Pareto member zero produced the lowest drag at the operational Mach number of 0.59, of 0.02175.

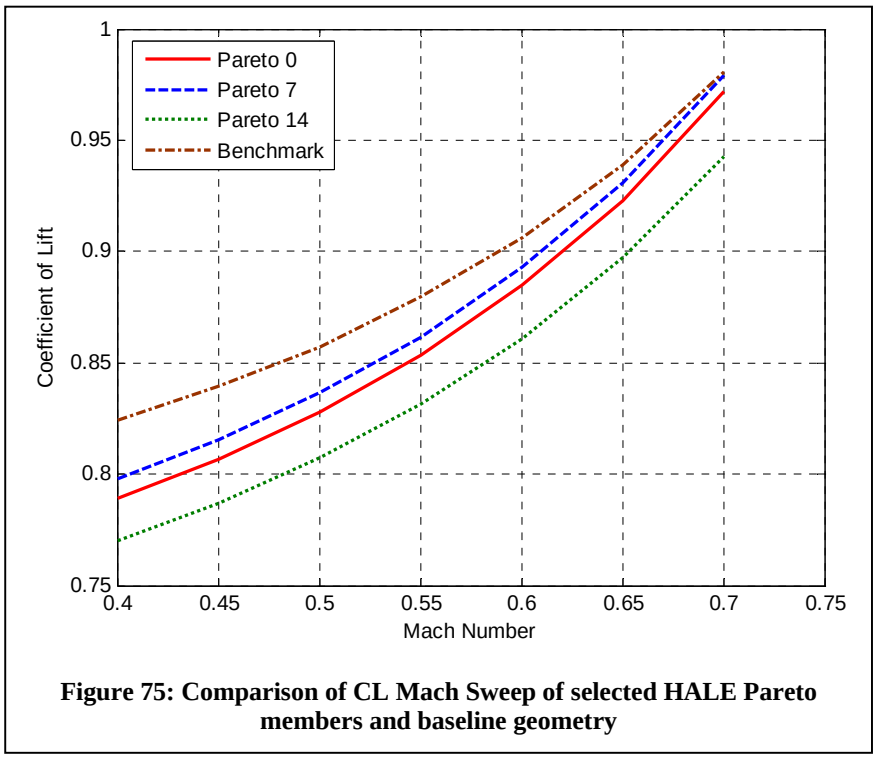

Figure 75: Comparison of CL Mach Sweep of selected HALE Pareto members and baseline geometry

For both the Coefficients of Lift and Drag, the trends in the Figures for the Pareto members are very similar.

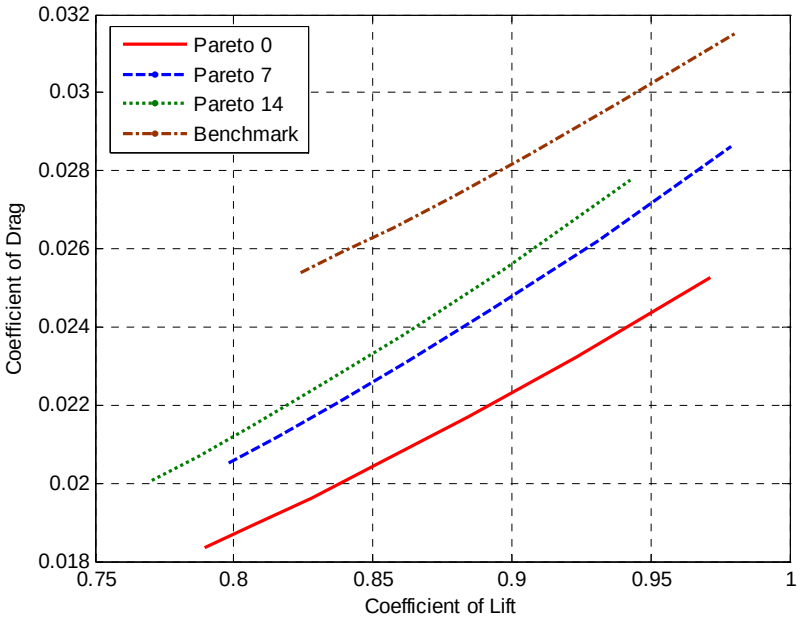

Figure 76: Coefficient of Lift vs Coefficient of Drag for HALE UAV

From Figure 76, the performance of the Pareto selected wings can be compared to that of the benchmark HALE UAV wing. As was indicated in the Pareto front shown in Figure 68, Pareto zero has the best L/D ratio and Pareto fourteen the worst. Even though Pareto fourteen has the best structural wing solution, it still has a better aerodynamic performance than the benchmark wing.

The second order external aerodynamic pressures are plotted for the upper and lower Pareto wing surfaces in Figures 77 and 78 respectively.

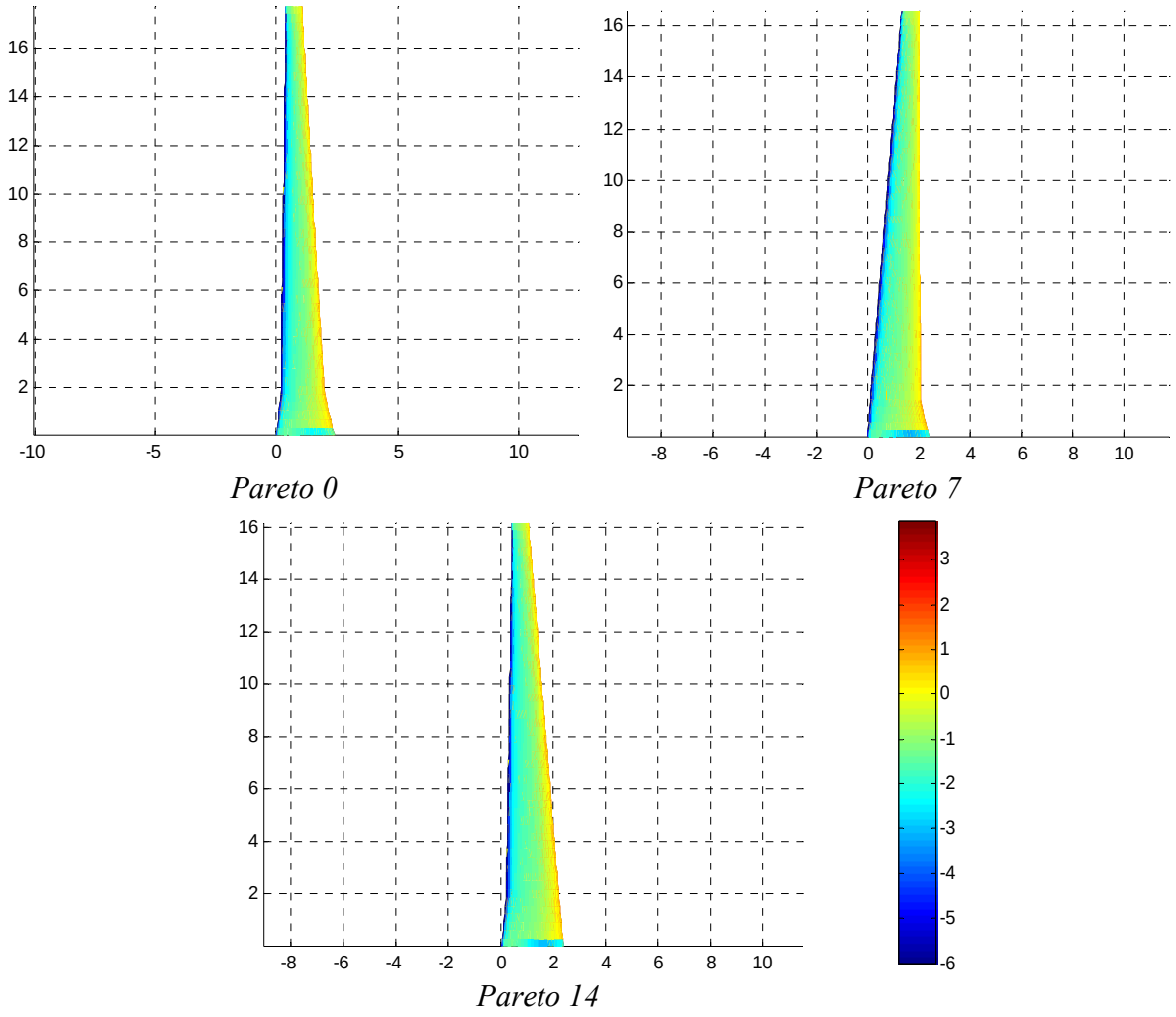

Figure 77: External Pressure Coefficients for selected HALE Pareto Members – Upper Surface

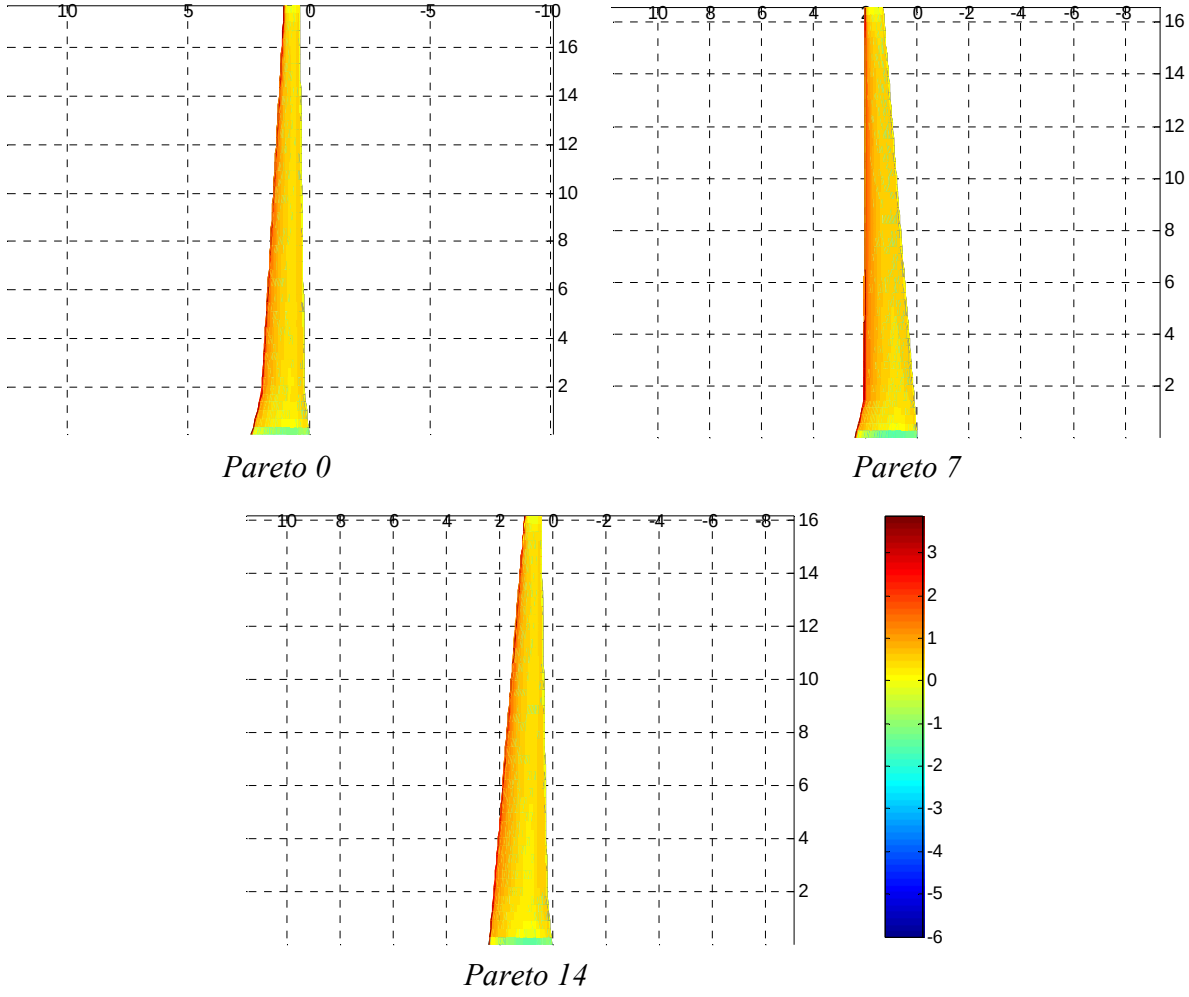

Figure 78: External Pressure Coefficients for selected HALE Pareto Members – Lower Surface

The pressure coefficients calculated by PANAIR about the Pareto wings are of a similar order of magnitude as those computed for the benchmark wing.

Figures 79 to 81 show the deflected Pareto wings. The original wing position and internal structure is shown as a wire frame for comparison.

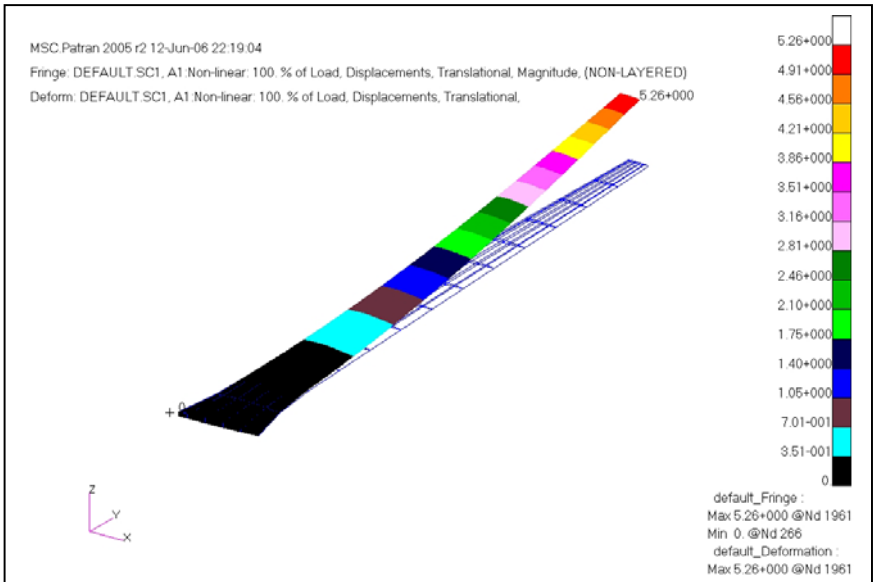

Figure 79: HALE Pareto 0 Displacement

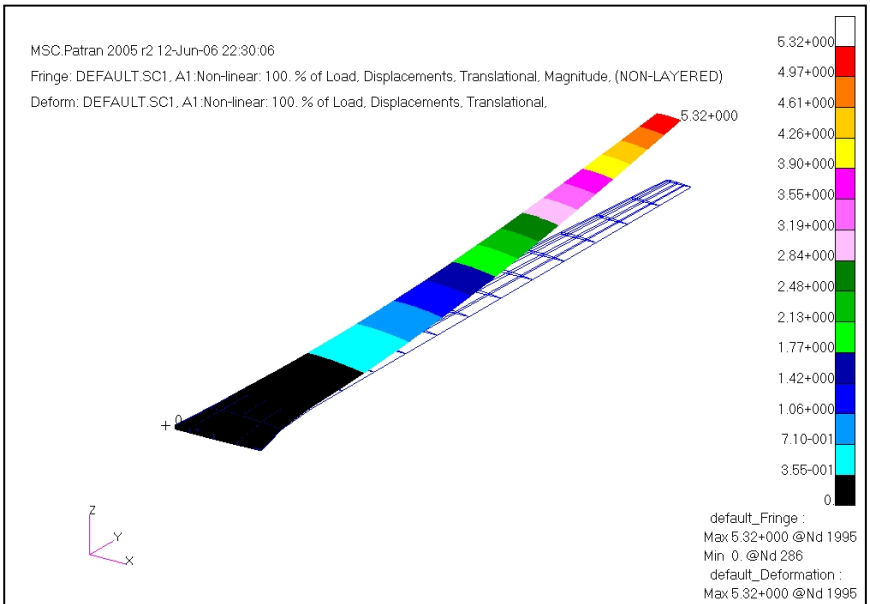

Figure 80: HALE Pareto 7 Displacement

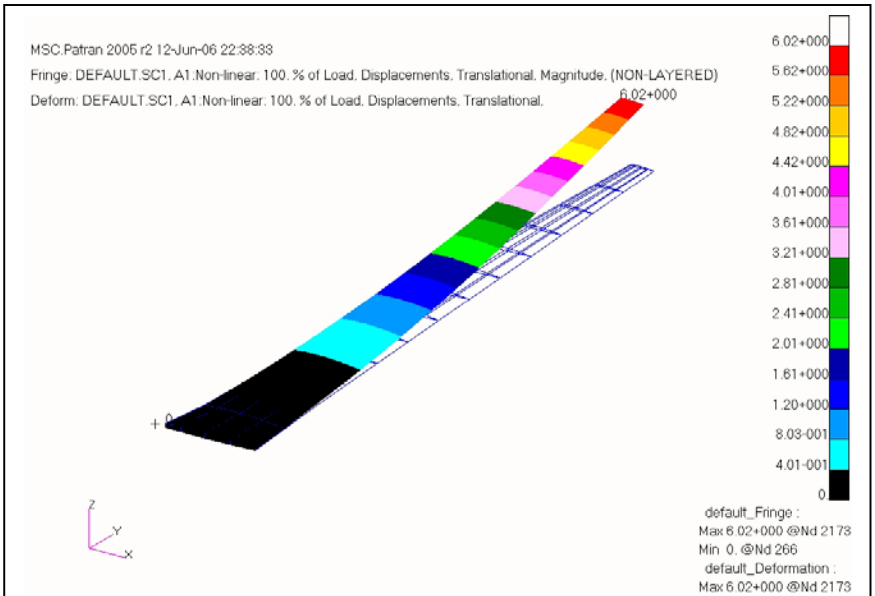

Figure 81: HALE Pareto 23 Displacement

From the above Figures showing the displacement of the HALE UAV wings it is quite evident that the wings deflected more than the twenty percent span value indicated in Table 15. Further testing is needed to analyse the effects of constraining the displacement.

An analysis of the strains produced by the aerodynamic forces is shown in Figures 82 to 84.

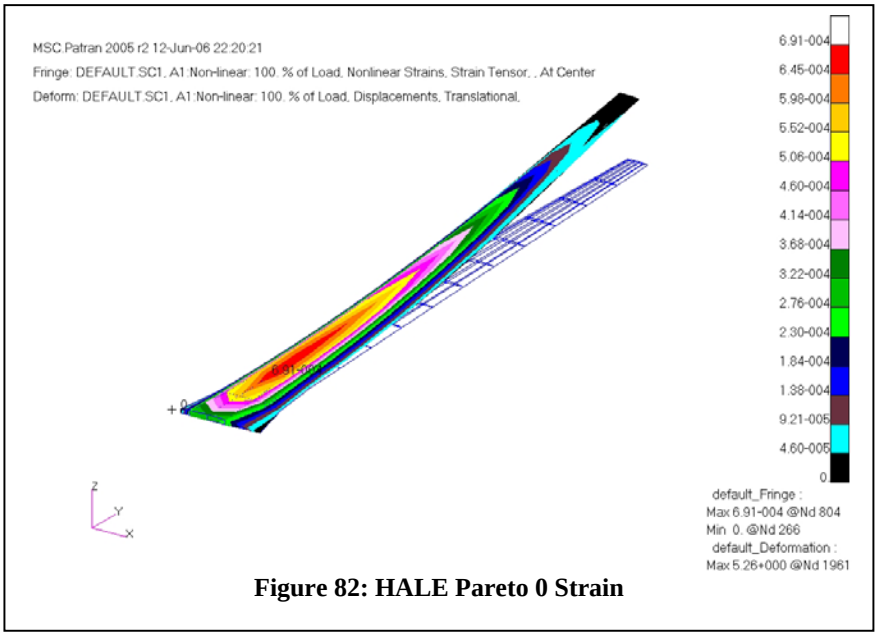

Figure 82: HALE Pareto 0 Strain

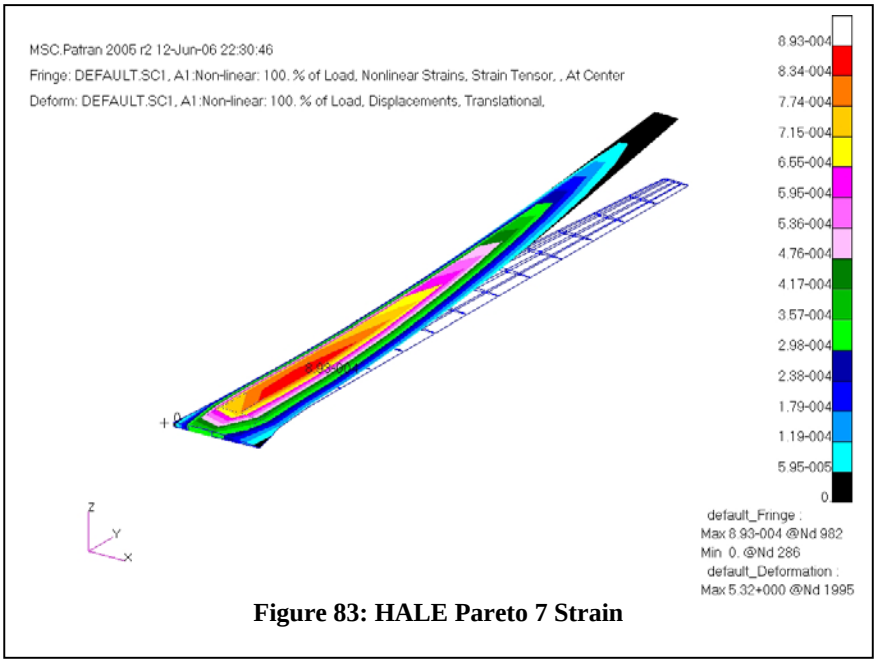

Figure 83: HALE Pareto 7 Strain

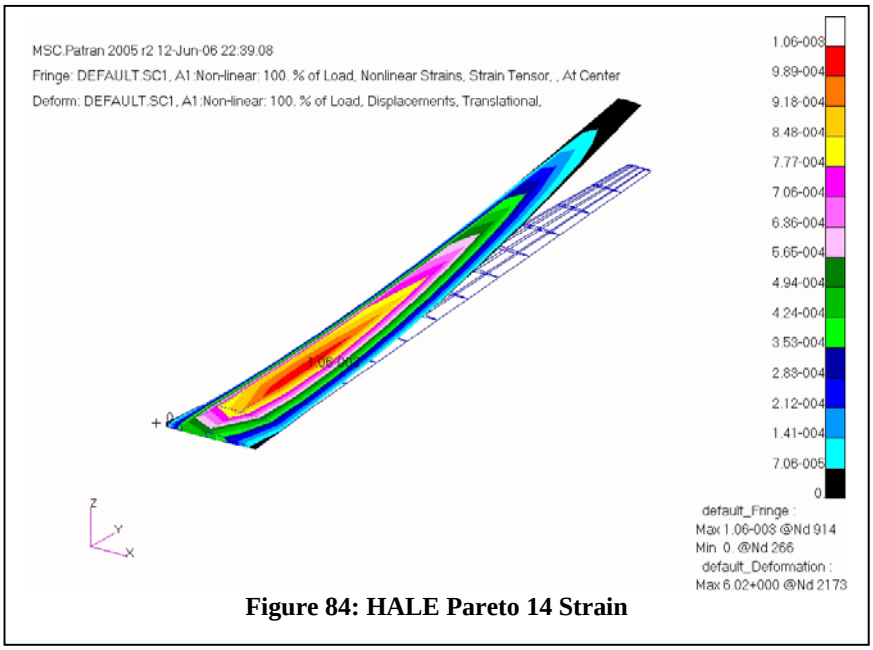

Figure 84: HALE Pareto 14 Strain

Due to the large displacements shown in Figures 82 to 84, the internal strains in the HALE UAV wings are very large with Pareto 0 failing the maximum strain allowable value specified in Table 14.

The results for the HALE UAV wing optimisation are summarised in Table 16 for comparison.

	Pareto 0	Pareto 7	Pareto 14	Benchmark
Deflection (%)	29.65	31.08	37.16	16.7
Maximum Strain	0.00691	0.000893	0.00106	0.000487
Mass (kg)	963.38	774.28	525.51	1138.15
L/D	40.805	36.559	36.197	31.729
Mass Penalty (kg)	286.55	235.65	167.69	0
Drag Penalty	0.0051	0.0074	0.0076	0

Table 16: Summary of Displacement, Strain and Mass for Selected HALE Pareto members

All the Pareto members selected from the Pareto front shown in Figure 68 had better Lift to Drag ratios.

The mass of the simulated Pareto members was lower than that of the benchmark, but the deflection of the wings was larger than the allowable twenty percent. The maximum strain values calculated by MSC.Nastran® were higher than those calculated for the MALE UAV Pareto wings. This is caused by the large displacements of the wings due to a less rigid wing internal structure.

Furthermore, all the HALE Pareto wings had penalties. This would have influenced the HAPMOEA code as it determined new generations of candidate solutions for evaluation.

Pareto 0 failed the maximum strain criteria as the maximum strain value was almost twice the allowable amount. This indicates that panels within the wing would fail due to the aerodynamic loads placed on the wing skin.

8 CONCLUSIONS

This report has described the characteristics and implementation details of a framework in which different aeronautical problems can be analysed. The framework is based on a Multi-objective Evolutionary Algorithm. The report indicates and addressed some of the limitation of current optimisation techniques and the need for alternative approaches. The report provides a description of the main components of the framework, i.e. an Aero-structural solver, a wing mesh generation capability, a robust MOEA optimiser and capabilities for parallel computing and post processing. Hence we have within the framework, a complete set of numerical tools for handling mathematical test functions and real world problems in aeronautics.

The methodology is illustrated on its application to the design optimisation of UAV wings as a multi-objective and MDO problem showing the benefits of the method. The method is found to be capable of identifying the trade-off between the multi-physics involved and provides classical aerodynamic shapes as well as alternative configurations from which the designer can choose. It is observed that there was a computational gain on using asynchronous evaluation and a hierarchical topology of fidelity models as compared to a single model during the optimisation.

Large gains in aerodynamics can be made for both the MALE and HALE UAV test cases through the use of the data calculated by the HAPMOEA code from the assumed benchmark wings. The lift to drag ratio can be extended to regions only seen previously within the flight envelopes of high performance gliders.

Structural gains can also be made, though as the true benchmark structures are more complex and probably include hard points within the wings and fuel tanks, the results obtained through the HAPMOEA code are only indicative of future possibilities given more accurate data.

A more detailed analysis needs to be performed on algorithms to better describe the internal structure of high aspect wings. This analysis could aid the optimisation of the HALE UAV test case and limit the penalties due to deflection and strain.

Although the implemented penalty functions and values worked when optimising both the MALE and HALE UAV wings, a more thorough investigation of the effect of different penalty functions and the calculation of penalty values on the optimiser simulation solution could yield better algorithms which, when used in the HAPMOEA code, could result in quicker solution times with results which didn't fail any of the constraints.

Given more accurate benchmark information, a more complex and detailed investigation and optimisation could be performed.

9 FUTURE WORK

A limitation to this study is that the solution found is not a full aero-elastic solution but rather a one iteration coupling of the aerodynamics of the candidate wing with the structural model. Furthermore, a rather low fidelity model is used to calculate the form and skin friction components of the drag produced by the candidate wing.

Further analysis methods and techniques could be incorporated into the Aero-Structural Solver framework, or modifications to the code could be made to perform calculations which would assist in designing more optimal wings based upon other constraints. The work could be divided into two sections namely the aerodynamics and aerodynamic package, and the structural model and structural simulation method.

9.1 AERODYNAMICS

9.1.1 SOLVER

The PANAIR aerodynamic solver could be upgraded to make use of a Navier-Stokes solver. This would increase the computational cost for each candidate wing simulation, but would also increase the accuracy of the solution attained if complex flow geometries were being analysed such as slotted flaps.

If the solver were upgraded, special consideration would have to be given when designing the program to automatically generate the domain meshes about the planned wings. If little consideration was given in defining mesh densities about areas of high macroscopic gradients, loss of accuracy could be significant.

9.1.2 DRAG CALCULATIONS

Currently the Aero-Structural Solver makes use of PANAIR and FRICTION to calculate the aerodynamic loads and aerodynamic fitness values for each candidate wing. As PANAIR is only applicable to linear potential flows, it would be beneficial to upgrade to a nonlinear flow solver such as TRANAIR®. Such an upgrade would allow the user or optimiser the ability to model complex flows which included shock waves at or near transonic speeds. This would also minimise any solution errors due to large Mach angles.

FRICTION is a low fidelity program which was passed a constant value for the percentage chord location where the transition from a laminar to turbulent boundary layer took place. The assumption was a crude estimate made by the authors and would not hold true for all the candidate wings analysed. For a more accurate skin friction drag coefficient calculation, a higher fidelity model could be incorporated into the solution sequence. Another simple addition which could be made to FRICTION could be a simple iterative method which could determine the Reynolds number at which the flow would make the transition from laminar to turbulent, and the corresponding chord ratio passed to FRICTION when calculating the required coefficients of drag.

9.2 STRUCTURES

9.2.1 MATERIALS

MSC.Nastran® has the ability to define materials that are made up of a number of plies. Hence graphite epoxy based materials could be correctly defined through the build up and orientation of the plies within the material. This could lead to a more detailed optimization where the material thickness could not only be a variable, but the make up of the material, fibre thickness, orientation and laminate layers, could also be added as design variables in the optimization process.

9.2.2 ELEMENTS

Most of the element input decks used when defining the elements in the structural model had the capacity to make use of material orientation within the element. Future work could entail the use of fibre orientation material properties such as those mentioned above. This would lead to a better understanding and optimisation as the element's true behaviour under loading could be studied.

If the position of the spars and ribs as functions of chord and span respectively were included as design variables within the simulation framework, the optimality of the spars could be increased as spars could be placed such that the bending moments generated by the aerodynamic forces could be minimised, and the variable rib placement could mean that better rib distributions could be achieved where sections of high strain which occur at crank locations could be minimised through the use of two closely spaced ribs.

More complex thickness functions could be devised, such as third or fourth order polynomials, to describe the way in which Spar and Rib thicknesses vary according to span. This could assist in the reduction of high strain concentrations which would occur where the wing geometry changes greatly.

CBAR or CBEAM elements could be used to describe the Rib and Spar Caps. The height and width of the sections could then be added to the design variables optimised by the Evolutionary Optimiser code. This would allow for more accurate deflection calculations and assist in the minimisation of the candidate wing structure.

9.2.3 SOLUTION METHOD

Further analysis could be conducted to incorporate buckling analysis to investigate the natural frequencies of the candidate wings. MSC.Nastran® can incorporate the MSC.Flightloads® package and undertake full aero-elastic analysis of candidate wing geometries. This would greatly increase the solution resolution of the candidate wings as solutions could be penalised against a final wing deflection value instead of the first solution iteration. This is beneficial as many wing solutions would solve to a position which would lie in the predefined constraints, but as the initial iteration indicates that the deflection is greater than this predefined value, the wing is discarded prematurely.

ACKNOWLEDGMENTS

The authors gratefully acknowledge Dr E.J. Whitney at Boeing Australia and Prof. Jacques Periaux at INRIA-CIMNE for fruitful discussions on Hierarchical Asynchronous Parallel EAs and the authors would like to acknowledge Mr K. White at Aeronautical Engineers Australia for his help and discussion on the structural model and MSC.Nastran®. Thanks are due to Prof. S W Armfield for allowing the authors the use of the computer cluster at the University of Sydney, Prof. L Tong for MSC.Nastran® licenses and Dr D J Auld for his assistance during the computer simulations. The project was funded by AOARD, Japan through their contract AOARD-044078. Furthermore, thanks to Lt. Col. (Dr) Bill Nace, Technical Director and Maj. (Dr.) Tony Mitchell, former Technical Director, AOARD, Japan for their continued support of our work.

REFERENCES

Abott, I. H. and A. E. V. Doenhoff (1980). Theory of Wing Sections, Dover.

Agarwal, R. K. (1999). "Computational Fluid Dynamics for Whole Body Aircraft." Annual Review of Fluid Mechanics **31**: 125–169.

Alexandrov, N. M. and R. M. Lewis (2000). "Analytical and Computational Properties of Distributed Approaches to MDO."

Ali, N. a. B., K. (2002). Conceptual Aircraft Design-A Genetic Search and Optimisation Approach. 23rd International Congress of Aeronautical Sciences (ICAS) Toronto, Canada.

Anderson, M. B. a. G., G. A. (1996). Using Pareto Genetic Algorithms for Preliminary Subsonic Wing Design. AIAA Paper 96-4023. AIAA. Washington, D. C.

Bäck, T., G. Rudolph, et al. (1993). Evolutionary programming and evolution strategies: Similarities and differences. Second Annual Conference on Evolutionary Programming, San Diego, CA, Evolutionary Programming Society.

Bäck, T., G. Rudolph, et al. (1993). Evolutionary programming and evolution strategies: Similarities and differences. Second Annual Conference on Evolutionary Programming, San Diego, CA.

Bäck, T. and H. P. Schwefel (1995). Evolution Strategies I: Variants and their computational implementation. Genetic Algorithms in Engineering and Computer Science Chichester: Wiley.

Bartholomew, P. (1998). The Role of MDO within Aerospace Design and Progress towards an MDO Capability. 7th AIAA/USAF/NASA/ ISSMO Symposium on Multidisciplinary Analysis and Optimization, St. Louis, Mo, AIAA.

Bertin, J. J. (2002). Aerodynamics for Engineers, Prentice Hall.

Cantu-Paz, E. (2000). Efficient and Accurate Parallel Genetic Algorithms, Kluwer Academic Publishers, New York.

Coello, A. C., D. A. V. Veldhuizen, et al. (2002). Evolutionary Algorithms for Solving Multi-Objective Problems, Kluwer Academic Publishers, New York.

Collard, P. and C. Escazut (1995). Genetic Operators in a Dual Genetic Algorithm. Seventh IEEE International Conference on Tools with Artificial Intelligence, Virginia, USA, IEE

Craidon, C. A. (1985). A Description of the Langley Wireframe Geometry Standard (LaWGS) Format, NASA.

Crispin, Y. (1994). Aircraft Conceptual Optimization Using Simulated Evolution,. AIAA and P. 94-0092.

Crossley, A. W. a. L., H (1996). "Design of Helicopters via Genetic Algorithm." Journal of Aircraft **3**(6).

Cvetkovic, D. a. P., I.C. (2000). Designer's Preferences and Multi-objective Preliminary Design Processes. Fourth International Conference
on Adaptive Computing in Design and Manufacture (ACDM'2000),, University of Plymouth, UK, Springer.

Deb, K. (2003). Multi-Objective Optimization Using Evolutionary Algorithms, Wiley.

Geist, A., A. Beguelin, et al. (1994). PVM: Parallel Virtual Machine. A User's Guide and Tutorial for Networked Parallel Computing, Massachusetts Institute of Technology.

Giesing, J. P. a. B., J. F. (1998). A Summary of Industry MDO Applications and Needs. Seventh AIAA/USAF/NASA/ISSMO Symposium on Multidisciplinary Analysis and Optimisation, St. Louis, Missouri, AIAA.

Giunta, A. A., Balabanov, V., Haim, D., Grossman, B., Mason, W. H. , Haftka, R. T. and Watson, L. T. (1997). "Multidisciplinary Optimization of a Supersonic Transport Using Design of Experiments Theory and Response Surface Modeling." The Aeronautical Journal(October 1997): 347–356.

Goldberg, D. (1989). Genetic Algorithms in Search, Optimization and Machine Learning, Addison-Wesley.

González, L., E. Whitney, et al. (2004). Multidisciplinary Aircraft Design and Optimisation Using a Robust Evolutionary Technique with Variable Fidelity Models. AIAA/ISSMO Multidisciplinary Analysis and Optimization Conference, Albany, NY, AIAA.

Gonzalez, L., Whitney, E. W., Srinivas, K., Armfield, S. and Periaux, J. (2005). "A Robust evolutionary technique for coupled and multidisciplinary design optimisation problems in aeronautics." Computational Fluid Dynamics Journal,: 142 – 153.

Gonzalez, L. F. (2005). Robust Evolutionary Methods for Multi-objective and Multidisciplinary Design in Aeronautics., Thesis, School of Aerospace, Mechanical and Mechatronic Engineering, J07 , NSW, 2006 Australia, . School of Aerospace, Mechanical and Mechatronic Engineering. Sydney, University of Sydney. **PhD** 222.

Gonzalez, L. F., E. J. Whitney, et al. (2004). A Robust Evolutionary Technique for Inverse Aerodynamic Design. Design and Control of Aerospace Systems Using Tools from Nature, Jyvaskyla, Finland, Computational Methods in Applied Sciences and Engineering.

Goraj, Z., A. Frydrychewicz, et al. (2004). "High altitude long endurance unmanned aerial vehicle of a new generation – a design challenge for a low cost, reliable and high performance aircraft." Bulletin of the Polish Academy of Sciences **52**(3).

Hansen, N. and A. Ostermeier (2001). "Completely Derandomized Self-Adaptation in Evolution Strategies." Evolutionary Computation **9**(2): 159 - 195.

Holland, J. H. (1975). Adaption in Natural and Artificial Systems, University of Michigan Press.

Kim, H. J. a. R., O. H. (1997). "Dual-Point Design of Transonic Airfoils Using the Hybrid
Inverse Optimization Method. ." Journal of Aircraft **34**(5): 612–618.

Kolbe, C. D. and R. W. Boltz (1951). The Forces and Pressure Distribution at Subsonic Speeds on a Plane Wing Having 45 of Sweepback, an Aspect Ratio of 3, and a Taper Ratio of 0.5. Washington, NACA.

Komzsik, L. (2001). MSC.Nastran 2001 Numerical Methods User's Guide.

Koza, J. R. (1992). Genetic programming : on the programming of computers by means of natural selection. Cambridge, Mass., MIT Press.

Koza, J. R. (1992). On the Programming of Computers by Means of Natural Selection. Cambridge MA, MIT Press.

Mäkinen, R., Neittaanmäki, P., Périaux, P. and Toivanen, J. (1998). A Genetic Algorithm for Multiobjective Design Optimization in Aerodynamics and Electromagnetics. . ECCOMAS 98 Conference, Athens, Greece, Wiley.

Margason, R. J., S. O. Kjelgaard, et al. Subsonic Panel Methods - A Comparison of Several Production Codes.

Marisarla, S. (2005). Structural Analysis of an Equivalent Box-Wing Representation of Sensorcraft Joined-Wing Confuration for High-Altitude, Long-Endurance (HALE) Aircraft. Mechanical Engineering. Cincinnati, University of Cincinnati. **Master of Science**.

Mason. (2001). "FRICTION." Retrieved September, 2005, from http://www.aoe.vt.edu/~mason/Mason_f/MRsoft.html.

Mason, W. H., Knill, D.L., Giunta, A. A., Grossman, B. , Haftka, R. T. and Watson, L. T. (1998). Getting the Full Benefits of CFD in Conceptual Design. AIAA 16th Applied Aerodynamics Conference,, Albuquerque, New Mexico, AIAA

Michalewicz, Z. (1992). Genetic algorithms + data structures = evolution programs. Berlin ; New York, Springer-Verlag.

MSC.Software (2005). Quick Reference Guide.

NASA. (2004). "Airborne Science Program - Altair Specifications." Retrieved August, 2005, from http://www.nasa.gov/centers/dryden/research/AirSci/UAV_Specs/altair_specs.html http://www.nasa.gov/centers/dryden/news/FactSheets/FS-073-DFRC.html.

Ng, T. T. H. a. L., G. S. B. (2002). "Application of Genetic Algorithms to Conceptual Design of a Micro-air Vehicle. ." Engineering Applications of Artificial Intelligence, **15**(5): 439-
445, .

NORTHROP-GRUMMAN. (2006). "UNMANNED SYSTEMS." 2006, from http://www.northropgrumman.com/unmanned/index.html.

Obayashi, S. (1998). Multidisciplinary Design Optimization of Aircraft Wing Planform Based on Evolutionary Algorithms. IEEE International Conference on Systems, Man, and Cybernetics, La Jolla, California, IEEE, October . IEEE.

Oyama, A., M.-S. Liou, et al. (September, 2002). Transonic Axial-Flow Blade Shape Optimization Using Evolutionary Algorithm and Three-Dimensional Navier-Stokes Solver. 9th AIAA/ISSMO Symposium on Multidisciplinary Analysis and Optimization, Atlanta, Georgia.

Oyama, A., Obayashi, S. and Nakamura, T. (2000). Real-Coded Adaptive Range Genetic Algorithm Applied to Transonic Wing Optimization. Lecture notes in Computer Science. Springer-Verlag. Berlin Heidelberg New York. **1917:** 712-721.

Parmee, I. and A. H. Watson (1999). Preliminary Airframe Design Using Co-Evolutionary Multiobjective Genetic Algorithms. The Genetic and Evolutionary Computation Conference, Orlando, Florida, USA, Morgan Kaufmann.

Parmee, I. and A. H. Watson (July 1999). Preliminary Airframe Design Using Co-Evolutionary Multiobjective Genetic Algorithms. Genetic and Evolutionary Computation Conference, Orlando, Florida, USA, Morgan Kaufmann.

Raymer, D. (2003). Use of Genetic and Evolutionary Algorithms for Aircraft Conceptual Design Optimization. . 41th AIAA Aerospace Sciences Meeting, Reno, Nevada.

Raymer, D. a. C., W. (2002). A Comparative Study of Genetic Algorithm and Orthogonal Steepest Descent for Aircraft Multidisciplinary Optimization- Paper 2002-0514. AIAA Aerospace Sciences Meeting. AIAA, Reno, Nevada.

Raymer, D. P. (1999). Aircraft design : a conceptual approach. Reston, VA., American Institute of Aeronautics and Astronautics.

Ruben, P., Chung, J., and Behdinan, K. and . (2000). Aircraft Conceptual Design Using Genetic Algorithms. 8th AIAA/USAF/NASA/ISSMO Symposium on Multidisciplinary Analysis and Optimization, Long Beach, California.

Saaris, G. R. (1992). A502I User's Manual - PAN AIR Technology Program for Solving Problems of Potential Flow about Arbitrary Configurations, Boeing.

Sacks, J., W. J. Welch, et al. (1989). "Design and Analysis of Computer Experiments." Statistical Science **4**(4): 409-435.

Sasaki, D., Obayashi, S., (2004). "Adaptive range multi objective genetic algorithms and self –organizing map for multi objective optimisation problem." in VKI Lecture Series 2004-07 , Optimization methods & tools for multicriteria/multidisciplinary design , Applications to Aeronautics and Turbomachinery , Eds, H. Deconinck, J. Periaux and K. Giannakoglou, 2004.

Sefioui, M., J. Periaux, et al. (1996). Fast convergence thanks to diversity. Evolutionary Programming V. 5th Annual Conference on Evolutionary Programming, MIT Press.

Sefrioui, M. and J. Périaux (2000). A Hierarchical Genetic Algorithm Using Multiple Models for Optimization. Parallel Problem Solving from Nature, Springer.

Selig, M. (2002). "UIUC Airfoil Coordinates Database." Retrieved August, 2005, from http://www.ae.uiuc.edu/m-selig/ads/coord_database.html.

Sobieski, J. and R. Haftka (1996). "Multidisciplinary Aerospace Design Optimization: Survey of Recent Developments."

Sobieszczanski-Sobieski, J. a. H., R.T. (1997). "Multidisciplinary Aerospace Design Optimization:Survey of Recent Development." Structural Optimization **14**: 1–23.

Takahashi, S., Obayashi, S. and Nakahashi, K (1997). Transonic Shock-free Wing Design with
Multiobjective Genetic Algorithms. Proceedings of the International Conference on Fluid Engineering, Tokyo, Japan, JSME.

Thierens (2002). Adaptive mutation rate control schemes in genetic algorithms. IEEE World Congress on Computational Intelligence: Congress on Evolutionary Computation IEEE Press.

Thomas, Z. a. G., A. (1999). AIAA Paper 1999-3798-Multidisciplinary Design Optimization Techniques: Implications
and Opportunities for Fluid Dynamics Research. 30th AIAA Fluid Dynamics Conference Norfolk, VA, .

Veldhuizen, D. A. V., J. B. Zydallis, et al. (2003). "Considerations in Engineering Parallel Multiobjective Evolutionary Algorithms." IEEE Transactions on Evolutionary Computation **7**(2): 144--173.

Venter, G. and J. Sobieszczanski-Sobieski (2004). "Multidisciplinary optimisation of a transport aircraft wing using particle swarm optimisaiton." Structural Mutidisciplinary Optimization **26**: 121-131.

Wakunda, J. and J. A. Zell (2002). Median-selection for parallel steady-state evolution strategies. Parallel Problem Solving from Nature Berlin, Springer.

Whitney, E., M. Sefrioui, et al. (2002). "Advances in Hierarchical, Parallel Evolutionary Algorithms for Aerodynamic Shape Optimisation." JSME (Japan Society of Mechanical Engineers) International Journal **45**(1).

Whitney, E. J. (2003). A Modern Evolutionary Technique for Design and Optimisation in Aeronautics. AMME. Sydney, University of Sydney. **PhD**.

www.airforce-technology.com. (2004). "Specifications - Global Hawk High Altitude, Long Endurance Unmanned Reconnaissance Aircraft, USA." Retrieved August, 2005, from http://www.airforce-technology.com/projects/global/specs.html.